Declaration

Name:	Justin Hettinga
Email:	justin.hettinga@gmail.com

Title of the Msc Dissertation:	Structural analysis of the roof of St Anne's Church
Supervisor(s):	Professor Pavel Kuklik
Year:	2008 - 2009

I hereby declare that all information in this document has been obtained and presented in accordance with academic rules and ethical conduct. I also declare that, as required by these rules and conduct, I have fully cited and referenced all material and results that are not original to this work.

I hereby declare that the MSc Consortium responsible for the Advanced Masters in Structural Analysis of Monuments and Historical Constructions is allowed to store and make available electronically the present MSc Dissertation.

University:	Czech Technical University
Date:	July 1, 2009
Signature:	_____

This page has intentionally been left blank.

Acknowledgements

This thesis would not have been possible without the extensive efforts of Professor Pavel Kuklik as he supervised this work. He was always willing to help and offer advice, kept a positive attitude, and spent large amounts of time assisting with the work. I am very grateful for the trips he organized to St Anne's Church and to the Broumov region, and for the multiple tours to sites and churches around Prague.

I would like to thank Mr. Dolezal for volunteering his time and letting us enter St Anne's Church. For the organization of this masters program in the Czech Republic, I would like to thank Professor Petr Kabele. Many thanks to Natalia Cavina for her tireless help with the visa, and for helping the students with any concerns or problems they had, this made the stay in the Czech Republic enjoyable and worry free. Finally I would like to acknowledge the Erasmus Mundus scholarship, as without this funding, I would not have been able to participate in this program.

This page has intentionally been left blank.

Abstract

Buildings in Prague with an original Gothic roof structure are the focus of this thesis. An overview of buildings from the Gothic period (13^{th} to 16^{th} c.) and relevant architects is given. As the history of Prague, Bohemia, and the Holy Roman Empire is relevant to the construction of Gothic structures in Prague, it is discussed briefly. The majority of the Gothic buildings in Prague suffered considerable damage from wars, invasions, or fires, and few still have their original roof trusses. St Anne's Church, Old New Synagogue, Pinkas Synagogue, and Church of St Wenceslas in Zderaz all have original gothic roof structures. Access to St Anne's Church was granted, so it was studied for this thesis.

Relevant documents relating to historic timber constructions are employed, such as "Evaluation and analysis of old timber structures," which uses non-destructive techniques. [1] Compliance with the Venice Charter [2] is required for all monuments and historic constructions, and the ICOMOS document "Principles for the preservation of historic timber structures" [3] is also followed.

A two dimensional model of a standard truss of St Anne's Church is modeled in the finite element program FIN 2D. Joints are modeled using pinned, fixed, and spring configurations, and no significant differences are found between them. Loading on the truss accounts for a 500-year return period, and for clay roof tiles that are not currently present, but could possibly be used in the future. The model is run under first and second order analysis. The stability is determined by increasing the loading until deflection and axial load limits are exceeded. Results are compared with limits set out in Eurocode 5: Design of Timber Structures.

By comparing the deflections from first and second order analysis, the structure can be checked against instability. Limits are established for comparing first and second order results, and can be used as alternatives to the Eurocode buckling equations.

This page has intentionally been left blank.

Abstract (in Czech)

Tato práce je zaměřena na stavební objekty s původní gotickou konstrukcí střechy. Je uveden přehled gotických budov a jejich architektů z rozmezí třináctého až šestnáctého století. Krátce je diskutována historie Prahy, Čech a Svaté říše římské a její podíl na vzniku gotických konstrukcí v Praze. Většina gotických budov v Praze byla v minulosti poškozena válkami, vpády nebo ohněm a pouze několik málo z nich má původní konstrukci krovu. Kostel sv. Anny, Staronová synagoga, Pinkasova synagoga, kostel sv. Václava ve Zderaze. Kostel sv. Anny byl vybrán pro studii zejména kvůli možnosti přístupu do objektu.

Byly využity relevantní dokumenty týkající se historických dřevěných konstrukcí jako: "Evaluation and analysis of old timber structures" (oceňování a analýza starých dřevěných konstrukcí), která používá nedestruktivních technik průzkumu [1]. V souladu s "Venice Charter" (benátskou chartou) [2] je tato doporučována pro všechny monumenty a historické konstrukce. Nebyl opomenut ani dokument ICOMOS "Principles for the preservation of historic timber structures" (principy ochrany historických dřevěných konstrukcí) [3].

Dvoudimenzionální model klasické příhradové konstrukce krovu sv. Anny byl modelován programem FIN 2D. Připojení ve styčnících bylo modelováno kloubově, vetknutím i pružným upnutím. Ve výsledcích nebyly shledány podstatné rozdíly pro jednotlivé případy připojení. Zatížení prutové soustavy krovu uvažujeme s pětisetletou periodu návratu. Jako krytina byly ve výpočtu uvažovány klasické pálené prejzy, ikdyž v současné době je střecha provizorně pokryta jinak. Výpočty byly prováděny podle teorie prvého i druhéhé řádu. Kritický stav konstrukce, lineární stabilita, byl určován zvyšováním zatížení do doby, dokud přetvoření nerostlo nade všechny meze. Výsledky jsou porovnány s limity stanovenými v eurokodu 5, Návrh dřevěných konstrukcí.

Prostřednictvím výpočtu přetvoření dle teorie prvého a druhého řádu, můžeme kontrolovat potencionální nestabilitu konstrukce. Tři limity byly zavedeny pro srovnání

výpočtů dle teorie prvého a druhého řádu. Tyto limity mohou být užity jako alternativy k rovnicím pro posouzení stability doporučovaných v eurokodu.

Table of Contents

1 Introduction 1
2 History of Prague 2
2.1 Political History of Bohemia 2
2.1.1 Establishment of Bohemia 2
2.1.2 Holy Roman Empire 2
2.1.3 Luxembourgs 3
2.1.4 Hussite wars 3
2.1.5 Habsburg rule 4
2.1.6 Twentieth century 5
2.2 The building of Prague: history of construction 6
2.2.1 Romanesque origins 7
2.2.2 Growth of Prague: Development of the towns 7
2.2.3 Further development and changes in Prague 8
2.2.4 Gothic architects in Prague 10
3 Gothic structures and architecture in Prague (13^{th} to 16^{th} c.) 12
4 St Anne's Church 22
4.1 History [5] 22
4.2 Geometry 24
4.3 Loading 31
4.3.1 Probability of exceedance 31
4.3.2 Dead load (DL) 31
4.3.3 Live load (LL) 31
4.3.4 Snow Load (SL) 31
4.3.5 Wind Load (WL) 32
4.4 Load Combinations [6] 33
5 Evaluation and analysis of old timber structures 35
6 The effect of age on material properties of timber 37
7 Timber strength classification 38

7.1 Service class [15] 38
7.1.1 Service class and St Anne's Church 38
7.2 Timber strength classification [9] 38
7.2.1 Timber strength classification of St Anne's Church 38
8 Second order theory, geometrical nonlinearities, linear stability and FINE 39
8.1 An ideal column [11] 40
8.2 Column with an initial deformation [10] 41
8.3 Linear Stability [12] 42
9 Eurocode and the reliability index 44
10 Structural analysis: FINE and St Anne's Church 45
10.1 Geometry of interior truss joints 45
10.2 Analysis of a standard truss 50
10.2.1 Geometry 50
10.2.2 Material strengths and properties 53
10.2.3 Loading 54
10.2.4 Results 56
10.2.5 Analysis of FINE results 64
10.2.6 Stability check by comparison of I and II order analysis 64
10.2.7 Out of plane stability 65
10.2.8 Analysis of results by Eurocode 5: Design of timber structures [15] 66
10.2.9 Linear stability: FINE 68
10.2.10 Linear stability: Eurocode 5 70
10.2.11 Discussion 71
10.3 Middle section with a different geometry 73
10.3.1 Geometry 73
10.3.2 Analysis 78
10.3.3 Summary of structural integrity 82
10.4 End of the roof 83
10.4.1 Analysis of FINE results: Eurocode 5 [15] 83
10.5 Irregularities due to damages, deteriorations, and imperfections 85
10.5.1 Decreased cross section due to missing material 85

10.5.2 Decreased cross section due to beetle damage 86
10.5.3 Truss irregularity 88
10.6 Summary of analysis 90
11 Conclusions 92
12 References 94
13 Appendix A: Loading calculation for St Anne's Church 95
13.1 Dead load (DL) 95
13.2 Live load (LL) 95
13.3 Snow Load (SL) 96
13.4 Wind Load (WL) 96
13.4.1 Basic wind velocity (v_b) 96
13.4.2 Reference height (z_e) 96
13.4.3 Terrain category 96
13.4.4 Peak Velocity Pressure 97
13.4.5 External pressure 98
13.4.6 Probability of Exceedance 98
13.4.7 Internal pressure coefficient 103
14 Appendix B: Timber grading criteria, as per DIN 4074-1 [9] 104
15 Appendix C: Derivation of equations 107
15.1 Buckling of an ideal column [11] from page 40 107
15.2 Buckling of a column with an initial deformation [10] from page 41 108
15.3 Eurocode buckling equations [15] from page 67 109

List of Symbols

A	Constant, or area
B	Constant
c	Distance from the neutral axis on a member cross section
$c_{pe, 10}$	External wind coefficient
D	Displacement {vector}
DL	Dead load
e	Eccentricity of a point load on a member
e_0	Initial eccentricity of a member from a straight geometry
E	Modulus of elasticity
f	Normal stress
F	Force {vector}
F_{krit}	Critical buckling force
I	Moment of inertia
k	Stiffness, load multiplier causing failure
k_m	Modification factor
l	Length
LL	Live load
M	Bending moment
n	Integer
P	Axial load on a member
P_{cr}	Axial load on a member that causes buckling
q_k	Live load (pressure)
Q	Shear force
Q_k	Live load (point load)
r	Radius of gyration
S	Stiffness [matrix form]

w	Deflection of a member perpendicular to its axis
W_e	External wind pressure
W_i	Internal wind pressure
WL	Wind load
x	Distance along a member
y	Distance from the neutral axis on a member cross section
ε	Strain
δ	Deflection
λ	Slenderness
ρ	Curvature
τ	Shear stress
σ	Normal stress

1 Introduction

During the Gothic period, there was no knowledge of structural mechanics, and the structures were built based on what had been done previously and the ideas of the designer. Of the few structures that have survived since their construction, their existence is evidence that they are structurally adequate. However, over time, the capacity of or loading on a structure can change, resulting in failure or irreversible loss of historic material. Of particular concern is that wood trusses are susceptible to deterioration from beetles and rot. The analysis on St Anne's roof truss accounts for deterioration in the members, missing members, and reduced cross-sectional dimensions of members so that the true state of the structure is examined.

When a structure is in need of repair after a catastrophic event like a fire or damage in a war, the current knowledge of structural mechanics is often employed when works are done. However, if the changes to a structure happen slowly over a period of months or years, they can often go unnoticed. Many historic constructions are privately owned, and as a result are not subject to regular maintenance or monitoring for changes such as the emergence of rot or beetle infestation. St Anne's Church has recently undergone modifications including the replacement of the roofing material, but it is unknown if any structural analysis was done on the roof truss, or if there has ever been any analysis performed in the past. This thesis provides a report on the current capacity and safety of the roof truss of St Anne's Church employing the current methods of analysis, namely second order analysis in a finite element program.

2 History of Prague

2.1 Political History of Bohemia

2.1.1 Establishment of Bohemia

The western half of what would become Bohemia was conquered and settled Germanic people (Bavarians) in the 1st c. BC. Some of these people later emigrated, likely encouraging the immigration of Slavic people in the 6th c. AD. The first ruler of the Slav people was Samo, who created one of the earliest Slav states from 623 to 658 as a supra-tribal union. In the 9th c. the manorial system declined, and a new nation based on a united Slav ethnic group was created in 833. It was called Greater Moravia, and included the area of modern day Czech Republic and Slovakia. Internal struggles and wars weakened Greater Moravia, and in 895 it fragmented and Bohemia gained independence. From 895 to 1306, the Přemyslid Dynasty ruled Bohemia.

During its inclusion in Greater Moravia in the 9th c., Bohemia was introduced to Christianity, which became widespread in the 10th c. This facilitated an alliance with the Frankish rulers, who were Christians as well. The East Frankish Kingdom originated from the Carolingian Empire, would go on to become East Francia then the Holy Roman Empire. In 950, under German King Otto I, Bohemia became a part of the Holy Roman Empire.

2.1.2 Holy Roman Empire

The Holy Roman Empire was made up of large amounts of central Europe, and was a union of territories during the Middle Ages to Early Modern period. For most of its history, the Empire consisted of hundreds of smaller sub-units, principalities, duchies, counties, and free imperial cities. Bohemia, under the Holy Roman Empire, was largely autonomous.

The Holy Roman Emperor would appoint the Duke or King of Bohemia, and from 993 to 1212 the Přemyslid Dynasty ruled Bohemia as appointed by the Emperor. In 1212, the Holy Roman Emperor awarded the hereditary title of King, and this bloodline would continue until 1306, when King Wenceslaus III died and no male heir to the throne remained.

2.1.3 Luxembourgs

When King Wenceslaus III died, the Holy Roman Emperor was Henry VII, a member of the Luxembourg family. His son, John I, married Elisabeth, daughter of the late King Wenceslaus II, and was elected King of Bohemia in 1310. Upon the death of John I, his son, Charles IV became the next King of Bohemia in 1347. In 1349 he was elected and crowned King of the Romans, and in 1355 he became the Holy Roman Emperor. Prague now became the capital, and developed into one of Europe's greatest cities, the third largest at one point, gaining landmarks such as Charles University, Charles Bridge, and St Vitus Cathedral.

Charles IV attempted to expand Bohemian crown lands in the 1350's, and acquired Silesia, the Upper Palatinate, and Franconia, known as "New Bohemia". In 1367, he annexed Lower Lusatia to Bohemia. The reign of Charles IV was a prosperous time for Bohemia. He divided the land between his three sons, and died in 1378. King Wenceslaus IV ruled over Bohemia from 1378 to 1419. Sigismund was the last of the Luxembourg dynasty, and was Holy Roman Emperor from 1433 to1437.

2.1.4 Hussite wars

The Hussite wars (Bohemian wars) were between the military and followers of Jan Hus, rector of Charles University and prominent reformer and religious thinker. They occurred from 1420 to 1434, and ended inconclusively. The Hussite movement gained momentum after the execution of Jan Hus in 1415, as the Hussites opposed the views of the Roman Catholic Church. Following the death of Holy Roman Emperor and King of Bohemia Wenceslaus IV in 1419, various Hussite committees ruled Bohemia. Holy Roman Emperor Sigismund launched the first anti-Hussite crusade in 1420, which was

successfully defended in Prague by Hussite forces during the Battle of Vitkov Hill. In the 1420s, the Hussites split into the Utraquists and Taborites. In 1434 the Utraquists accepted Sigismunds' rule in exchange for religious tolerance, and the Taborites kept fighting and were defeated. Utraquist George of Podebrady ruled Bohemia as a Hussite king from 1452 to 1471, followed by two kings from the Polish Jagiellonian dynasty, though the majority of the power remained with the Utraquist nobles, the "Bohemian Estate."

2.1.5 Habsburg rule

The Czech nobility asked the Austrian Catholic Habsburgs to rule Bohemia in 1526, and Bohemia became a constituent state. The provinces of the Habsburg Monarchy enjoyed considerable religious and cultural freedom. The capital of the Habsburg Monarchy was originally Vienna, moved to Prague from 1583 to 1611, then returned to Vienna. Emperor Ferdinand II began oppressing rights of the Protestants in Bohemia, which started the Thirty Years' War in 1618. A quarter of the Bohemian population died in this war.

In 1618, the Bohemian Estates started an uprising by throwing two Habsburg councilors and a secretary out the window of the Old Royal Palace. The next year the Bohemian Estates elected Frederick of the Palatinate as ruler. In 1620, he lost the Battle of Bila Hora to the Habsburgs, and he fled. In 1621, 27 nobles who started the revolt were executed, and Prague was no longer the head of the Empire. During the Thirty Years' War, Saxons occupied Prague from 1631 to 1632, the Swedes occupied Hradčany and Malá Strana in 1648, and Stare Mesto was bombarded for months. From 1620 to 1648, the population of Prague dropped from 60,000 to 24,600. The Czechs had Catholicism forced on them, their culture was threatened by Germanisation, and they lost their independence for almost 300 years. German was spoken by the administration controlling the region. Prague was reduced to a provincial town, as the throne was moved to Vienna.

The indivisibility of the Habsburg Empire and the centralization of its rule were secured in 1749, which prevented any possibility of Bohemian independence. The 19th c. saw success for the Czech in their culture, as Czech language journalism, literature and drama

was reborn in the Czech National Revival. The Revolution of 1848 aimed for autonomy for Bohemia, but was defeated. The Czechs gained control of Prague in council elections of 1861, and the Germans lost their influence over the city in the next few decades. Austria was defeated in the Austro-Prussian war in 1866, creating an Austrian-Hungarian empire with equality between the two. Bohemia pushed for a tripartite monarchy, but failed in 1871.

2.1.6 Twentieth century

The Czechs and Slovaks did not want to fight for Germany or Austria in World War I, and many fought in renegade legions against them. In 1918, Czechoslovakia declared independence as World War I ended, with Prague as the capital.

Before World War II, three million German speakers were living in Bohemia and Moravia. In October 1938, Nazis occupied the Sudetenland, and in 1939 occupied all of Bohemia and Moravia. In 1945, Czechoslovakia once again became an independent country.

In 1946, the communist Party of Czechoslovakia won the elections and formed a coalition government. In 1948 they staged a coup d'etat with the support of the Soviet Union. A movement for democracy, "Prague Spring," was crushed in 1968 by the Soviets.

In 1989, the Berlin wall fell, and the peaceful Velvet Revolution resulted in elections in 1990. The Czech Republic and Slovakia were now separate countries.

2.2 *The building of Prague: history of construction*

A map of Prague is shown, with the neighborhoods indicated, which kept the names of the historic towns.

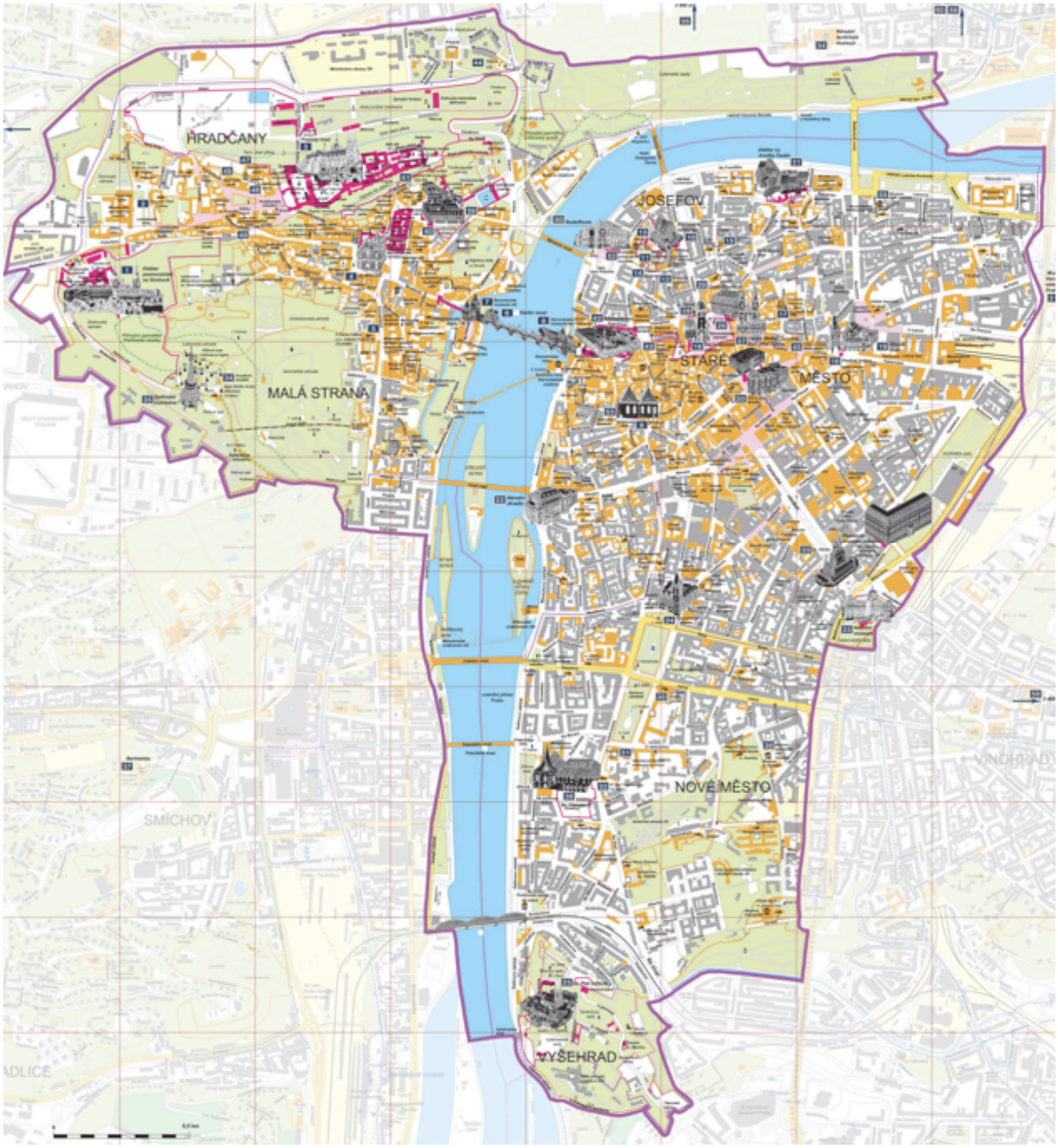

Figure 1 Map of Prague, focusing on the historic areas [4]

2.2.1 Romanesque origins

The Prague settlement became the seat of the Přemyslid princes between 880 and 890. Romanesque buildings were built on the location that is now Prague Castle, the first being the Church of Our Lady. Prince Borivoj I founded it prior to 885, and now only part of the floor and foundation remain. This church is the oldest in Prague, and second oldest in Bohemia, and was a single nave building with an apse. Under what is now St Vitus Cathedral are remains of St Vitus Rotunda, which was founded in the 930's. The remains of the Romanesque Basilica of St Vitus are also present in this area, as well as the 11th c. Episcopal Chapel of St Maurice. At the foot of the hill Prague Castle is on, a settlement was started next to the shallow crossing points over Vltava River, as trade routes converged at this location. In the 12th c, a Romanesque palace replaced some of the previous buildings.

A church and fortified trading post were built on the cliff on the other side of the Vltava River at Vysehrad in the 10th c. This occurred 70 years after the establishment of buildings on the Prague Castle site. Prince Vratsilav II of the Přemyslid dynasty built the castle Vysehrad in 1085. The following Přemyslid rulers returned to Prague Castle where the city would then grow around, instead of Vysehrad.

In the 11th c, the city expanded from the banks of Vltava River around the marketplace that is now the old town square (Staromestske námestí). The city became quite multicultural, as German merchants settled Na Porici and a Jewish settlement was established at the end of the 11th c.

2.2.2 Growth of Prague: Development of the towns

2.2.2.1 Staré Město

Settlements in what would become the Old Town, Staré Město, started around the 9th c. In the 12th c, the settlement was linked to the Prague Castle area by Judith Bridge, which would later be destroyed and replaced by Charles Bridge. In 1231, Wenceslaus I gave it a

town charter, and had Vaclav II build stone fortifications and a moat on its south and east side, which protected it in combination with the Vltava River on its north and west. The wall and moat are gone, but the main gate, Powder Gate, remains.

Starting in the 13th c, the buildings were gradually raised by building new constructions on top of old foundations, in order to reduce the damage when Vltava River flooded. The majority of the town was Gothic, but many buildings had Romanesque foundations. Johann of Luxembourg gave the town the right to set up its own town hall in 1338.

2.2.2.2 Malá Strana

A market settlement was present in this are in the 8th or 9th c, and the population grew over the next few centuries. Přemysl Otakar II of the Přemyslid dynasty founded the town of Mensi Mesto, later renamed the Lesser Town, Malá Strana, by combining these settlements beneath Prague Castle in 1257. The town is located on the west bank of the Vltava River, and the residents were largely German craftsmen invited by the King.

2.2.2.3 Hradčany

The third town of Prague, Hradčany was established around 1320 - 1330 under the administration of Prague Castle. It encompasses Prague Castle and the surrounding area.

2.2.2.4 Nove Mesto

In 1348 Charles IV founded the New Town, Nove Mesto. Most of the fortifications surrounding this area were demolished in 1875.

2.2.3 Further development and changes in Prague

In the 15th and 16th centuries, Prague strengthened its role as a merchant city, and many noteworthy Gothic buildings were erected.

2.2.3.1 Hussite wars and Habsburg Rule

In the Hussite wars, Hradčany and Malá Strana sustained major damage. Malá Strana was almost destroyed in the battles in 1419.

In 1541, a huge fire (the Great Fire) started in Hradčany square, and ruined many sections of Malá Strana and Hradčany. The houses were mostly wooden and occupied by merchants and artisans, and burned easily.

The rebuilding of Malá Strana and Hradčany after the damages sustained in the Hussite wars and the Great Fire resulted first in Renaissance architecture, and in the 17th and 18th c, Baroque architecture. The Habsburg nobility built many palaces in Hradčany in the 17th c. to try increase their influence on the leaders in Prague Castle.

A major fire in 1689 caused significant damage to Stare Mesto, and the rebuilding was of Baroque style.

In 1784, Joseph II united the Prague towns of Staré Město, Nove Mesto, Malá Strana, and Hradčany by imperial degree.

During the Czech National Revival of the 19th c., a distinctive architecture emerged including Prague landmarks the National Theatre and the National Museum.

2.2.3.2 Twentieth century

Prague became capital of Czechoslovakia in 1918. On January 1, 1922, Greater Prague was established by annexing surrounding towns, and had a population of 677,000. An industrial boom occurred until the Great Depression of the 1930's, and by 1938 the population was one million. Prague had little damage during WWII.

2.2.4 Gothic architects in Prague

2.2.4.1 Matthias of Arras (Matyas z Arrasu, Mathieu d'Arras) (1290? - 1352)

Matthias of Arras was a French architect who was summoned to Prague from the papal court of Avignon by Charles IV to lead works on the newly founded St Vitus Cathedral. He likely worked on Karlstein Castle in Karlstein, Central Bohemia, which was founded in 1348. He also likely was a town planner of Nove Mesto (New Town) of Prague. When Matthias of Arras died in 1352, Peter Parler, then 23 years old, continued works on St Vitus Cathedral and Charles IV supervised works on Karlstein Castle.

2.2.4.2 Peter Parler (1330 – 1399)

Peter Parler was a German architect that moved to Prague in 1356, where he would spend the rest of his life. He was the architect of a number of works in Bohemia, but most are in Prague. His work included:

- The primary planning of the New Town of Prague (likely started by Matthias of Arras)
- Charles Bridge and its towers
- All Saints' Chapel in the Royal Palace of Prague Castle, which after the fire of 1541 was redecorated in the Baroque style
- Likely the architect of Church of Our Lady (Frauenkirche) (stone masonry) in Nuremburg, Bavaria, Germany, built from 1352 to 1356 under Charles IV, as the area around Nuremberg was then a part of Bohemia and called "New Bohemia"
- The chancel of the St. Bartholomew Church in Kolin, Central Bohemian Region, Czech Republic, between 1360 – 1378
- Co-author of the draft design of St Barbara Church in Kutna Hora

His Gothic style was characterized by extensive ornamentation that reflected a display of wealth and luxury. He built the first real net vaults, which are vaults with hanging bosses

and ribs rising free through space. Upon his death, his sons, Wenzel Parler and Johann Parler, continued his work.

2.2.4.3 Wenzel Parler (1360? – 1404)

The son of Peter Parler, Wenzel Parler worked on St Vitus Cathedral from the late 1370s to 1392. In 1398 he left Prague and worked on buildings in Germany and Austria.

2.2.4.4 Johann Parler (1359? – 1405 or 1406)

Johann Parler continued Peter Parlers' work on St Vitus Cathedral. He later moved to Kuttenburg (later named Kutna Hora), and was likely the first architect of St Barbara Church, of which Peter Parler participated in the draft design.

2.2.4.5 Matěj Rejsek (1445? – 1506)

Matěj Rejsek was a Czech architect who worked on St Barbara Church in Kutna Hora in 1482, after works had ceased for 60 years under the Hussite wars. He did the upper triforium and vault of the choir of this church. He was the architect of the south tower of the Church of Our Lady of Týn, which was finished in 1511, and also was the architect of Powder Tower in Prague.

2.2.4.6 Benedikt Rejt (1453 – 1534)

Benedikt Rejt was a German architect, who worked on the following structures in Bohemia:

- Vladislav Hall (1497 – 1500) and Louis Tract in Prague Castle
- Church of St. Nicolas (1517 – 1537) in Louny
- The palace of the castle in Blatna
- Reconstructed the Prague Castle fortification
- St. Barbara Church in Kutna Hora (1482), works restarted after the Hussite wars

He was buried in the Church of St. Nicolas in Louny.

3 Gothic structures and architecture in Prague (13th to 16th c.)

Note: Buildings outside Prague included only for significant Gothic architects

Table 1 Gothic structures and architecture in Prague (13th to 16th c.)

Building	Location	Year	Builder or event
Staré město			
Church of St Martin in the Wall *Roof likely not original*	Martinská 8, Stare Mesto, Prague	1178 – 1187 13th c. 1355 – 1378 1488 1678 1779 1905 - 1906	Construction of the one nave Romanesque church Town walls are built that divide the church Gothic reconstruction, the nave was elevated and a new vault was built Completion of a reconstruction in late-Gothic style, including addition of two transepts Major damage in a fire, followed by rebuilding Baroque reconstruction Rebuilt under Kamil Hilbert
Convent of St Agnes *Roof likely not original*	U milosrdnych 17, Staré Město, Prague	1233 1234 – 1380 Unknown Currently	Founded by King Wenceslaus I, is the oldest Gothic construction in Prague Construction Church St Francis had a partially collapsed nave and dome roof, now rebuilt and used as a concert hall Restored, one building is the National Gallery

Old New Synagogue ***Roof likely Gothic***	Červená 2, 110 00, Josefov (historically Staré Město), Prague 1	1270 Middle Ages	Completed, with a twin nave design, is one of Prague's first Gothic buildings, likely the same architects that designed the Franciscan St Agnes Convent Roof built
House at the Stone Bell *Gothic roof was likely replaced by a Baroque roof*	Staromestske námestí 13, Staré Město, Prague	Late 13th c. Mid 14th c. 1685 – 18th c. 19th c. 1988	Construction begins Rebuilding Baroque adaptations Neo-Baroque façade Restoration, original Gothic façade revealed
St Anne's Church ***Roof original***	Zlatá ulice 110 00, Staré Město, Prague 1	1313 – 1330 Late 17th c. 20th c.	Construction Repairs and interior decorations Reconstruction and replacement of roof coverings
Old Town Hall *Roof likely not original*	Staromestske námestí 1, Staré Město, Prague	1338 1364 Unknown 1939 – 1945 20th c.	Founded Tower completed Ongoing expansions and constructions leave the buildings with Gothic and Renaissance styles Significantly damaged in world war II Rebuilt

Church of Our Lady before Týn *Roof not original*	Staromestske námestí, Staré Město, Prague	1365 – 1511 1450's 1511 1670 Unknown	Construction, early Gothic style, possibly designed by Matthias of Arras and Peter Parler Roof completed Southern tower completed under Matěj Rejsek Lightning strike caused a fire, burning down the vault Interior decorated in Baroque
Church of St James *Roof likely not original*	Malá Stupartska 6, Staré Město, Prague	1373 1689	Built by Minorites (a branch of the Franciscans) Suffered extensive damage in the fire, and was rebuilt in the Baroque style
Old Town Bridge Tower *Roof not original*	Charles Bridge, Prague 1	1380 1648	Completion, done by Peter Parler Partially damaged by the Swedes attempted occupation
Bethlehem Chapel *Roof not original*	Betlémské námestí 3, Staré Město, Prague 6	1391 – 1394 1402 - 1413 1661 1786 1950 - 1952	Construction, built by rich courtier Hanus of Mühlheim and tradesman Vaclav Kriz Jan Hus preaches in the church Altered to become a Catholic church Mostly torn down Replica built by Jaroslav Fragner, using existing wall fragments and original plans

Powder Tower (or Powder Gate) *Roof likely not original*	Náměstí Republiky, Staré Město, 110 00 Prague 1	1475 1477 – 1485 1757 1875 – 1886 1990s	Construction starts, done by Matěj Rejsek, based on the Old Town Bridge Tower, under the reign of King Vladislav II, late Gothic style Construction interrupted as riots forced King Vladislav II to flee the city. Severely damaged during the Prussian occupation Rebuilt by Josef Mocker Renovated
Pinkas Synagogue ***Main sanctuary has preserved Gothic arches (roof), other areas have late Renaissance vaults***	Siroka 3, Stare Mesto, Prague	1535 1607 - 1625	Constructed in late Gothic / Renaissance style Renovated and expanded in late Renaissance style
Charles Bridge	Malá Strana / Staré Město, Prague	1357 – early 15th c.	Done by Peter Parler

Malá Strana			
Church of St John at the Laundry	4 Říční, Southern Malá Strana, 118 00, Prague	1142 1235 Mid 13th c. 18th c. 2002	Founded Construction of the protestant church, used by the Hussites, in early Gothic style New chancel Renovated in Baroque style Renovations done
Church of Our Lady Below the Chain *Roof likely not Gothic*	Lázeňská 118 00, Southern Malá Strana, Prague 1	1182 1314 15th c. 16th c. 17th c.	Completion of a three nave Romanesque basilica Rebuilding of the church after previous damages starts in early Gothic style using fragments of the original walls Rebuilding is interrupted by the Hussite wars, the towers are completed but not the nave Rebuilt in Renaissance style Baroque features added

St Thomas Church *Roof not original*	Josefská 28/8, 118 00, Malá Strana, Prague 1	1315 15th c. 1584 – 1592 1727 - 1731	Completion Destroyed by Hussite riots Rebuilt by Augustinian solitaires with the participation of Bernard di Alberto in Renaissance style Renovated in Baroque style
Lesser Town Bridge Tower	Malostranská mostecká věž, Malá Strana, Prague 1	1462	Construction under King George of Podebrady using the Old Town Bridge Tower as a model
Hradčany			
Old Royal Palace *Roof likely not original*	Prague Castle, 118 00, Hradčany, Prague 1	1135 14th c. 1487 - 1500 1541	Sobeslav I built a Romanesque palace Rebuilt in Gothic style by Charles IV Vladislav Hall and the Louis Tract built by Benedikt Reid in late Gothic style Large fire, rebuilding of portions including the All Saint's Chapel
St Vitus' Cathedral *Roof not original*		1344 1354 - 1399 1541	Begun under Matthias of Arras Peter Parler worked on it, specifically the eastern portion, followed by his sons, Wenzel and Johannes Parler, then Master Petrlik Fire considerably damages the cathedral
Fortifications improved		Unknown	Fortifications improved by Benedikt Rejt
Living quarters		Unknown	Done by Benedikt Rejt

Nové Mesto			
Church of St Wenceslas in Zderaz ***Ceiling dates to 1586-1587, roof possibly from this time period or older***	Resslova, near Charles Square, Nové Mesto, Prague	14th c 1586-1587	Construction, incorporating parts of a wall and windows from a previous 12th c Romanesque construction Ceiling built by K. Mělnický
Church of the Assumption of the Virgin Mary and Charlemagne *Roof not original*	Ke Karlovu, Nové Mesto, Prague	1350 1575 1755	Constructed under Charles IV, modeled on Charlemagne's burial chapel in Aachen Ribbed vault added Fire and reconstruction
Church of St Stephen *Roof not original*	Štěpánská, Nové Mesto, Prague	1351 – 1401 1600 - 1604 1686 1866 1876 – 1879	Construction under Charles IV of the triple aisled church, in Gothic style Detached belfry constructed, roof replaced in 1731 Chapels Koronelská and Brangeberg added on the south and north sides of the church Addition of a neo-Gothic hall on the north side of the church Renovation by Josef Mocker in neo-Gothic style

Emmaus Monastery *Roof likely not original*	Vysehradska 49, Nové Mesto, Prague	1372 1945 1960s 1990	Founded for a Slavonic Benedictine order as requested by Charles IV Almost destroyed by an Allied fire-bomb Church of Our Lady (part of the monastery) has twin spires added Reconstruction of the monastery began
New Town Hall *Majority of roof not Gothic, east wing unknown*	Karlovo námestí 23, Nové Mesto, Prague	1377 15th c 1559 1722-1725	Records mention the building, but not much of it remained Construction of portions, including the tower Lightning strike causes a fire, west and north wing built in Renaissance style and the east wing renovated Roof of the tower rebuilt
Church of Our Lady of the Snows *Roof not original*	Jungmannovo námestí 18, Nové Mesto, Prague	1397 1422 1566 17th c	Founded, done by Peter Parler Unknown damages to the building Roof and temple dome fell down Reconstruction after years of negligence and significant damage, including the collapse of a choir arch

Jindrisska Tower *Roof not original*	Jindrisska 1, Nové Mesto, Prague	1472–1476 1745 1870s 2002	Bell tower is built in Gothic style A major fire destroys much of the building, and it is rebuilt in Baroque style Rebuilt in Gothic style by Mocker Reconstruction
Bohemia, excluding Prague			
St James Church	Kutná Hora, Central Bohemia	1330 Currently	Constructed, late Gothic style Closed to the public
St Barbara's Church	Kutná Hora, Central Bohemia	14th c. 1388 1420 – 1482 1482 1588 - 1884 1905	Peter Parler likely the co-author of the draft design Construction began, the first architect likely Johann Parler Hussite wars interrupt construction Works restart under Matěj Rejsek and Benedikt Rejt Construction halted Completed

Blatná Castle	Blatná, Southern Bohemia	13th c. Late 14th c. 1520 – 1530 Unknown	Constructed Moat built Benedikt Rejt adds buildings to the castle Portions changed to Renaissance style
Karlstejn Castle	Karlstejn, Central Bohemia	1348	Founded, likely started by Matthias of Arras
St. Bartholomew Cathedral	Kolin, Central Bohemian	Late 13th c., 1360 - 1378	Construction, late Gothic style Chancel built, done by Peter Parler
The Church of St Nicholas	Louny, Northern Bohemia	Unknown 1517 1519 - 1538 Post 1534 End of 19th c	Constructed Fire destroys much of the church except the tower Benedikt Rejt rebuilds the church in late Gothic style, noteworthy is the triple nave Benedikt Rejt is buried in the church Rebuilt in Gothic style

4 St Anne's Church

St Anne's Church is one of the few structures with an original Gothic roof truss in Prague. As it is the only one that was accessible, it is the focus of this thesis. The history of it is reviewed, followed by the geometry of the roof, and loading. Methodology for working with historic wood structures is described, followed by analysis of the roof structure. First and second order results are compared using FINE software. Areas of the roof structure with a different geometry or damages are examined, and conclusions on analysis methods and the roof capacity are made.

4.1 History [5]

927 Church built by St Wenceslas on the site (known as Prague Crossroads) of the current church, who dedicates it to St Lawrence. There are no remains of this church.

1100 A Romanesque rotunda was built, still dedicated to St Lawrence, the foundations of which are now part of St Anne's Church

1312 Knights Templar settles and expands the church

1313 – 1330 Nuns of the Order of St Dominic and St Anne beneath Petřín purchase the church and monastery, the later being called St Anne's Convent. The church is reconstructed and expanded, and the nave and presbytery are built in Gothic style. The walls and roof are from this construction

1676 Baroque alterations, including to the choir loft above the rear of the nave.

1782 Emperor Joseph II dissolved the convent and the Church of St Lawrence was deconsecrated. The convent was turned into dwellings and the church was used as a storehouse for coaches and joinery products.

1816 Taken over by Schönfeld's (later Haas') printing works

19th c. Masonry Gothic vaults removed and multiple floors were built into the church for storing paper

1970's Printing works leave the building, and the National Theatre occupies it and uses it for storing their archives

1980's-90's Alterations were done by the Vize '97 Foundation. "Inappropriate additions" were removed, such as the inserted wooden floors. Flooring lay with under-floor heating, interior lighting and sound equipment installed. Re-roofing, a functional conversion to the choir loft, and a new façade were added.

4.2 Geometry

The roof of St Anne's Church is very steep, at 64° (see Figure 2). One end of the roof is a masonry wall, while the other has 10 timber beams joining at the peak of the roof, forming the shape of half of an inverted hexagon (see Figure 3).

Figure 2 External view of the south side of St Anne's Church

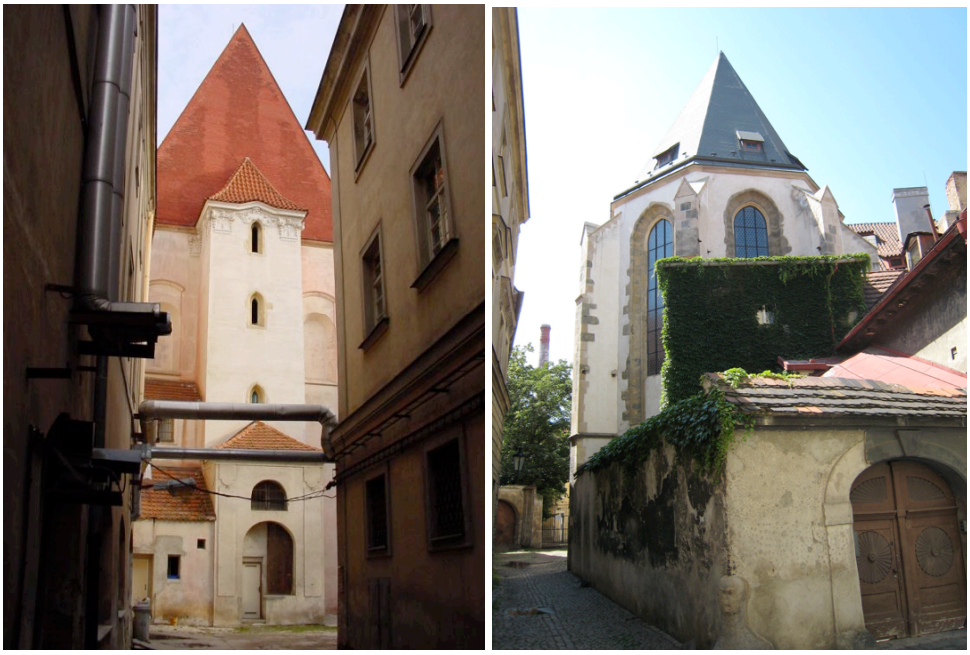

Figure 3 View of the west and east sides of the church

The roof structure of St Anne's Church consists of 48 trusses spaced at 0.84 m. A tension chord of new glulam timber is present at every second truss. The trusses that do not have this tension member still have a portion of it that extends out far enough to support the walkway that goes around the entire roof. This can be seen in Figure 4 below.

The two long members supporting the roof covering of each truss are 20 cm by 20 cm. The tension members (on alternating trusses) are 20 cm by 25 cm (width by height), and all other members of the truss are 12 cm by 20 cm.

The roof covering consists of two layers of 20 mm thick boards, which are nailed directly onto the main diagonal chords of the truss. These two layers are orientated at a 45° angle from the horizontal, and perpendicular to each other. This is a very stiff configuration; as each board is long enough to be attached to multiple trusses, the average board spans three trusses. Because they are on an angle, stiff triangular elements are produced.

Figure 4 Views of the roof structure of St Anne's Church, the first looking to the south, the second to the north

The glulam tension members on the bottom of every other truss and the roofing boards were added in the alterations done in the 1980's and 90's. As the entire truss rests on the glulam member, jacks were likely used to lift each truss and put in the member.

On each truss, roman numerals can be seen on at least two members. The numbering starts at the west side of the church (the side with the masonry wall). The trusses were intentionally placed in a specific order. Two members marked with roman numerals are shown in Figure 5.

Figure 5 Roman numerals on the members done by the carpenter

The joints were constructed using square wooden dowels with a cross section of 2 cm by 2 cm. The members at all joints are cut so that approximately half of each member is removed. At interior joints of the truss, both members are continuous past the joint, which is made possible by cutting back the member. The joints, in addition to the original wooden dowels, have had two steel bolts of diameter 12 mm added (see Figure 6).

Figure 6 Joint with the members cut back and continuing past each other (left picture), and wooden dowels visible (both pictures)

The following AutoCAD drawings illustrate the overall geometry of the church.

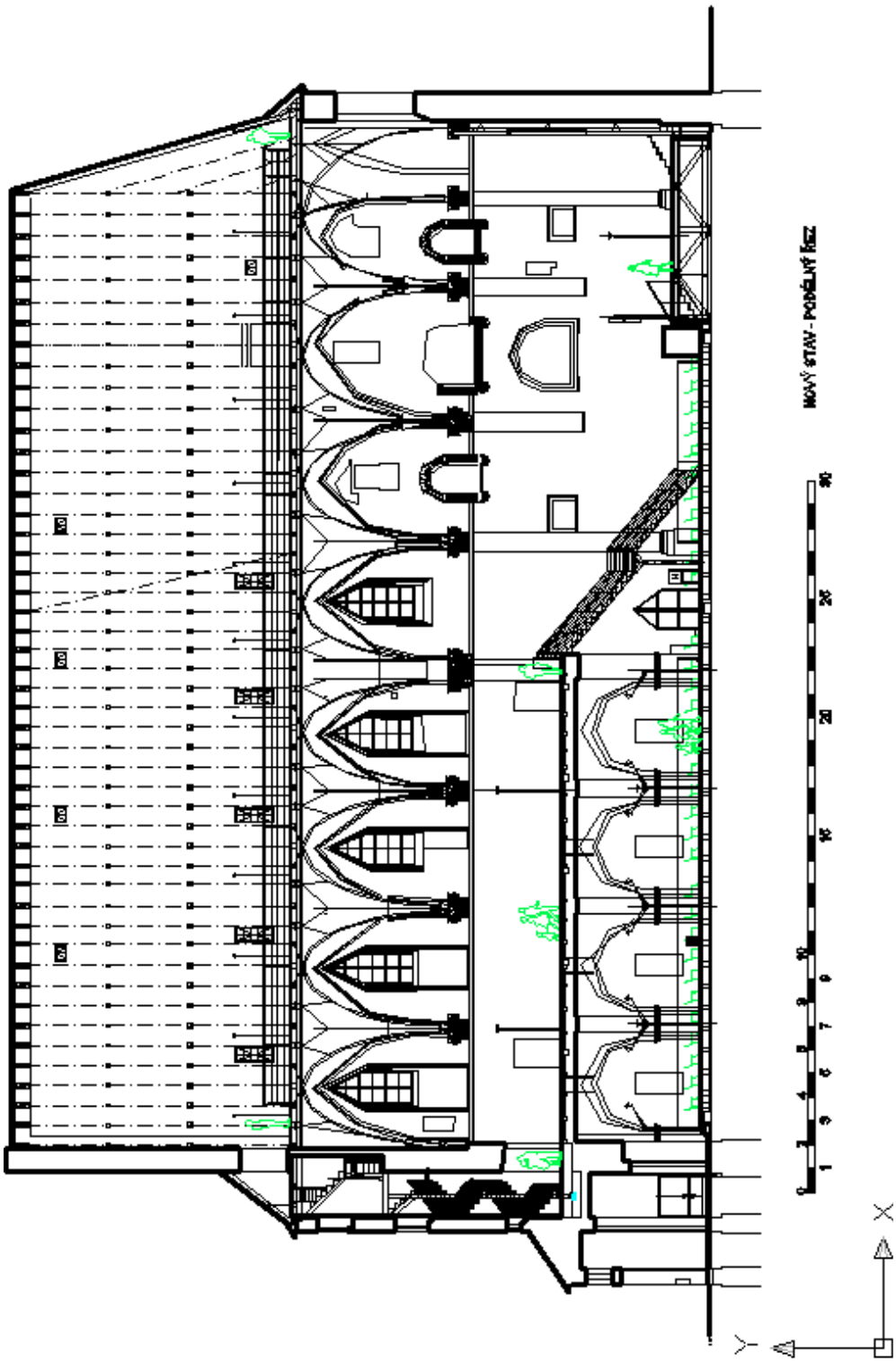

Figure 7 Elevation view of the south side of St Anne's Church

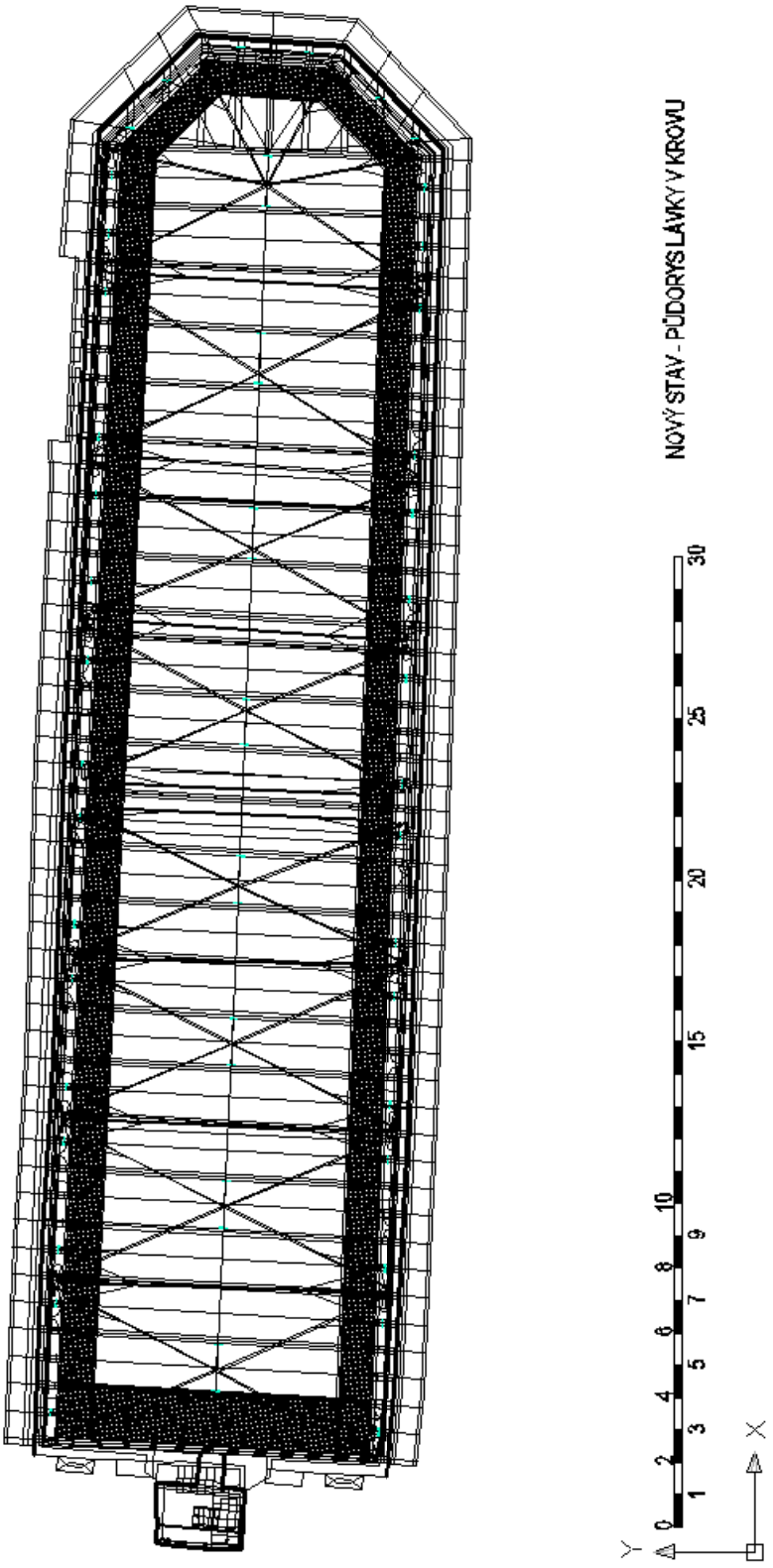

Figure 8 Plan view of St Anne's Church, the x-axis points east

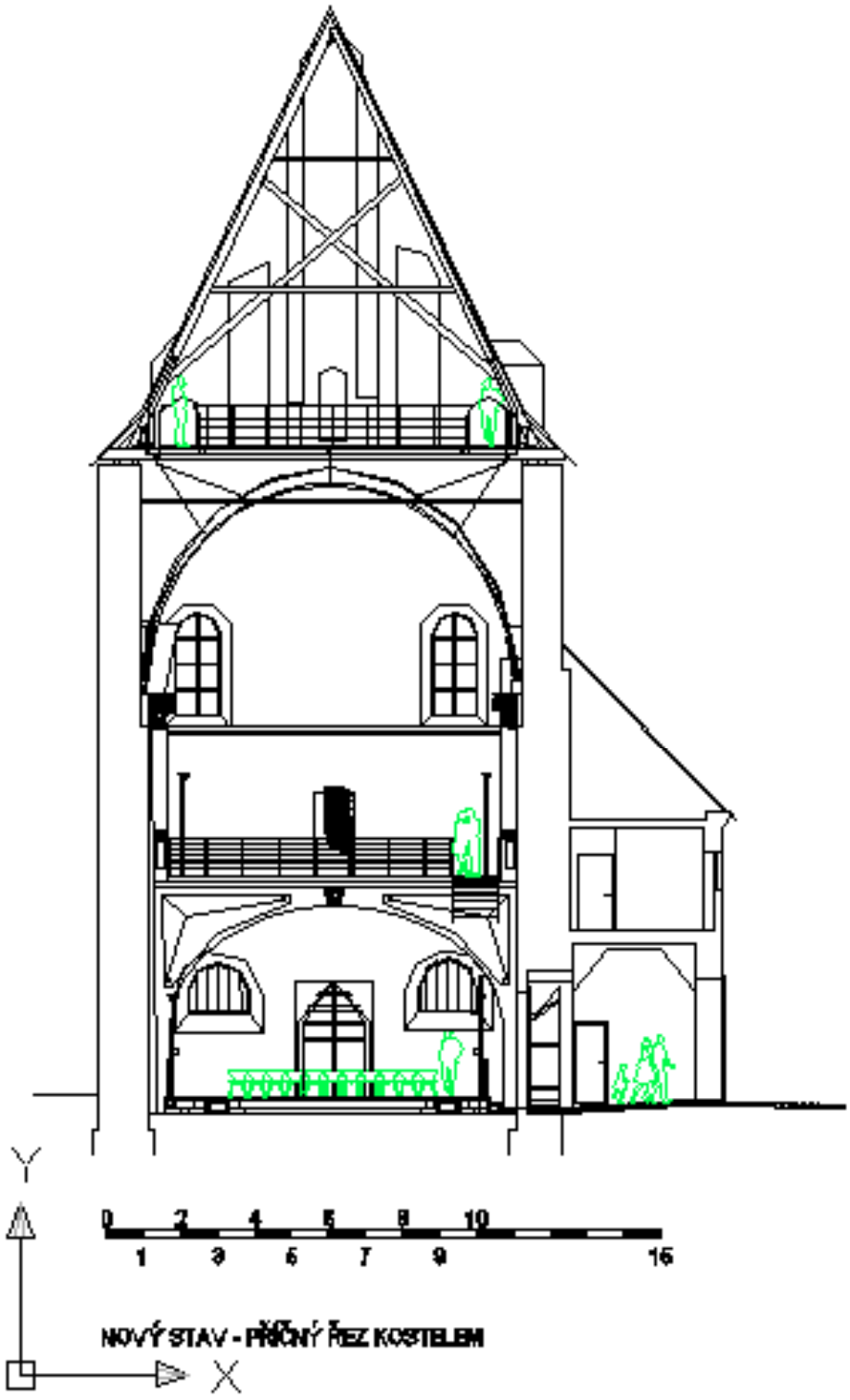

Figure 9 Cross-section of St Anne's Church, the x-axis points north

4.3 Loading

The load calculation is based on the Eurocode 1: Actions on structures. [6] "Appendix A: Loading calculation for St Anne's Church" has a detailed calculation of the loading.

4.3.1 Probability of exceedance

The Eurocode considers a return period of 50 years for new constructions. It is recognized that St Anne's Church will be standing for centuries if it is properly maintained. A life of 500 years is being considered as the best use for the return period.

4.3.2 Dead load (DL)

There are two layers of wood planks, each of thickness 20 mm directly on top of the trusses. The roof is covered with shingles. However, it is plausible that standard clay tiles are used in the future, so the roof capacity is checked both with and without these tiles, which weigh = 100kg/m^2.

- DL = 0.12 kPa, for the existing roofing shingles
- DL = 1.10 kPa, for standard clay tiles

4.3.3 Live load (LL)

The live loads are as follows:

- q_k = 0.4 kN/m^2 or a point load of Q_k = 1 kN

4.3.4 Snow Load (SL)

The slope of the roof is high enough that no snow load needs to be considered.

4.3.5 Wind Load (WL)

4.3.5.1 External pressure

Two cases are considered, where the wind direction is perpendicular to a longitudinal wall, then to an end wall.

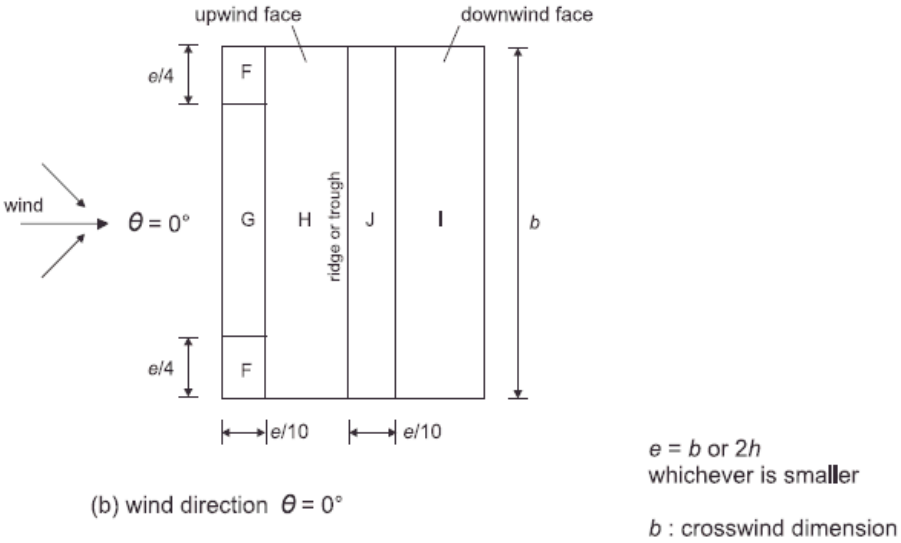

Figure 10 W_e for a 1/500 return period at wind direction θ = 0° (Pitch angle = 64 °), coefficient e = {smaller of 2h = 60, or b = 44m} = 44m

The resulting pressure, W_e, for each zone shown in Figure 10 is shown in Table 2.

Table 2 External coefficient ($c_{pe,10}$) at wind direction θ = 0°

Zone	**F**	**G**	**H**	**I**	**J**
$c_{pe,10}$	0.727	0.727	0.727	-0.200	-0.300
W_e (kPa)	0.530	0.530	0.530	-0.146	-0.219

Similarly, for the other wind load case, the zones and corresponding pressures are shown in Figure 11 and Table 3.

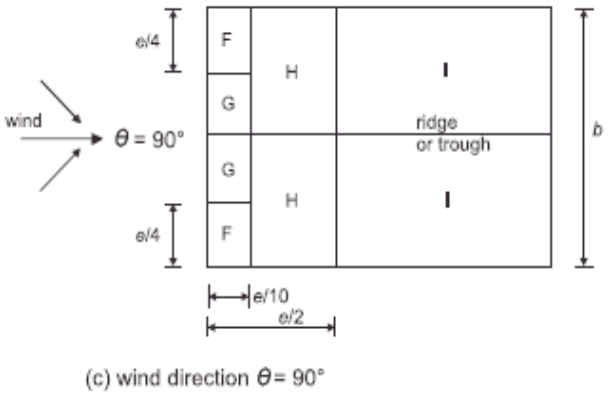

(c) wind direction θ = 90°

Figure 11 W_e for a 1/500 return period at wind direction θ =90º (Pitch angle = 64 º), coefficient e = {smaller of 2h = 60, or b = 12.6} = 12.6 m

Table 3 External coefficient ($c_{pe,10}$) at wind direction θ = 90º

Zone	**F**	**G**	**H**	**I**
$c_{pe,10}$	-1.100	-1.200	-0.800	-0.500
W_e (kPa)	-0.802	-0.875	-0.583	-0.365

4.3.5.2 Internal pressure

There is no dominant face to the building. The internal pressure coefficient shall be taken as 0.200 or -0.300 whatever one is critical. Both W_i = -0.098 kPa or 0.146 kPa should be considered.

4.4 Load Combinations [6]

The following load combinations follow this notation:

DL = dead load, LL = live load, WL = wind load

Ultimate limit states:

$$1.35\ DL + 1.5\ LL \qquad \text{[Eq. 1]}$$

$$1.35\ DL + 1.5\ LL + 0.75\ WL\ (\text{pressure}) \qquad \text{[Eq. 2]}$$

$$1.35\ DL + 1.5\ WL\ (pressure) \quad [Eq.\ 3]$$

$$1.00\ DL + 1.5\ WL\ (suction) \quad [Eq.\ 4]$$

Serviceability limit states:

$$DL + LL \quad [Eq.\ 5]$$

$$DL + WL \quad [Eq.\ 6]$$

5 Evaluation and analysis of old timber structures

The following is a method for evaluating the actual load-bearing performance of an ancient timber construction using a non-destructive approach, as recommended by A. Ceccotti in the paper "Evaluation and analysis of the old timber structures" [1].

Evaluation is important as the material characteristics and geometry of the structure must be determined as accurately as possible. Table 4 describes what is done in the evaluation phase.

Table 4 Evaluation of the structure, done by a wood technologist

Evaluation
Decay detection: residual cross section dimensions, *b* and *h*
Strength grading, in situ: timber grade
Anticipated strength: $f_{m,k(5\%)}$
Uncertainties: γ_M, material safety coefficient

The wood technologist evaluates biological decay across the member cross section and along the member, provides cross section dimensions for design, and performs in-situ grading using the applicable grading rules. The structural engineer then uses this data for the calculations, as shown in Table 5.

Table 5 Analysis of the structure, done by a structural engineer

Analysis (Structural engineer)
Actions (loads, q_k)
Structural scheme for calculations: q_k to M_k
Stresses on elements: M_k to $\sigma_{m,k}$
Uncertainties: γ_f, action side safety coefficient

Analysis is begun using a simple structural scheme, and then accounting for the actual restraints and actual mechanical behavior of the materials as much as possible increases accuracy of the analysis. Possibilities include semi-rigid behavior of joints (including

slip) and structural deformations and disorders. Anisotropy or second order analysis is modeled only when the complexity requires it.

This methodology is followed for this thesis, except that second order analysis is performed regardless of whether complexity requires it.

6 The effect of age on material properties of timber

There is no real evidence that long lasting pre-loading of timber or timber structures to a limited load level has produced any damage. [7] At higher loads, the timber loses strength as the duration and magnitude of the load increases. Figure 12 below shows the value of k_1, a modification factor, which are used in the Eurocode as a result of the duration of the peak load. It is important to note that the duration of the peak load is the same for a structure with a 500-year design life as that for one with a 50-year design life. The loading is higher for a structure that will be standing longer, which is accounted for by the return period, but the peak load on each structure will have a similar duration, which is accounted for by the sampling period.

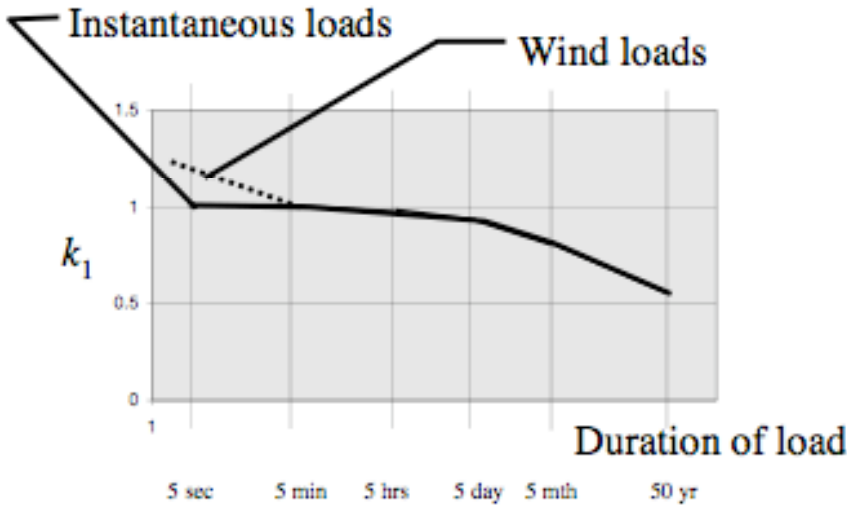

Figure 12 The effect of load duration on strength, which is multiplied by factor k_1 [8]

The strength of a timber structure is not affected by age, and the structural condition of many historic timber structures is a testament to this. Given this, and as no testing has been performed, the material properties of new spruce are used. The modification factor k_1 is used according to the proper loading duration.

7 Timber strength classification

7.1 Service class [15]

The service class is used for assigning strength values and for calculating deformations, using set environmental conditions. Service class 1 is for an environment with a temperature of 20°C and a relative humidity only exceeding 65% for a few weeks per year. For most softwood species, the average moisture content will not exceed 12%.

7.1.1 Service class and St Anne's Church

St Anne's Church meets service class 1, so it is used. The trusses are softwood, spruce, so the material properties used are chosen with consideration to the moisture content likely not exceeding 12%.

7.2 Timber strength classification [9]

The FINE programs require the strength classification of the timber to be specified as grade S7, S10, or S13. This is in accordance with the German classification system for sawn timber set out in DIN 4074-1 (2004). See Appendix B for the requirements that need to be met for the three grades. Grades S7, S10, and S13 correspond to strength classes C16, C24, and C30, respectively, according to the EN 338 classification system.

7.2.1 Timber strength classification of St Anne's Church

The majority of the roof trusses of St Anne's Church meet grade S13. The standard truss analyzed uses this grade in the FINE program. Further models examining specific trusses account for observed damages and deteriorations and use the applicable grade determined from inspection.

8 Second order theory, geometrical nonlinearities, linear stability and FINE

Figure 13 below illustrates the force deflection relationship for different initial conditions and curvature equations.

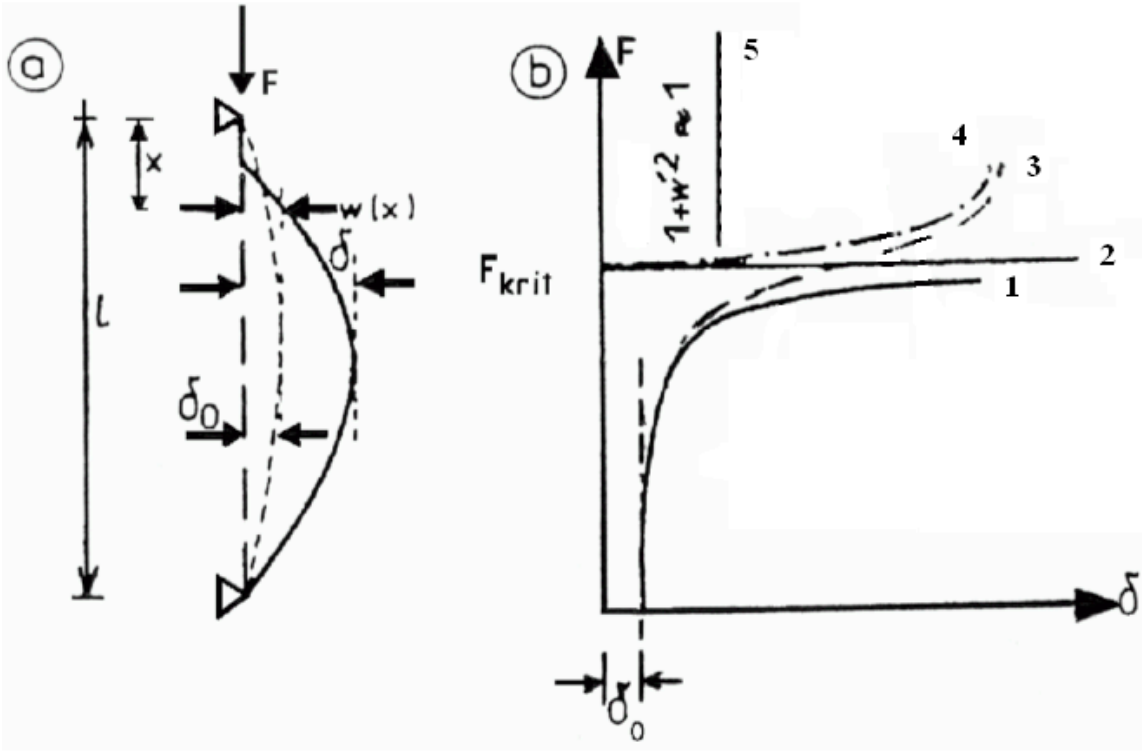

Figure 13: Stability and critical loading for different curvature equations and initial deflections [10]

In Figure 13, part b above, lines 1 and 3 represent columns with an initial deflection $w_0(x)$, described at a location as δ_0. Lines 2 and 4 represent ideal columns that are perfectly prismatic and homogeneous.

Curves 3 and 4 on Figure 13 represent geometric nonlinear analysis, which uses the following equation for curvature

$$\frac{1}{\rho} = -\frac{w''}{\left(1 + w'^2\right)^{3/2}} \qquad \text{[Eq. 7]}$$

Second order theory is a simplification of geometric nonlinear analysis. For second order theory the term *w'* is assumed to be small enough that it has no effect, and the equation becomes

$$\frac{1}{\rho} \approx -w'' \qquad \text{[Eq. 8]}$$

This equation is used for lines 1 and 2. Second order analysis is characterized by [10]:

- A linear relationship between deformations and strains
- Distribution of axial forces in the deformed shape is the same as in the undeformed shape
- Static equilibrium is on the deformed shape

Line 5 corresponds to the limit where $(1+w'^2)$ stops being approximately 1, and the approximate equation for curvature (and therefore second order analysis) can no longer be used [11].

If the difference between the deflections from first and second order analysis differs by 15% or more, the design is inefficient and unstable.

8.1 An ideal column [11]

Line 2 on Figure 13 is that of an ideal column using the approximate equation for curvature:

$$\frac{1}{\rho} \approx -w'' \qquad \text{[Eq. 8]}$$

$$w'' = \frac{M}{EI} = \frac{-Pw}{EI} \qquad \text{[Eq. 9]}$$

This differential equation is solved for, providing the critical buckling load:

$$P_{cr} = \frac{\pi^2 EI}{l^2} \qquad \text{[Eq. 10]}$$

This derivation is shown in "Appendix C: Derivation of equations." Because equation 8 was used instead of equation 7, it is not possible to solve for the failure at deflection so it is unknown. When $P < P_{cr}$ the equation describing the shape of the column cannot be satisfied, and therefore, the column is straight.

In FINE, it is important to apply a small initial deflection by means of a moment, lateral load, eccentric load, or displacement to the member so that the member does not behave as an ideal column.

8.2 Column with an initial deformation [10]

As no column is perfect in terms of geometry or material, a column (Line 1 on Figure 13) is examined with an initial deformation given as

$$w_0(x) = e_0 \sin\left(\frac{\pi x}{l}\right) \qquad \text{[Eq. 11]}$$

Modifying equation 9 to account for the initial deflection given by equation 11:

$$(w(x) - w_0(x))'' = \frac{-Pw(x)}{EI} \qquad \text{[Eq. 12]}$$

This differential equation is solved for, providing the second order deflections:

$$w = \frac{w_0}{1 - \frac{P}{P_{cr}}} \qquad \text{[Eq. 13]}$$

The derivation is shown in "Appendix C: Derivation of equations." Equation 13 represents line 1 on Figure 13, and is the equation used by FINE to calculate second order deflections. The deflection w_0 is from first order analysis.

Two limits are present for preventing buckling of a member. In the Czech Republic, the following limit is used:

$$P < (1/4)\, P_{cr} \qquad \text{[Eq. 14]}$$

And elsewhere in Europe, the following limit is used:

$$P < (1/10)\, P_{cr} \qquad \text{[Eq. 15]}$$

As the second order deflection varies with the first order deflection and load to critical load ratio, these limits from equation 14 and equation 15 can be put into equation 13. Limits for comparing the deflections of first and second order analysis are produced. Corresponding to the buckling check for the Czech Republic:

$$w < (4/3)\, w_0 \qquad \text{[Eq. 16]}$$

And corresponding to the buckling check for elsewhere in Europe:

$$w < (10/9)\, w_0 \qquad \text{[Eq. 17]}$$

These equations are summarized in Table 6 below.

Table 6 Limits for comparing first and second order results to prevent instability

Limit	**Stability criteria**
$P < (1/10)\, P_{cr}$	$w < (10/9)\, w_0$
$P < (1/4)\, P_{cr}$	$w < (4/3)\, w_0$

Previously, it was established that the deflections from first and second order analysis must not differ by more than 15%, or the design will be inefficient and unstable. The two limits for the buckling load provide two more guidelines for comparing first and second order analysis, based on buckling criteria. However, if the first and second order deflections must not differ by more than 15%, the limit $w < (4/3)\, w_0$ cannot be used because it exceeds this criteria.

These buckling limits, intended for each specific member, can be applied to the entire structure or the portion modeled in the finite element program to check for instability.

8.3 Linear Stability [12]

Linear stability determines the critical value of the ideal load as a multiple of the current load when instability is reached.

The axial force causing buckling is estimated to be a constant (α) multiplied by the current load, that is, the buckling load is $\{P(\alpha)\}$. Given these axial forces, it is possible to calculate the stiffness matrix, $[S(\alpha)]$, where the elements of this matrix are a function of α. Using the equation:

$$[S(\alpha)]\ \{D\} = \{F\} \qquad \text{[Eq. 18]}$$

If α corresponds to the critical buckling value, then the structure can acquire additional displacements $\{\delta D\}$ without applying any more forces. The equation becomes

$$[S(\alpha)]\ \{\delta D\} = 0 \qquad \text{[Eq. 19]}$$

For a nontrivial solution to exist, the stiffness matrix $[S(\alpha)]$ must be singular, that is, the determinant

$$|S(\alpha)| = 0 \qquad \text{[Eq. 20]}$$

There are multiple solutions to this equation, each value of α obtained corresponds to a different mode of failure. The lowest value of α corresponds to the collapse load.

9 Eurocode and the reliability index

By applying modification factors and load factors, and taking into account the return period and sampling duration (for wind load), the Eurocode employs a reliability index. This is a measure of the number of standard deviations between the effect of loading and resistance probability distribution functions, and is known as reliability based design. The reliability index establishes a set level of safety for the structure and all elements in it, and is shown in Figure 14 below.

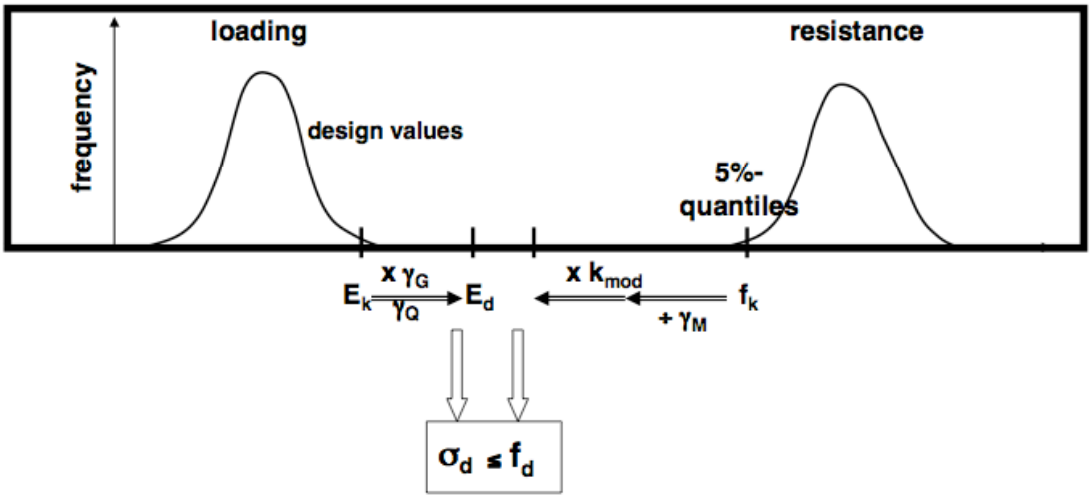

Figure 14 Probability distribution functions of the effect of loading and of the load carrying capacity [13]

For historical constructions, it is desirable to meet the reliability index that is required for new constructions by the Eurocode. However, it must be recognized that conservative equations or values may be used, often because the actual properties or behavior of the material, loading, or structure is unknown, or must be applicable to all situations. Second order analysis can more accurately represent the true state of the timber truss than the buckling equations in the Eurocode, without changing the standard deviation of the resistance probability distribution function. The same modification and material safety factors are used to employ the same reliability index. However, despite the second order results being more accurate, it is not possible to compare the levels of safety employed by the different limits for comparing first and second order deflections. No conclusions can be made on the reliability index employed for each limit.

10 Structural analysis: FINE and St Anne's Church

Two FINE programs are used, FIN 2D, and FIN 3D. These programs use beam elements only, with cubic shape functions. No other elements are possible.

A typical truss is modeled in FIN 2D, and the capacity and failure loading determined. The trusses in the middle of the church with a different geometry are then modeled using FIN 3D. However, as FINE has no plate elements, the roofing material cannot be modeled so lateral deflection of the truss is not permitted for the members attached to the roofing boards. Two-dimensional models with reduced cross sections or missing members are used to simulate observed damages and deteriorations.

For typical joints, pinned connections are used in the FINE programs. However, at interior joints, the members are continuous past the joint. The following is a calculation of the stiffness of the joint, with the purpose of determining the spring constant to use in FINE.

10.1 Geometry of interior truss joints

On interior joints on the truss, both members are cut back so that they fit into each other. On Figure 15 below, joints 26, 27, and 28 are of this nature. The members crossing a joint are both continuous.

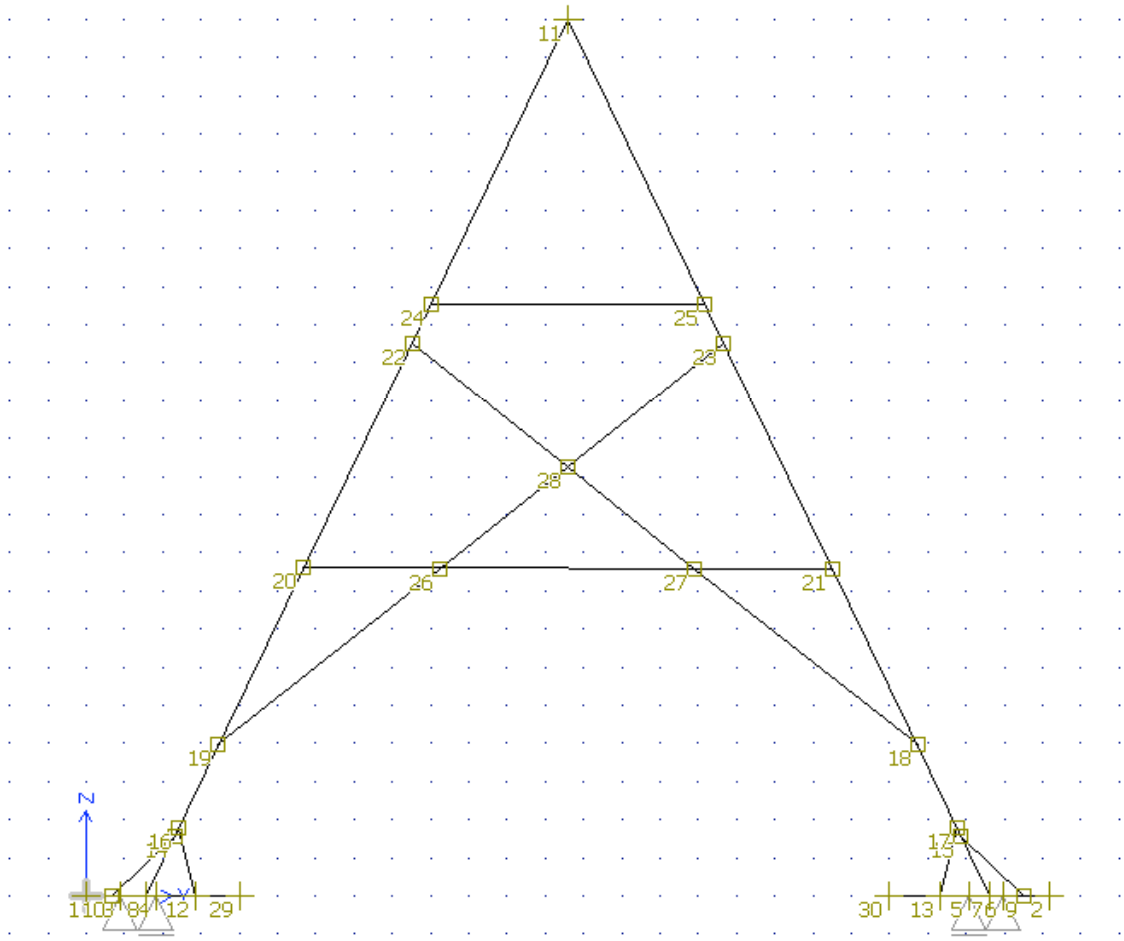

Figure 15 Standard truss of St Anne's Church

In Figure 16 below, one member is shown how it is cut back at a joint. Rotation of the other member causes two couples, indicated by the blue and red arrows.

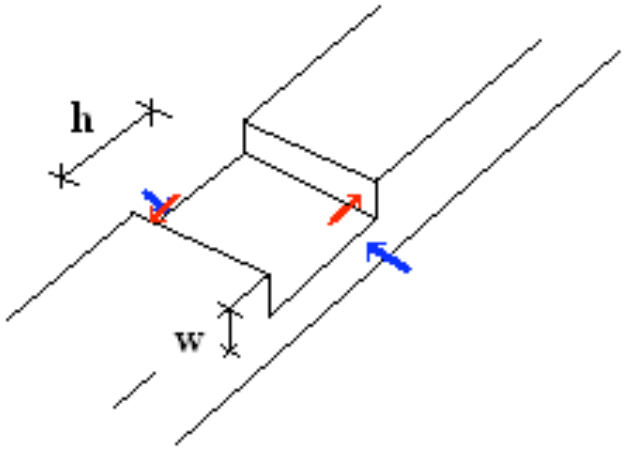

Figure 16 Member of dimension 20 cm by 12 cm, cut out at the joint

The members do not cross at a 90° angle, but at a 102.8° angle, resulting in h = 205.1mm. When one member is rotated, it is resisted at the locations indicated by the blue and red arrows in the previous figure. These forces are all equal, so only one pair will be examined, and then the second will be accounted for later.

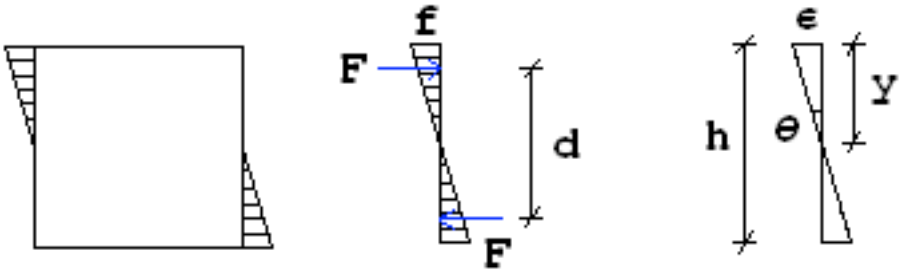

Figure 17 Approximate the strain as linear and perpendicular to the surface of the beam

As seen in Figure 17, the resistance of the wood is assumed to be perpendicular to the surface, which is an approximation assuming small displacements. The stiffness of the joint is determined:

$$F = \frac{fwy}{2} \quad \text{[Eq. 21]}$$

$$d = \frac{2}{3} h \quad \text{[Eq. 22]}$$

$$\theta = \frac{\epsilon}{y} \quad \text{[Eq. 23]}$$

$$y = \frac{h}{2} \quad \text{[Eq. 24]}$$

$$f = E\epsilon \quad \text{[Eq. 25]}$$

$$M = k\theta \quad \text{[Eq. 26]}$$

$$M = Fd \quad \text{[Eq. 27]}$$

$$k\theta = Fd \quad \text{[Eq. 28]}$$

$$k \frac{\epsilon}{y} = \frac{fwy}{2} d \qquad \text{[Eq. 29]}$$

$$k\epsilon = \frac{fw \left(\frac{h}{2}\right)^2 \left(\frac{2}{3}\right) h}{2} \qquad \text{[Eq. 30]}$$

$$\epsilon k = \frac{Eewh^3}{12} \qquad \text{[Eq. 31]}$$

$$k = \frac{Ewh^3}{12} \qquad \text{[Eq. 32]}$$

Equation 32 is solved for, where E = 0.077 x 10 000 MPa to account for the modulus perpendicular to the grain, w = 60 mm, and h = 205.1 mm. There are two couples (shown in Figure 16), so the stiffness calculated in equation 32 is multiplied by two. The resulting joint stiffness is 66.43 MNm / rad.

The stiffness of the joint is compared to the stiffness of the continuous member. Joint 28 of Figure 15 is examined. A unit rotation is applied to one end of the beam, as seen in Figure 18.

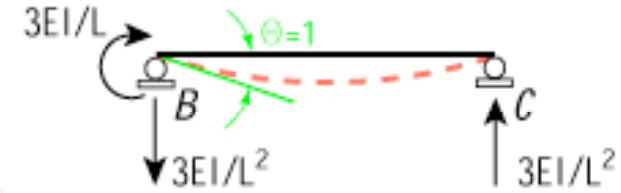

Figure 18 Forces resulting from a unit rotation on a beam

If one of the two members crossing each other has a unit rotation applied, the other member must follow. The rotational stiffnesses provided by the two portions of this member are:

$$k_1 = \frac{3\,EI}{l_1} \qquad \text{[Eq. 33]}$$

$$k_2 = \frac{3\,EI}{l_2} \qquad \text{[Eq. 34]}$$

The length l_1 = 2608 mm, length l_2 = 2127 mm, E = 10 000 MPa and I = 8 x 10^7 mm^4. Solving equation 33 and equation 34 and adding the results together produces a stiffness of 2.05 MNm / rad.

The stiffness of the joint is considerably larger than that of the members. The effect of the stiffness of the joint on the entire connection is:

$$\frac{1}{k_{total}} = \frac{1}{k_{joints}} + \frac{1}{k_{members}} \qquad \text{[Eq. 35]}$$

Equation 35 is solved using the joint and member stiffnesses 66.43 MNm / rad and 2.05 MNm / rad, respectively. The total stiffness is 1.99 MNm / rad.

This result shows that, assuming a perfectly cut joint, the behavior will be very close to a fixed connection. However, variability must be present between joints, and small gaps present between members. To account for variability, three models are considered in the FINE model of a 2D truss, using fixed, pinned, and spring connections with the spring stiffness equal to the joint stiffness previously calculated.

In all three models, both members are continuous past the joint. A fixed connection is easily input in FINE. The pinned and spring joints are modeled by first creating a relative joint (27 on Figure 19 below) on one of the intersecting members. The other member is split into two members, which are attached by a pin or a spring to this relative joint. Close to the joints, the members are divided, creating new members 12 and 31. Joints 35 and 36 are fixed to keep the members continuous. To complete the continuity of the member, a short member 32 is added from joint 35 to 36. The dimensions of members 12, 31, and 32 are adjusted for the appropriate cross section.

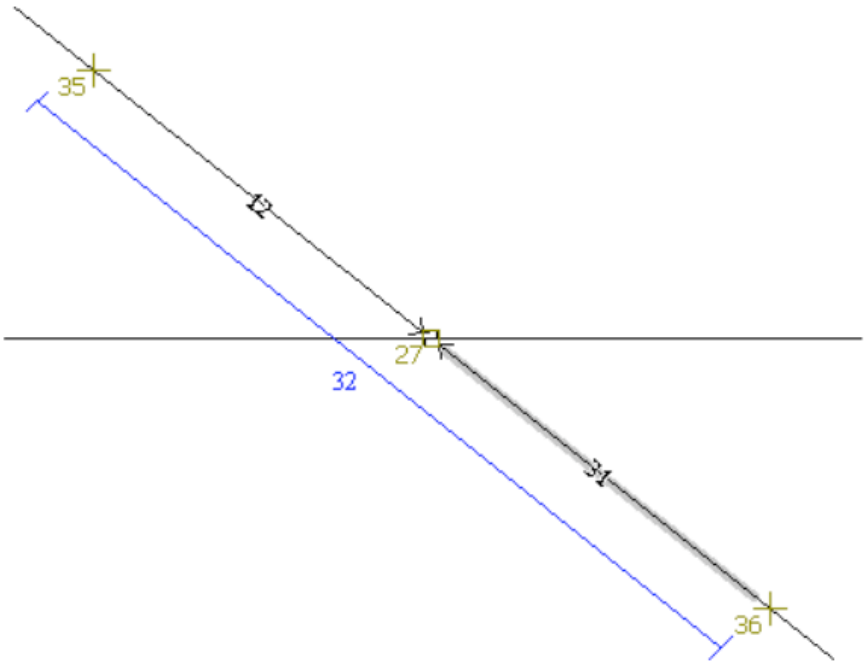

Figure 19 Schematic of the joint in FINE for a spring connection

It is possible to reduce the cross section of the members at the joint to account for material removal. However, the effect of this is minimal, and it is therefore not done.

Similar trusses with pinned, fixed, and spring joint were examined using first and second order analysis. The deformations and stresses were within 5%, indicating that the joint type in FINE is of low importance.

10.2 Analysis of a standard truss

10.2.1 Geometry

The following three figures show the geometry of the FIN 2D model. The tables following these figures in the results section reference the member and joint numbers shown on them. All joints are pinned, with the exception of joints 26, 27, and 28, which have the members passing each other, and are modeled as fixed, pinned, or springs in three separate models.

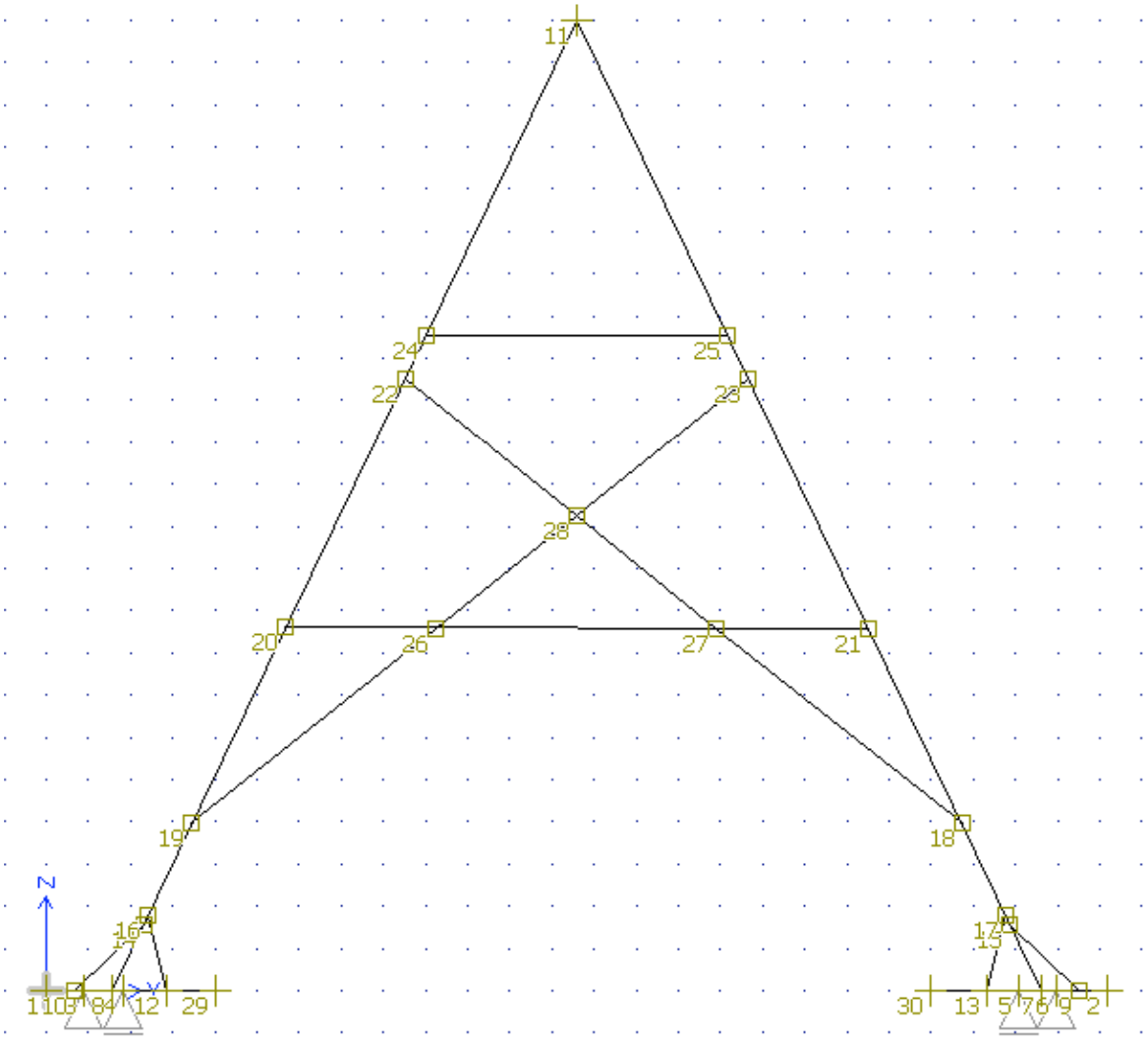

Figure 20 Joints

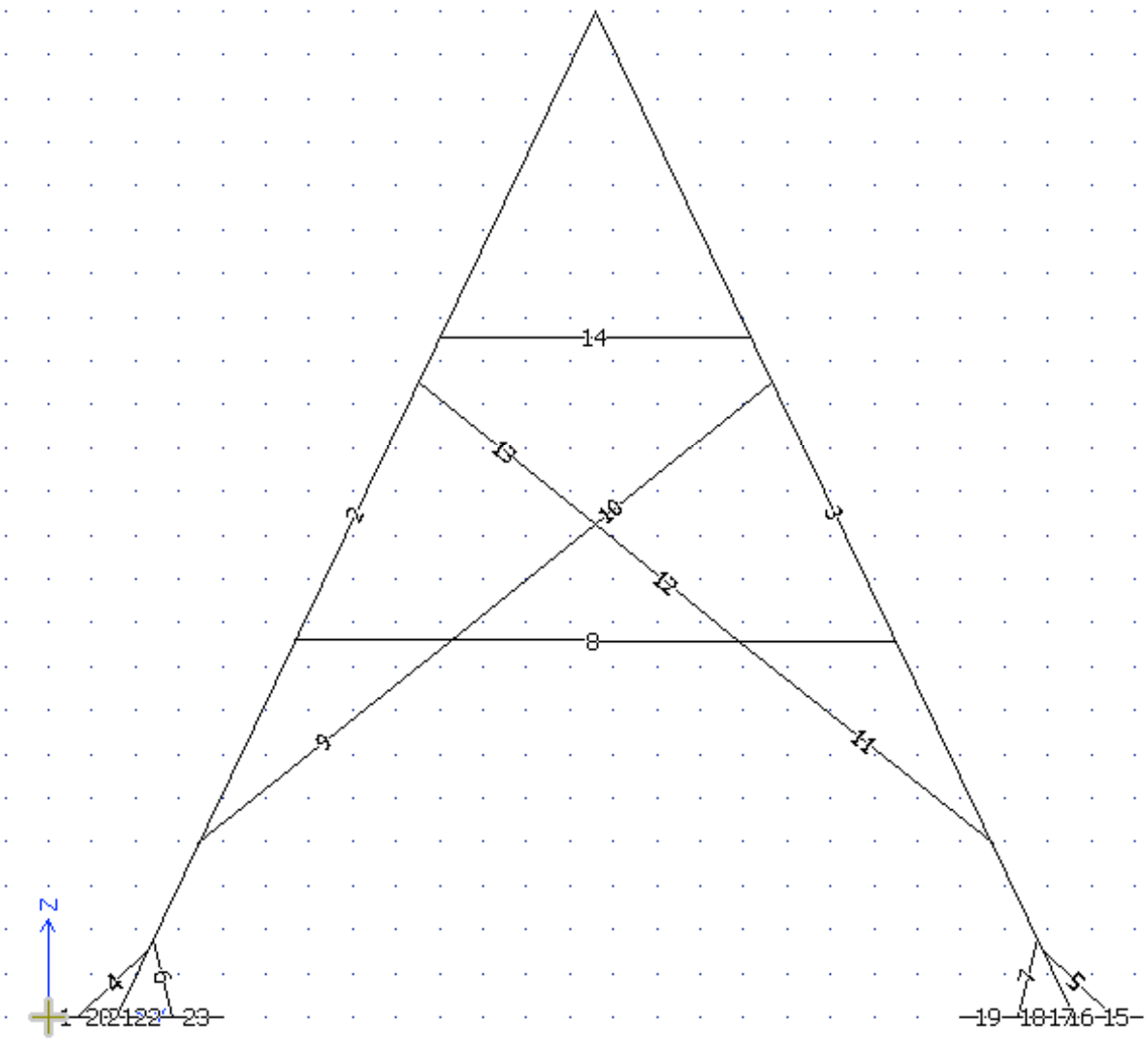

Figure 21 Members

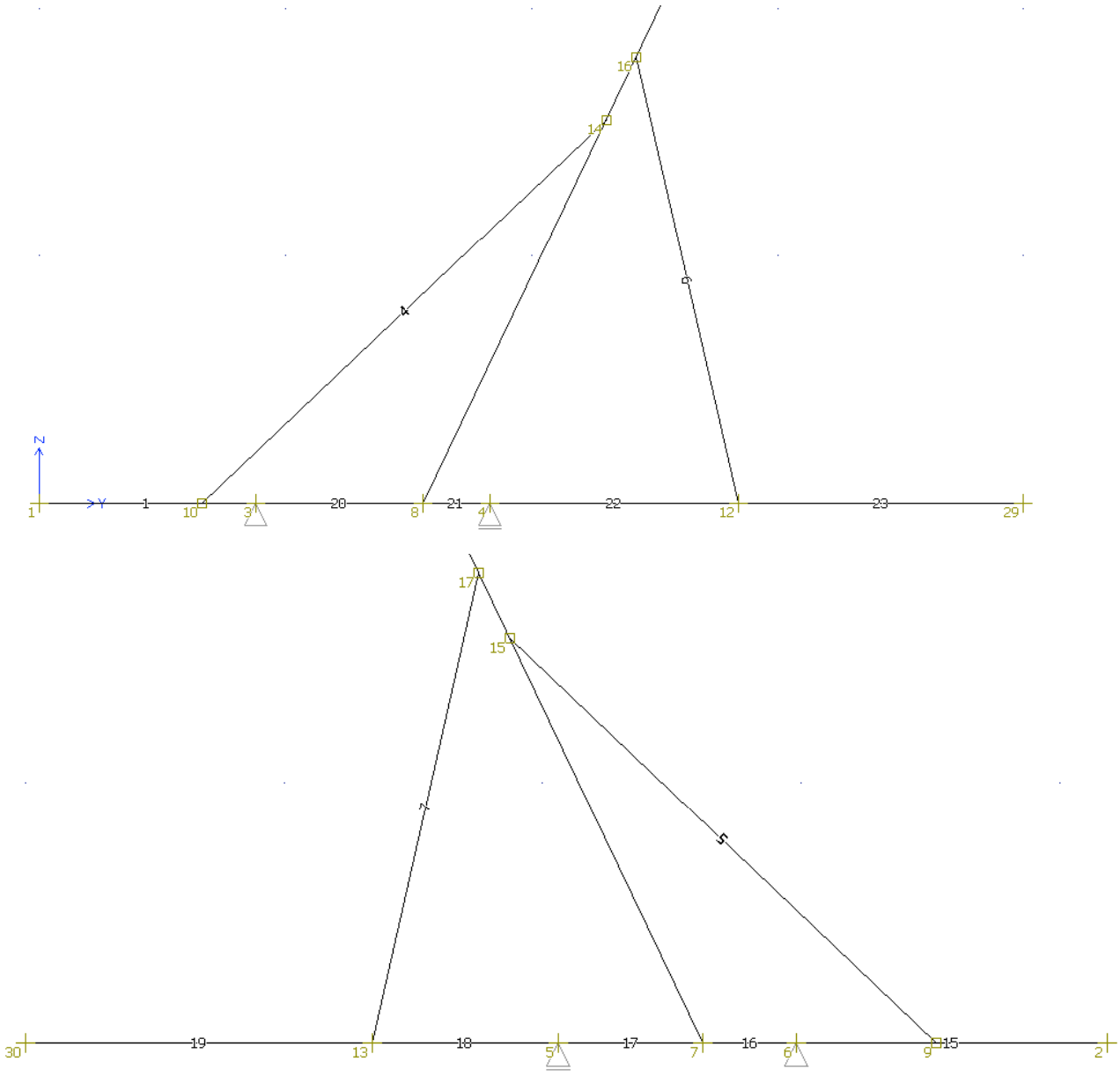

Figure 22 Node and member numbers at the supports

10.2.2 Material strengths and properties

As discussed in section 6, "The effect of age on material properties of timber," material properties of new spruce are used. However, it was not possible to obtain the European standards document EN 338, which provides material properties for European wood. Therefore, the best information available was used, which were the properties of American spruce averaged over the different subspecies, as shown in Table 7.

Table 7 Summarized Mechanical properties of American spruce at 12% relative humidity, averaged over the different subspecies [14]

Mod of rupt (kPa)	E (MPa)	Comp paral grain (kPa)	Comp perp grain (kPa)	Shear paral grain (kPa)	Tens perp grain (kPa)	Tens paral grain (kPa)
72 000	9 000	15 000*	3 100	8 000	2 400	60 000

*Property is not that of American spruce, but as recommended by Professor Kuklik

The material property: compression parallel to the grain was identified to be significantly different to that expected for European wood. Therefore, it was changed from 35 000 kPa to 15 000 kPa.

10.2.3 Loading

The following two figures show the wind load cases.

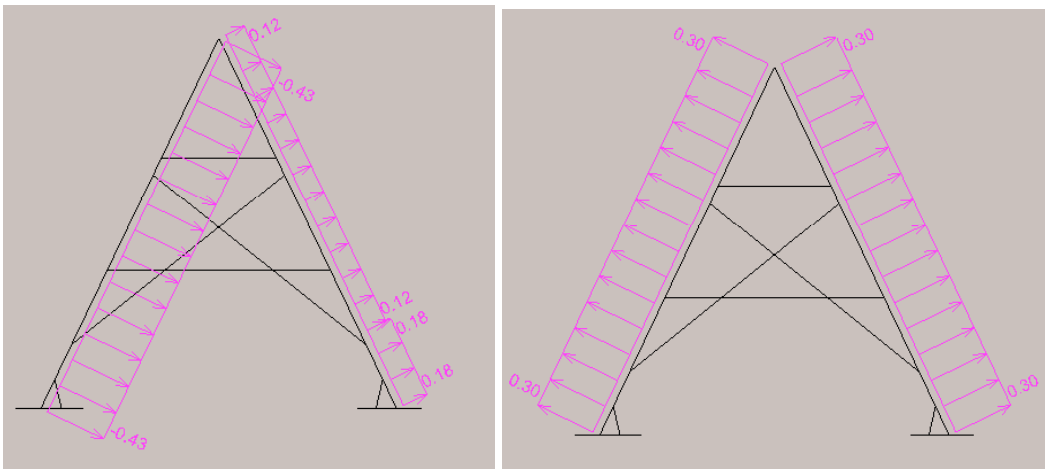

Figure 23 External wind pressure from wind load case 1 (left picture, shown in Figure 10) and wind load case 2 (right picture, shown in Figure 11)

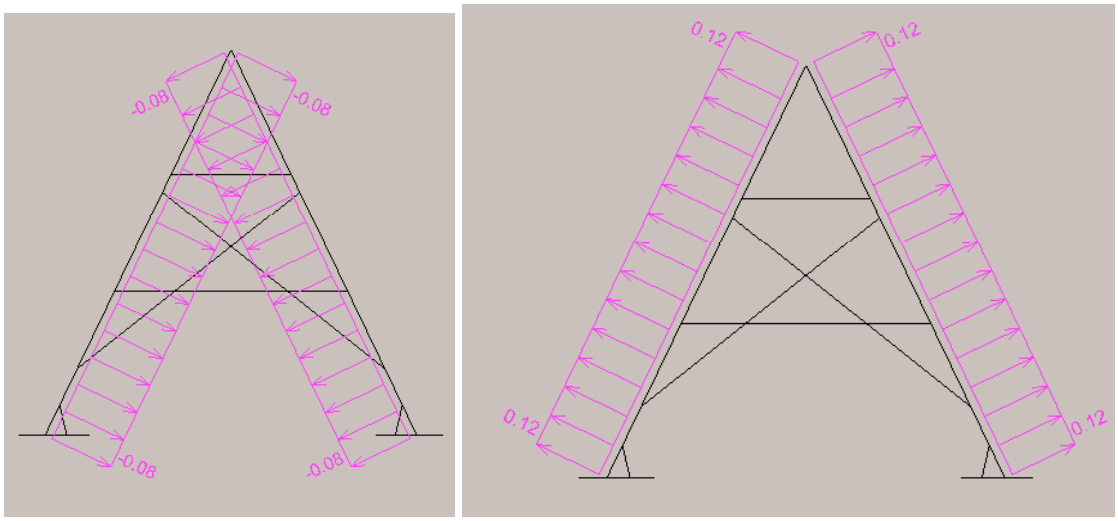

Figure 24 Internal wind pressure, suction case (left) and pressure case (right)

Four possible combinations of the case 1.35 DL +1.5 WL are considered for different wind combinations. Wind load case 1 is considered with internal suction as one case, and with internal pressure as another. Wind load case 2 is then considered with internal suction and pressure accordingly.

10.2.4 Results

Figures from FINE are provided for a visual interpretation of the results. Tables follow, from which the data is analyzed and discussed.

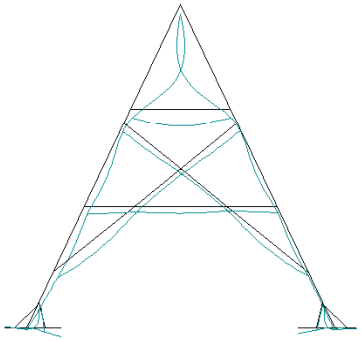

Figure 25 Deflected shape from load combination 1.35 DL + 1.5 LL

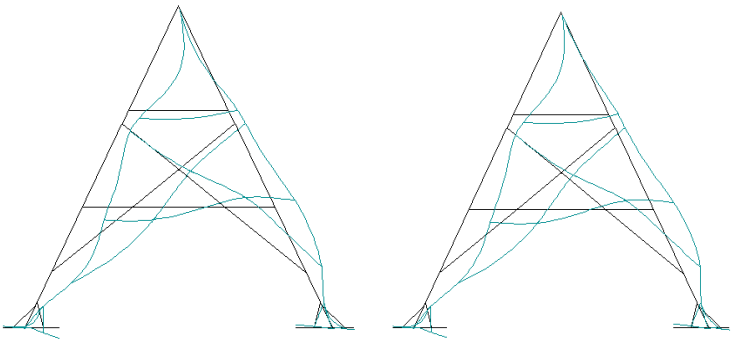

Figure 26 Deflected shape from load case 1.35 DL + 1.5 WL case 1, with internal suction (left) and internal pressure (right)

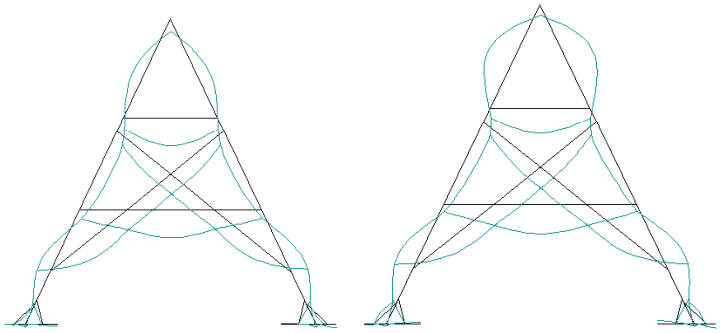

Figure 27 Deflected shape from load case 1.35 DL + 1.5 WL case 2, with internal suction (left) and internal pressure (right)

The following diagrams show the axial and shear forces and bending moments in the members for three load cases: 1.35 DL + 1.5 LL, 1.35 DL + 1.5 WL case 1 internal suction, and 1.35 DL + 1.5 WL case 2 internal suction. The wind load cases with internal pressure are very similar to those with internal suction, and are therefore not shown.

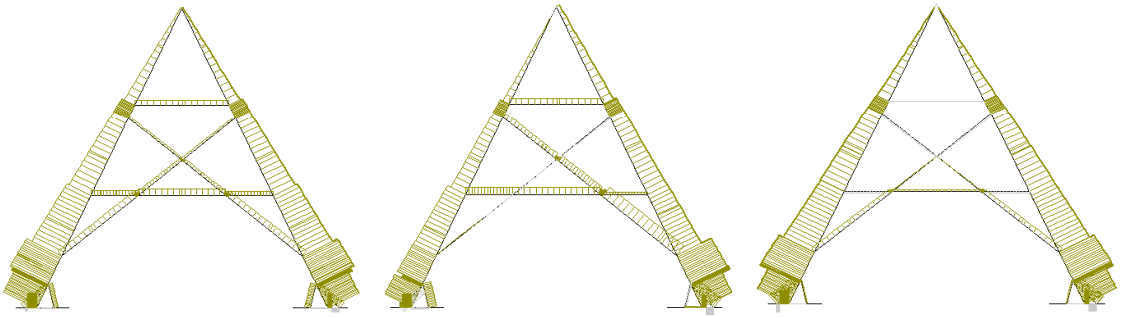

Figure 28 Axial force diagrams for load combinations 1.35 DL + 1.5 LL, 1.35 DL + 1.5 WL case 1 internal suction, and 1.35 DL + 1.5 WL case 2 internal suction

Examining the axial force diagrams above, it can be seen that the truss is well designed to prevent buckling. As the axial force increases closer to the base of the truss, the effective length of each truss segment decreases. The stiff roofing boards would prevent buckling, however, the original geometry of the construction did not have roofing boards but a gap between the members and spaced runners supporting the tiles. The roofing boards were not present to prevent buckling of these members.

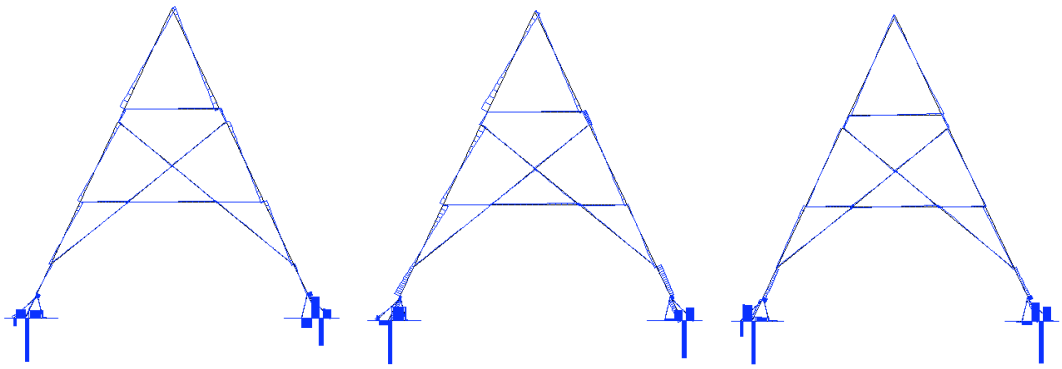

Figure 29 Shear force diagrams for load combinations 1.35 DL + 1.5 LL, 1.35 DL + 1.5 WL case 1 internal suction, and 1.35 DL + 1.5 WL case 2 internal suction

As seen in the shear force diagrams above, the maximum shear forces occur in the members at the bottom of the truss. This is because the supports are not directly under the truss members, as seen previously in Figure 22 (page 53). However, these bottom horizontal members are not original, but are new glulam beams of very high strength.

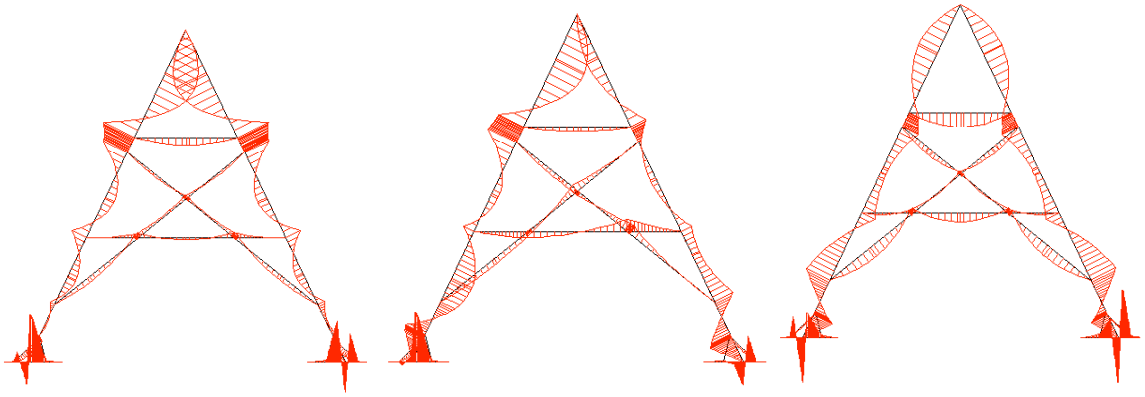

Figure 30 Bending moment diagrams for load combinations 1.35 DL + 1.5 LL, 1.35 DL + 1.5 WL case 1 internal suction, and 1.35 DL + 1.5 WL case 2 internal suction

As the load is applied to the exterior members, the bending moments are highest in these members. As well, the nature of a truss is such that members primarily carry axial loads. The exterior members are 20 cm by 20 cm, while the interior members are 12 cm by 20 cm. The truss is well designed as the members with the highest bending moments have the largest cross sections.

The maximum deformations are shown in Table 8 and Table 9. The notation of the wind loads is "WL 1" corresponds to the wind loading shown in Figure 10 (page 32), and "WL 2" to Figure 11 (page 33). Internal suction is referred to as "suc," and internal pressure as "pres." The "Z" deflection is vertical, and the "Y" direction perpendicular to it in the plane of the member.

For comparing first and second order results, the joint deflections are easily compared using the text output of the program. The member deflections are not easily comparable, due to the lack of output. FINE provides the maximum deflection in the y-direction and the distance along the member this occurs for the critical member only. However, it does not provide the deflection in the z-direction at this location as well. Therefore, to determine the maximum deflection of the member, the assumption is made that deflection occurs perpendicular to the member axis (Dmax in the table below).

The maximum member deflections provided by FINE are with respect to the global coordinate system. Therefore, to obtain the true deflection of the member, the deflection

of the joints must be considered. In Table 8 and Table 9, the deflection of the member relative to the joints it is attached to is given, as indicated by "Corrected for joint displacements."

The displacement outputs for FINE only provide member deflections for those with maximum values. Once the displacements corresponding to the strains in the member are calculated, they may no longer be the maximum deflections. By inspection, the maximum member deflection should occur at the top of member 2 or 3, as these are the longest spans and are directly loaded by wind and live loads. In Table 9, the top section of member is critical, so the maximum deflections are considered.

Table 8 Deformations for positive extremes

Joint def.	Load combo	Mem	Dist from memb begin (m)	I (mm, mrad)	II (mm, mrad)	e_0/l
Pinned Positive Extremes						
DY	1.35DL+1.5WL 1 suc	2	3.394	3.4	3.5	
Dmax				3.8	3.9	
Corrected for joint displacements				0.778	0.888	3.5E-4
DZ	1.35DL+1.5WL 1suc	11	3.130	1.4	1.4	
Dmax				0.229	0.229	6.2E-5
Corrected for joint displacements						
OX	1.35DL+1.5WL 1 suc	2	12.472	2.5	2.5	
Spring Positive Extremes						
DY	1.35DL+1.5WL 1 suc	2	3.480	3.4	3.4	
Dmax				3.8	3.8	
Corrected for joint displacements				0.778	0.778	3.0E-4
DZ	1.35DL+1.5WL 1 suc	11	3.250	1.2	1.3	
Dmax				1.2	1.3	
Corrected for joint displacements				0.048	0.559	1.5E-6
OX	1.35DL+1.5WL 1 suc	2	12.335	2.4	2.4	
Fixed Positive Extremes						
DY	1.35DL+1.5WL 1 suc	2	3.394	3.4	3.4	
Dmax				3.8	3.8	
Corrected for joint displacements				0.778	0.778	3.0E-4
DZ	1.35DL+1.5WL 1 suc	11	3.220	1.2	1.3	
Dmax				1.2	1.3	
Corrected for joint displacements				0.048	0.559	1.5E-6
OX	1.35DL+1.5WL 1 suc	2	12.472	2.5	2.5	

Table 9 Deformations for negative extremes

Joint def.	Load combo	Mem	Dist from memb begin (m)	I (mm, mrad)	II (mm, mrad)	e_0/l
Pinned Negative Extremes						
DY	1.35DL+1.5LL	3	10.824	-1.5	-1.5	
Dmax				-1.6	-1.6	
Corrected for joint displacements				-1.600	-1.600	3.9E-4
DZ	1.35DL+1.5WL1pres	9	2.166	-2.2	-2.2	
Dmax				-2.8	-2.8	
Corrected for joint displacements				-0.844	-0.844	2.3E-4
OX	1.35DL+1.5WL 1 suc	4	0.075	-3.2	-3.1	
Spring Negative Extremes						
DY	1.35DL+1.5LL	3	10.686	-1.5	-1.5	
Dmax				-1.6	-1.6	
Corrected for joint displacements				-1.600	-1.600	3.9E-4
DZ	1.35DL+1.5WL1pres	9	2.166	-2.1	-2.1	
Dmax				-2.7	-2.7	
Corrected for joint displacements				-0.716	-0.716	1.9E-4
OX	1.35DL+1.5WL 1 suc	4	0.113	-3.1	-3.1	
Fixed Negative Extremes						
DY	1.35DL+1.5LL	3	10.824	-1.5	-1.5	
Dmax				-1.6	-1.6	
Corrected for joint displacements				-1.600	-1.600	3.9E-4
DZ	1.35DL+1.5WL1pres	9	2.229	-2.1	-2.1	
Dmax				-2.7	-2.7	
Corrected for joint displacements				-0.716	-0.716	1.9E-4
OX	1.35DL+1.5WL 1 suc	4	0.075	-3.2	-3.1	

The midspan member deflections are negligible, as indicated by the midspan deflection over span ratios e_0/l.

Table 10 shows the maximum and minimum horizontal and vertical reactions.

Table 10 Reactions

Reaction	Load combo	Joint	I order (kN)	II order (kN)
Pinned Positive extremes				
RY	1.35DL+1.5LL	3	12.88	12.88
RZ	1.35DL+1.5WL 1 suct	4	28.39	28.51
Spring Positive Extremes				
RY	1.35DL+1.5LL	3	12.88	12.89
RZ	1.35DL+1.5WL 1 suct	4	28.34	28.45
Fixed Positive extremes				
RY	1.35DL+1.5LL	3	12.89	12.89
RZ	1.35DL+1.5WL 1 suct	4	28.33	28.45
Pinned Negative Extremes				
RY	1.35DL+1.5WL 1 suct	6	-15.42	-15.41
RZ	1.35DL+1.5WL 1 suct	3	-4.26	-4.37
Spring Negative Extremes				
RY	1.35DL+1.5WL 1 suct	6	-15.42	-15.42
RZ	1.35DL+1.5WL 1 suct	3	-4.21	-4.32
Fixed Negative Extremes				
RY	1.35DL+1.5WL 1 suct	6	-15.42	-15.42
RZ	1.35DL+1.5WL 1 suct	3	-4.20	-4.31

The internal stresses are calculated from the internal forces, as shown in Table 11 and Table 12.

Table 11 Internal stresses for positive extremes

Memb		**Area**	**y**	**I**	**P**	**Q**	**M**	σ_{max}*	σ_{min}*	τ
		m^2	mm	mm^4	kN	kN	kNm	kPa	kPa	kPa
Pinned Positive extremes										
1.35DL+1.5WL 1pres										
I	15	0.04	100	1.3E8	6.25	-6.51	-1.76	1476.3	-1163.8	
II	15	0.04	100	1.3E8	6.27	-6.54	-1.77	1484.3	-1170.8	
1.35DL+1.5WL 1suct										
I	21	0.04	100	1.3E8		21.69				542.3
II	21	0.04	100	1.3E8		21.76				544.0
1.35DL+1.5WL 1suct										
I	2	0.04	100	1.3E8	-1.85	0.03	2.23	1626.3	-1718.8	
II	2	0.04	100	1.3E8	-1.85	0.03	2.24	1633.8	-1726.3	
Spring Positive extremes										
1.35DL+1.5WL 1suct										
I	15	0.04	100	1.3E8	6.24	-6.50	-1.76	1476.0	-1164.0	
II	15	0.04	100	1.3E8	6.27	-6.53	-1.77	1484.3	-1170.8	
1.35DL+1.5LL										
I	21	0.04	100	1.3E8		21.66				541.5
II	21	0.04	100	1.3E8		21.72				543.0
1.35DL+1.5WL 1suct										
I	2	0.04	100	1.3E8	-1.83	0.05	2.24	1634.3	-1725.8	
II	2	0.04	100	1.3E8	-1.83	0.05	2.24	1634.3	-1725.8	
Fixed Positive extremes										
1.35DL+1.5WL 1pres										
I	15	0.04	100	1.3E8	6.24	-6.50	-1.76	1476.0	-1164.0	
II	15	0.04	100	1.3E8	6.27	-6.53	-1.77	1484.3	-1170.8	
1.35DL+1.5WL 1suct										
I	21	0.04	100	1.3E8		21.65				541.3
II	21	0.04	100	1.3E8		21.72				543.0
1.35DL+1.5WL 1suct										
I	2	0.04	100	1.3E8	-1.84	0.04	2.24	1634.0	-1726.0	
II	2	0.04	100	1.3E8	-1.85	0.04	2.24	1633.8	-1726.3	

*Calculated as $\sigma = P/A \pm My/I$

Table 12 Internal Stresses for negative extremes

Memb		**Area**	**y**	**I**	**P**	**Q**	**M**	σ_{max}*	σ_{min}*	τ
		m^2	mm	mm^4	kN	kN	kNm	kPa	kPa	kPa
Pinned Negative extremes										
1.35DL+1.5WL 1suct										
I	3	0.04	100	1.3E8	-32.05	-1.31	1.63	421.3	-2023.8	
II	3	0.04	100	1.3E8	-32.09	-1.27	1.67	450.3	-2054.8	
1.35DL+1.5LL										
I	17	0.04	100	1.3E8		-10.05				251.3
II	17	0.04	100	1.3E8		-10.05				251.3
1.35DL+1.5WL 1suct										
I	21	0.04	100	1.3E8	1.44	21.69	-3.40	2586.1	-2514.1	
II	21	0.04	100	1.3E8	1.45	21.76	-3.42	2601.3	-2528.8	
Spring Negative extremes										
1.35DL+1.5WL 1suct										
I	3	0.04	100	1.3E8	-32.05	-1.32	1.63	421.3	-2023.8	
II	3	0.04	100	1.3E8	-32.09	-1.28	1.66	442.8	-2047.3	
1.35DL+1.5LL										
I	17	0.04	100	1.3E8		-10.04				251.0
II	17	0.04	100	1.3E8		-10.04				251.0
1.35DL+1.5WL 1suct										
I	21	0.04	100	1.3E8	1.44	21.66	-3.39	2578.5	-2506.5	
II	21	0.04	100	1.3E8	1.44	21.72	-3.41	2593.5	-2521.5	
Fixed Negative extremes										
1.35DL+1.5WL 1suct										
I	3	0.04	100	1.3E8	-32.05	-1.32	1.62	413.8	-2016.3	
II	3	0.04	100	1.3E8	-32.09	-1.28	1.66	442.8	-2047.3	
1.35DL+1.5LL										
I	17	0.04	100	1.3E8		-10.04				251.0
II	17	0.04	100	1.3E8		-10.04				251.0
1.35DL+1.5WL 1suct										
I	21	0.04	100	1.3E8	1.44	21.65	-3.39	2578.5	-2506.5	
II	21	0.04	100	1.3E8	1.44	21.72	-3.41	2593.5	-2521.5	

*Calculated as $\sigma = P/A \pm My/I$

10.2.5 Analysis of FINE results

The differences between the three models (fixed, pinned, and spring interior joints) are negligible, as seen from the preceding tables, and it is concluded that the type of joint chosen does not affect the results.

The stresses in the above tables from second order analysis are compared to the material strengths shown in Table 7, which is repeated below, using the relevant modification factors.

Table 7 Summarized Mechanical properties of American spruce at 12% relative humidity, averaged over the different subspecies [14]

Mod of rupt (kPa)	E (MPa)	Comp paral grain (kPa)	Comp perp grain (kPa)	Shear paral grain (kPa)	Tens perp grain (kPa)	Tens paral grain (kPa)
72 000	10 000	15 000*	3 100	8 000	2 400	60 000

* Property is not that of American spruce, but as recommended by Professor Kuklik

The comparison of every stress is not shown due to the different modification factor for each type of loading, and all stresses present are well below the capacity.

10.2.6 Stability check by comparison of I and II order analysis

Below are the limits previously established for comparing first and second order results and for preventing instability such as buckling.

Table 13 Stability criteria for comparing second order results to first order

Load limit	**Deflection limit**	**Type of limit**
	$w < 1.15\ w_0$	Comparison of I and II order
$P < (1/10)\ P_{cr}$	$w < (10/9)\ w_0$	Instability (buckling)
$P < (1/4)\ P_{cr}$	$w < (4/3)\ w_0$	Instability (buckling)

The deflections of first and second order analysis are compared from the model with spring connections to see if the limits in Table 13 are met. The maximum deviation using the limit $w < (10/9)\ w_0$ is $1.3mm < (10/9) * 1.2\ mm = 1.33\ mm$. The other limits compare 1.3 to values of 1.38 and 1.60. It is recognized that these deflections are not entirely

correct, as FINE does not provide enough significant digits on the deflections but rounds them to 0.1 mm.

This check ensures against failure by buckling, and ensures stability. The failure mechanism (buckling, material failure, or a mix) depends on the slenderness ratio of each member, and the geometry of the structure. Previously, the stresses in the members were checked, ensuring against material failure. As both material strength and stability criteria are met, the FINE results show the truss is safe.

10.2.7 Out of plane stability

The two dimensional model of the truss does not allow for out of plane movement, so the truss is checked in FIN 3D. The shape at instability is shown in Figure 31 below.

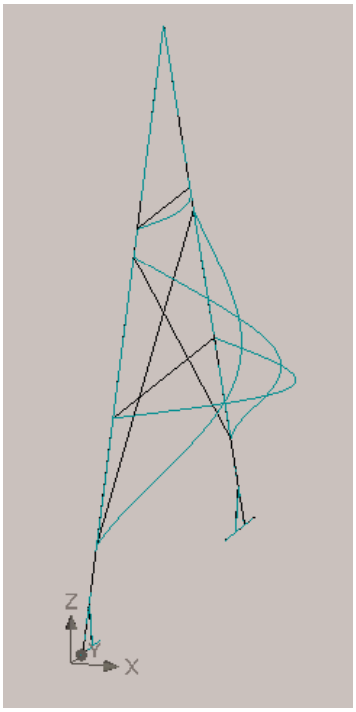

Figure 31 Shape at failure for the load case 1.35 DL + 1.5 WL, case 1, internal suction

The load multiplier, k, causing instability for this load case is 26.78. When the three-dimensional model is placed under the loading placed on the two-dimensional model, there is no measured deflection in the x-direction (out-of-plane). The two-dimensional model of the truss is therefore acceptable.

10.2.8 Analysis of results by Eurocode 5: Design of timber structures [15]

The model with spring connections is examined, as it is most representative of the actual state of the structure. The Eurocode specifies, "structures shall be analyzed using static models which consider in a realistic way the static behavior of the structure and of the supports" (5.4.1 (1)). The second order results are more representative of the true behavior of the structure, and are therefore used in the analysis, with the exception of buckling checks.

10.2.8.1 Bearing

At the supports, the members are subjected to compression perpendicular to the grain. At joint 4 (Figure 22, page 53) the member is subject to a factored load of 28.51 kN, corresponding to a pressure of 1425 kPa, which is less than the 5 438 kPa capacity, or as a ratio, $0.262 \leq 1$.

10.2.8.2 Negative reactions at supports

The reactions are checked to ensure that the wind loading is not high enough to pull the roof off of the structure. The load combinations are modified to use 1.00 DL instead of 1.35 DL, using the current weight of the roof with shingles, not with the clay roof tiles that may be used in the future. On each side of the truss there are two supports. If one of these has a negative reaction, the restraint is removed and the model was run again. The loading combination 1.00 DL + 1.50 WL case 2 internal pressure caused negative reactions at the supports. The total reactions were -0.4 kN, so the wind load is just high enough to counter the self-weight of the roofing. However, as the roofing self-weight causes reactions of 13.97 kN, the limit is exceeded by 2.9%, which is within the acceptable 5% margin.

10.2.8.3 Shear

The maximum shear stress of 434 kPa is less than the 4 846 capacity, or as a ratio, 0.090 ≤ 1.

10.2.8.4 Combined bending and axial tension

The criteria

$$\frac{\sigma_{t,0,d}}{f_{t,0,d}} + k_m \frac{\sigma_{m,y,d}}{f_{m,y,d}} \leq 1 \qquad \text{[Eq. 36]}$$

Is met as 0.102 ≤ 1.

10.2.8.5 Combined bending and axial compression (material failure)

The criteria

$$\left(\frac{\sigma_{c,0,d}}{f_{c,0,d}}\right)^2 + \frac{\sigma_{m,y,d}}{f_{m,y,d}} \leq 1 \qquad \text{[Eq. 37]}$$

Is met as 0.189 ≤ 1.

10.2.8.6 Buckling: Members subjected to compression or compression and bending (Eurocode section 6.3.2)

The following formulas use the stresses from first order analysis.

$$\frac{\sigma_{c,0,d}}{k_{c,y} f_{c,0,d}} + \frac{\sigma_{m,y,d}}{f_{m,y,d}} + k_m \frac{\sigma_{m,z,d}}{f_{m,z,d}} \leq 1$$
$$\frac{\sigma_{c,0,d}}{k_{c,z} f_{c,0,d}} + k_m \frac{\sigma_{m,y,d}}{f_{m,y,d}} + \frac{\sigma_{m,z,d}}{f_{m,z,d}} \leq 1 \qquad \text{[Eq. 38]}$$

This criteria is met as 0.567 ≤ 1. The factors $k_{c,y}$ and $k_{c,z}$ consider buckling of the member. The equations used for these factors are shown in "Appendix C: Derivations of equations." The buckling length used is measured from joint to joint. The use of this

effective length is conservative, as it for some cases it may be lower. The buckling shape determines the effective length, which is measured between the inflection points (change in curvature).

10.2.8.7 Beams subject to either bending or combined bending and compression

The following formula is used to check lateral torsional buckling, using stresses from first order analysis:

$$\left(\frac{\sigma_{m,d}}{k_{crit}\, f_{m,d}}\right)^2 + \frac{\sigma_{c,d}}{k_{c,z}\, f_{c,0,d}} \leq 1 \qquad \text{[Eq. 39]}$$

This criterion is met as 0.555 ≤ 1, for member 11. Lateral torsional buckling is of particular concern for members with a large height to width ratio, subjected to a high bending moment. The first term of the above equation is very close to zero for all truss members. This is to be expected as the members have a reasonable height to width ratio, and the bending moment on interior members is only from self-weight. As this is a type of buckling check, first order analysis results and there is no moment in the member resulting from an axial load.

10.2.9 Linear stability: FINE

In FIN 2D, the loading is increased until the deflection limit $w < (10/9)\, w_0$, $w < 1.15\, w_0$, or $w < (4/3)\, w_0$ is exceeded. The limit $w < (10/9)\, w_0$ is exceeded when a factor is applied to the entire loading combination of k = 4.3, the limit $w < (4/3)\, w_0$ is exceeded when k = 11.5, and the limit $w < 1.15\, w_0$ is exceeded when k = 5.8.

The buckling behavior of the members is illustrated in Figure 32 below. The slenderness of the most slender member, the top section of member 2, is shown by the yellow line marked "2-top."

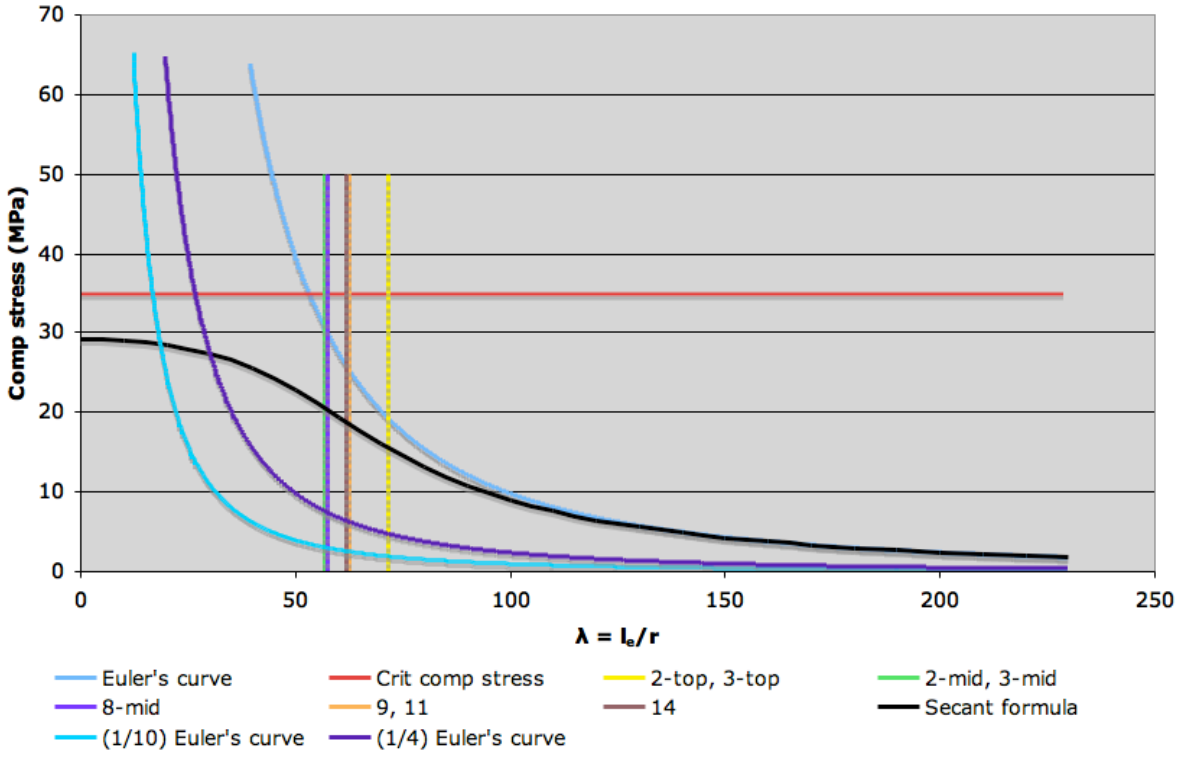

Figure 32 Behaviour in compression of members subject to buckling (non-short columns)

The blue line indicates Euler's buckling curve, the red line indicates the material strength, and the vertical lines indicate the slenderness ratios of the most slender members. The member numbers refer to Figure 21 on page 52. As some members are continuous past multiple joints, the location of the span on the truss is indicated, for example "8-mid" refers to the middle span of the three spans of member 8.

The most slender columns are considered to be medium length, that is, both material strength and slenderness play a part in the failure. Euler's curve and the material strength are idealized capacities, and are unconservative. The secant formula, represented by the black line, is closer to the actual capacity.

$$\frac{P}{A} = \frac{\sigma_{max}}{1 + \frac{ec}{r^2} \sec\left(\frac{1}{2}\sqrt{\frac{P}{EA}}\,\frac{L_e}{r}\right)} \qquad \text{[Eq. 40]}$$

The secant formula plotted used $ec / r^2 = 0.2$, where e is the eccentricity of the load, c is the distance of half the cross section height, and r is the radius of gyration. Despite being more accurate, the secant formula is still unconservative when compared to the actual behavior of a member.

Euler's curve, $\sigma_{cr} = P_{cr}/A$, is calculated directly from the critical buckling load. The force limits can be divided by area to provide $\sigma < (1/10)\sigma_{cr}$ and $\sigma < (1/4)\sigma_{cr}$, which are plotted as (1/10) and (1/4) of Euler's curve. The behavior of columns is very complex, and experimental results usually find the column to be weaker than theoretical values. There are many equations used for the behavior of a column, as there is no common agreement on which is most correct.

10.2.10 Linear stability: Eurocode 5

To determine linear stability, the coefficient k is determined such that $k*P = P_{crit}$. Equation 38 is repeated below:

$$\frac{\sigma_{c,0,d}}{k_{c,y} f_{c,0,d}} + \frac{\sigma_{m,y,d}}{f_{m,y,d}} + k_m \frac{\sigma_{m,z,d}}{f_{m,z,d}} \leq 1$$

$$\frac{\sigma_{c,0,d}}{k_{c,z} f_{c,0,d}} + k_m \frac{\sigma_{m,y,d}}{f_{m,y,d}} + \frac{\sigma_{m,z,d}}{f_{m,z,d}} \leq 1 \qquad \text{[Eq. 38]}$$

The terms $k_{c,y}$, $k_{c,z}$, $f_{c,0,d}$, $f_{m,y,d}$, and $f_{m,z,d}$ are all constants and independent of the load. Since this is a linear analysis, the stresses vary linearly with the loading. Given the current state of stress, and as there is no bending in the z-direction, it can be said that:

$$k \times \left(\frac{\sigma_{c,0,d}}{k_{c,y} f_{c,0,d}} + \frac{\sigma_{m,y,d}}{f_{m,y,d}} \right) \leq 1 \qquad \text{[Eq. 41]}$$

Which is solved for k = 1.8.

For lateral torsional buckling:

$$\left(\frac{k \times \sigma_{m,d}}{k_{crit}\, f_{m,d}}\right)^2 + \frac{k \times \sigma_{c,d}}{k_{c,z}\, f_{c,0\,d}} \leq 1 \qquad \text{[Eq. 42]}$$

Which is solved for k = 1.8.

For each design criteria, the load multiplier *k* required to cause failure is calculated and shown in Table 14.

Table 14 Load multiplier, k, required for failure by different paths

FINE comparison		**k**
Stability, w < (10/9) w_0 limit		4.3
Stability, w < (4/3) w_0 limit		11.5
Limit on II order validity, w < 1.15 w_0		5.8
Eurocode	**Limit (≤ 1)**	
Bearing	0.262	3.8
Shear	0.090	11.2
Bending and axial tension	0.102	9.8
Bending and axial comp (material failure)	0.189	5.3
Buckling	0.567	1.8
Lateral torsional buckling	0.555	1.8

10.2.11 Discussion

Focusing on the *k* values for stability, the load multiplier required for failure is considerably lower using the Eurocode result (k = 1.8) compared to that from the most conservative instability limit, $w < (10/9)\, w_0$ (k = 4.3). The load multiplier is much higher for the $w < (4/3)\, w_0$ limit at k = 11.5, however the accuracy of this result is unknown. These limits are derived from the accepted limits in the Czech Republic ($P < (1/4)\, P_{crit}$ corresponding to $w < (4/3)\, w_0$), and the rest of Europe ($P < (1/10)\, P_{crit}$ corresponding to $w < (10/9)\, w_0$). The limit on the validity of second order analysis produced a stability multiplier of 5.8.

Methods for checking buckling:

1. Eurocode equation

$$\frac{\sigma_{c,0,d}}{k_{c,y} f_{c,0,d}} + \frac{\sigma_{m,y,d}}{f_{m,y,d}} + k_m \frac{\sigma_{m,z,d}}{f_{m,z,d}} \leq 1$$

$$\frac{\sigma_{c,0,d}}{k_{c,z} f_{c,0,d}} + k_m \frac{\sigma_{m,y,d}}{f_{m,y,d}} + \frac{\sigma_{m,z,d}}{f_{m,z,d}} \leq 1 \qquad \text{[Eq. 38]}$$

2. Czech Republic limit for axial loading

$$P < (1/4)\, P_{cr} \qquad \text{[Eq. 14]}$$

   Or when using FINE to compare first and second order results:

$$w < (4/3)\, w_0 \qquad \text{[Eq. 16]}$$

3. European limit for axial loading

$$P < (1/10)\, P_{cr} \qquad \text{[Eq. 15]}$$

   Or when using FINE to compare first and second order results:

$$w < (10/9)\, w_0 \qquad \text{[Eq. 17]}$$

4. Comparison of deflections from first and second order analysis for stability, beyond which the results lose accuracy:

$$w < 1.15\, w_0 \qquad \text{[Eq. 43]}$$

Examining the Eurocode buckling equations and the first and second order analysis comparison, the loading causing instability of St Anne's Church roof structure is more than twice that allowed in the Eurocode equations for the limit $w < (10/9)\, w_0$. The Eurocode is likely overly conservative for the buckling equation, as it most accurate or conservative for all cases. However, it isn't possible to determine which limit is acceptable. The inaccuracies in second order analysis mean that anything beyond $w < 1.15\, w_0$ cannot be used.

10.3 Middle section with a different geometry

Four trusses near the center of the church have a different geometry than the others. This section is modeled in FIN 3D. The analysis section is limited to relevant observations, and differences from the standard truss. This is for clarity and to avoid repetition.

10.3.1 Geometry

The location of the trusses is shown in Figure 33 below.

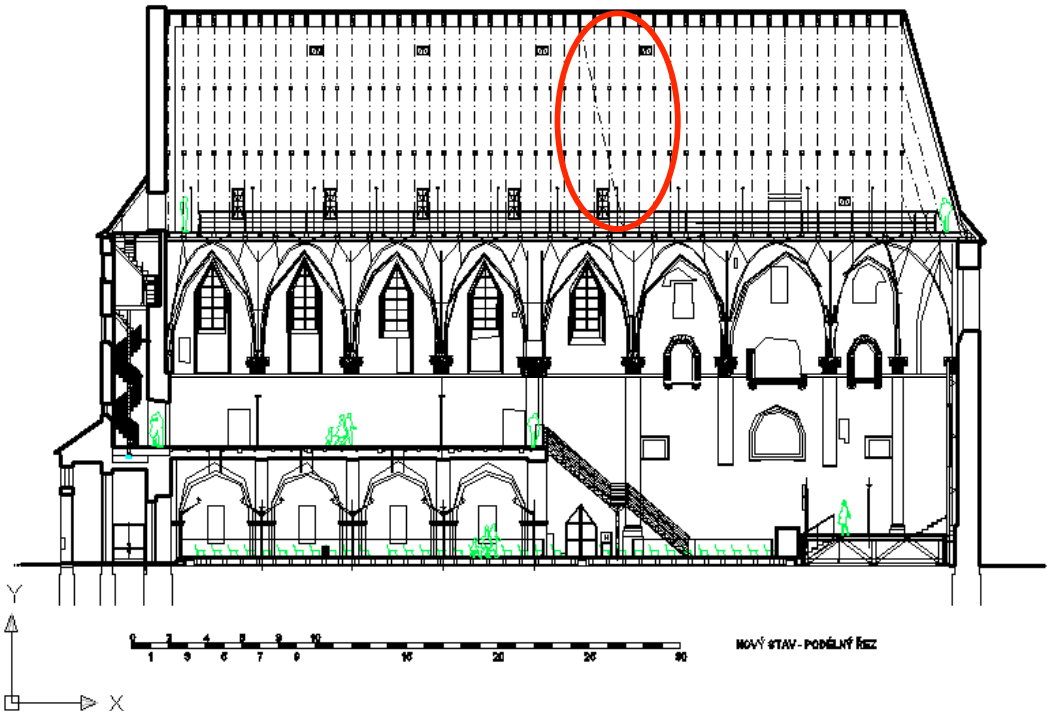

Figure 33 Truss section with irregular geometry as indicated by the red oval

This portion of the truss is shown in Figure 34 and Figure 35.

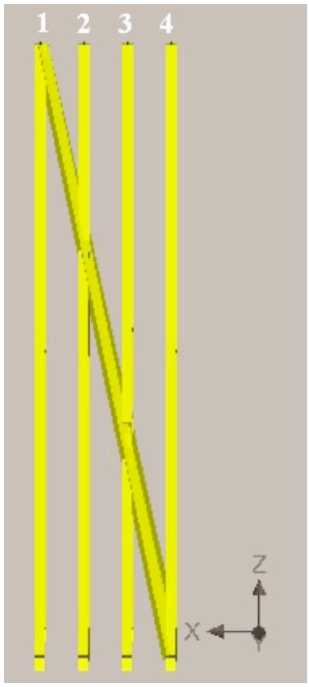

Figure 34 Section with irregular geometry, viewed from the south

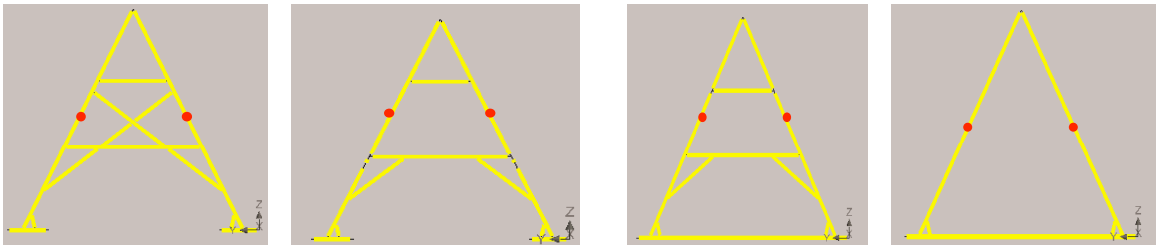

Figure 35 Trusses 1, 2, 3, and 4 from Figure 34

There are two members connecting the four trusses, seen in Figure 34 extending from the top of truss 1 to the bottom of truss 4. These members start at the peak of truss 1, and run along the surface of the roof to either side of the base of truss 4. The following pictures further illustrate the geometry.

Figure 36 Interior views of the section with irregular geometry

The loading distribution on the trusses is based on the stiffness of each truss. To start, the load is evenly distributed on all of the trusses. As shown in Figure 37 below, the diagonal members redistribute some of the load, as seen by the uneven reactions.

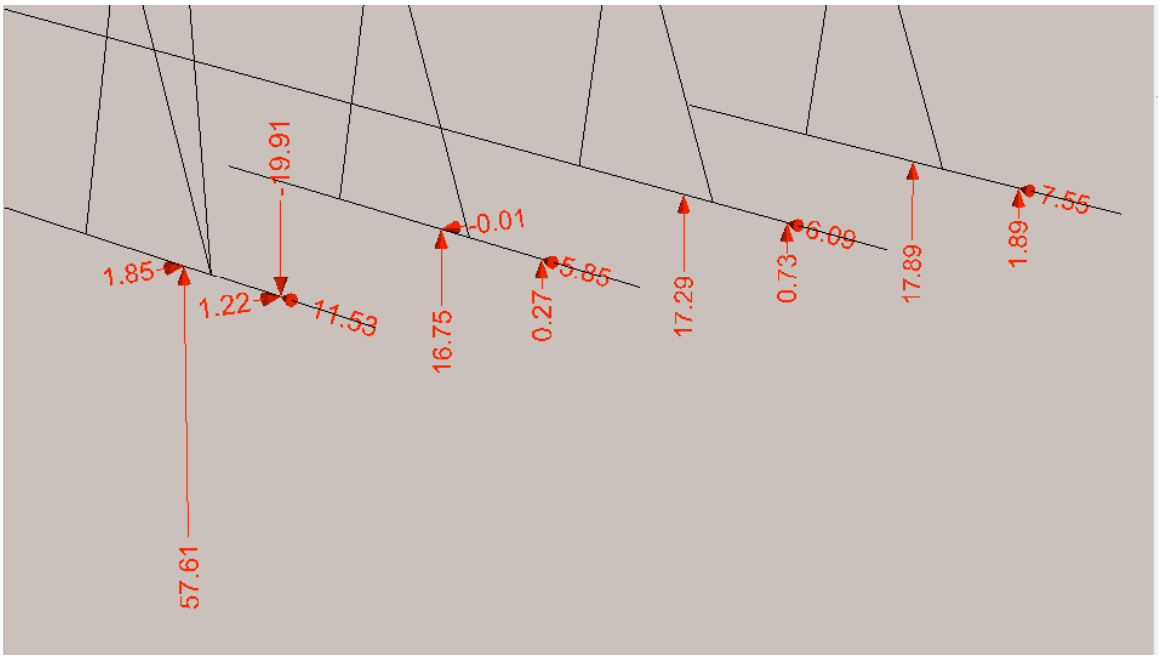

Figure 37 Reactions at the supports on the north side of the trusses with irregular geometry, for load case 1.35DL + 1.5 LL

Table 15 Truss reactions from the case of an even load distribution, for load combination 1.35DL + 1.5LL

Truss	Reaction 1 (kN)	Reaction 2 (kN)	Reaction 3 (kN)	Reaction 3 (kN)	Net reaction (kN)	% of orig load
1	17.89	1.89	11.83	7.93	39.54	85.3
2	17.29	0.73	12.17	6.01	36.02	77.7
3	16.75	0.27	11.45	5.76	34.22	73.8
4	57.61	-19.91	51.02	-13.26	75.49	162.9
5 (regular truss)	20.40	2.77	13.26	9.92	46.35	100.0

The reactions of the four trusses are compared to that of a regular truss, referred to as truss 5 in Table 15.

The roof membrane, made of two layers of 20 mm boards, is very stiff, and capable of redistributing some of the load. If the roof membrane were assumed to be infinitely stiff, then the deflections at all locations on the exterior members of each truss would be the same, across the entire roof. Therefore, the membrane is assumed to be infinitely stiff between these five trusses: the four shown in the figures, and a fifth regular truss adjacent to the fourth.

To achieve load distribution based on stiffness, the displacement must be compared at set points on each truss. The most appropriate points to measure the deflection are at the mid-span of the exterior truss members, as indicated by the red dots in Figure 35.

The load is distributed evenly on each truss based on the same tributary area for each truss. The force on the truss is known, and the deflection has been measured, so the stiffness is calculated:

$$[S]\ \{D\} = \{F\} \qquad \text{[Eq. 44]}$$

Now that the stiffnesses of the trusses are known, the distribution of the loading must be determined. Assuming an infinitely stiff roof membrane across the five trusses, the

deflection of all the trusses will be the same. The force is related directly to the stiffness, and knowing the total load to be applied, it can be distributed accordingly.

Table 16 Load attracted to each truss, as a percent of the original load on it

Truss	% of original load on the truss for 1.35 DL + 1.5 LL	% of original load on the truss for wind load combos
1	232.5	291.5
2	138.0	94.5
3	65.5	55.0
4	4.0	2.5
5 (regular truss)	160.0	156.5

Two iterations of calculating the applied loads were made to achieve equal deflections. Iterations were required because the two diagonal members connecting the trusses redistribute some of the load, causing uneven displacements between measurement points. The vertical loads (dead and live) were distributed differently than the wind loads. The deflections for the points at mid-span differed by 5.4% for the load case 1.35DL + 1.5LL, and by 8.4% for the wind load cases. The self-weights were not considered when the loads were distributed based on stiffness. By doing this, the relationship between stiffness, deflection, and force is linear, as the self-weight is constant and would void this relationship.

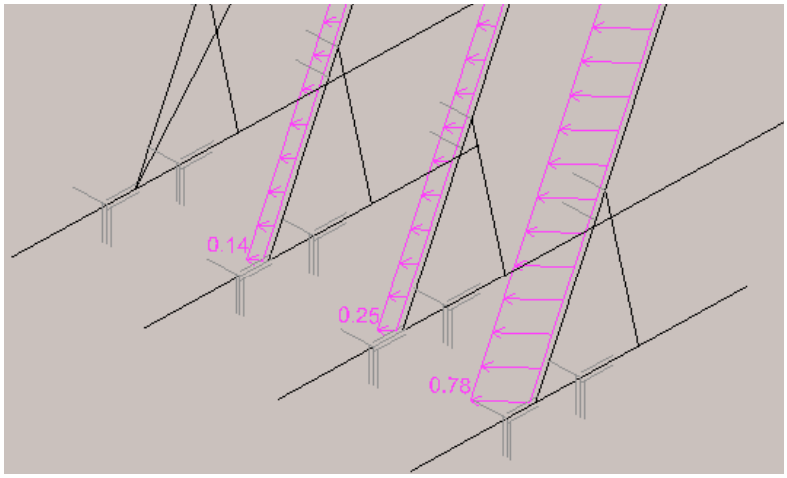

Figure 38 Load distributed based on stiffness for load case 2 (external wind loading)

Figure 38 above shows the load distribution for external wind load case 2. There is no wind loading on truss 4 because the smallest increment of load applied, 0.01 kN/m produced deflections much higher for this member than the others at mid-span.

In the FIN 3D model, the trusses are restrained in the x-direction to simulate the very stiff roof membrane. The model is analyzed similar to the analysis performed on the single regular truss previously, except only one model is analyzed with the interior joints pins. Previously, three models were done with interior joints examined as fixed, pinned, and spring connections, but it was shown that there were negligible differences between the models.

10.3.2 Analysis

The deflected shapes of the four trusses are very close, as seen in Figure 39 below for the load combination 1.35 DL + 1.5 LL. The figure is not very clear, but it can be seen that the top of truss 1, which is attracting the most load, has the highest deflections.

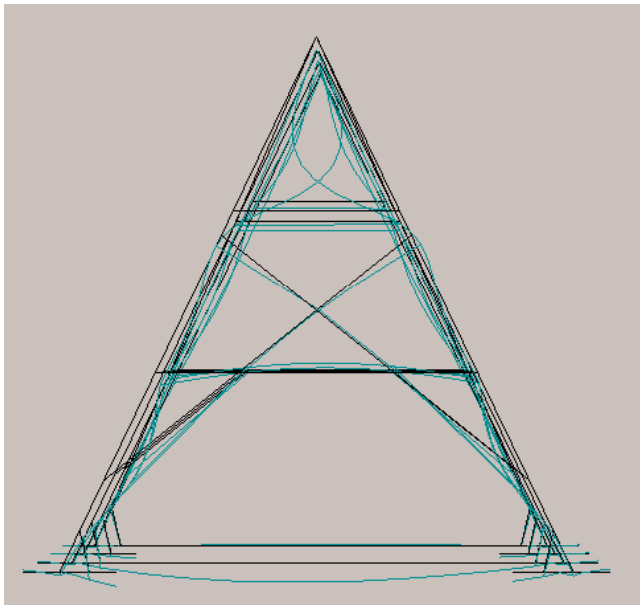

Figure 39 Deflected shape of the four trusses for combination 1.35 DL + 1.5 LL

The bending moment, shear force, and axial force diagrams are very similar to those of the standard truss, except accounting for the decreased or increased loading. The display outputs of FINE are such that it is very difficult to view these diagrams and make any observations from them.

10.3.2.1 Analysis of FINE results

The second order results are checked according to the following formulas, using capacities shown in Table 7 (page 54).

$$\frac{\sigma_{c,0,d}}{f_{c,0,d}} + \frac{\sigma_{m,y,d}}{f_{m,y,d}} + k_m \frac{\sigma_{m,z,d}}{f_{m,z,d}} \leq 1$$

$$\frac{\sigma_{c,0,d}}{f_{c,0,d}} + k_m \frac{\sigma_{m,y,d}}{f_{m,y,d}} + \frac{\sigma_{m,z,d}}{f_{m,z,d}} \leq 1 \qquad \text{[Eq. 45]}$$

The maximum tensile stress that occurs is 4 562 kPa, which is less than the 54 000 kPa capacity (accounting for modification factors). The maximum compressive stress is 4 773 kPa, which is less than the 13 500 kPa capacity.

10.3.2.2 Stability check by comparison of I and II order analysis

Table 13 is repeated below, and shows the acceptable limits for comparing first and second order results to prevent instability.

Table 13 Stability criteria for comparing second order results to first order

Load limit	**Deflection limit**	**Type of limit**
	$w < 1.15\ w_0$	Comparison of I and II order
$P < (1/10)\ P_{cr}$	$w < (10/9)\ w_0$	Buckling
$P < (1/4)\ P_{cr}$	$w < (4/3)\ w_0$	Buckling

All second order deflections meet all three limits. The largest difference between first and second order was $w_0 = 7.64$ *mm*, and $w = 7.84$ *mm*. This is smaller than the most conservative limit of $(10/9)\ w_0 = 8.49$ *mm.*

10.3.2.3 Linear stability

Unlike FIN 2D, the program FIN 3D solves for the linear stability for each load combination. This calculation was described previously in the "linear stability" section, but in brief, the equation $[S(\alpha)]\ \{D\} = \{F\}$ is solved such that the structure can acquire

additional displacements {δD} without applying any more forces. The constant (α) multiplied by the current load causes buckling. A visual interpretation of this was provided previously in Figure 13 (page 39), in this figure as line 1 approaches line 2, the load F_{krit} is reached.

Table 17 Linear stability from FIN 3D causing failure

Load combination	**k (also known as α)**
1.35 DL + 1.5 LL	17.52
1.35 DL + 1.5 WL case 1, internal suction	13.89
1.35 DL + 1.5 WL case 1, internal pressure	21.01
1.35 DL + 1.5 WL case 2, internal suction	33.54
1.35 DL + 1.5 WL case 2, internal pressure	39.64

Examining the values in the previous table, the load case "1.35 DL + 1.5 WL case 1, internal suction" has the highest loading on the structure, and also has the lowest *k* value. As well, wind load case 1 is an unsymmetrical load. It makes sense that this load case has the lowest load multiplier causing instability.

Comparing the two wind loadings of case 2, the internal pressure is a slightly higher load than internal suction. However, the direction of the internal pressure is opposite to wind load case 2, while the internal suction is in the same direction. These values for linear stability make sense.

The shapes of the trusses at failure are shown in the following figures.

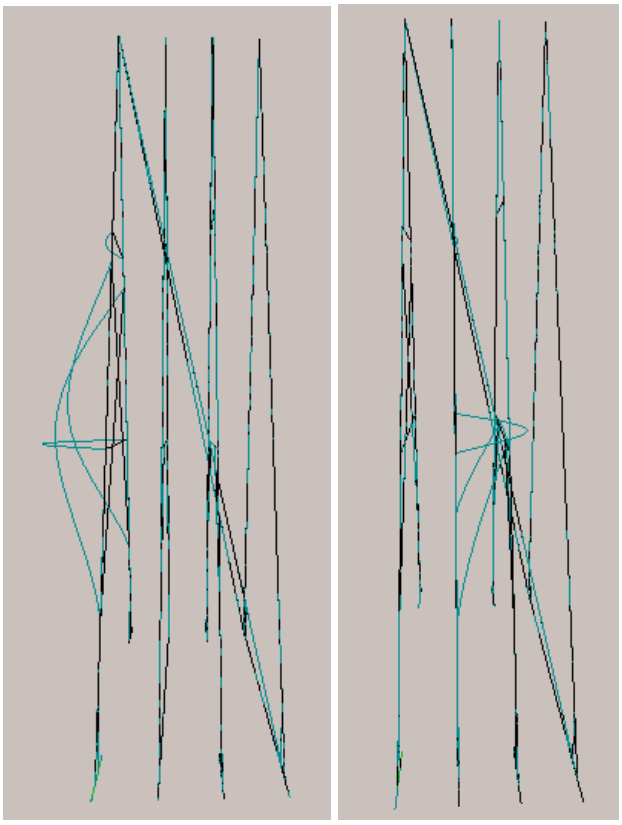

Figure 40 Shape of the structure at failure due to linear stability for load cases 1.35 DL +1.5 LL, 1.35 DL + 1.5 WL case 1 int suct, and 1.35 DL + 1.5 WL case 1 int pres (left), and for load case 1.35 DL +1.5 WL case 2, int suct (right)

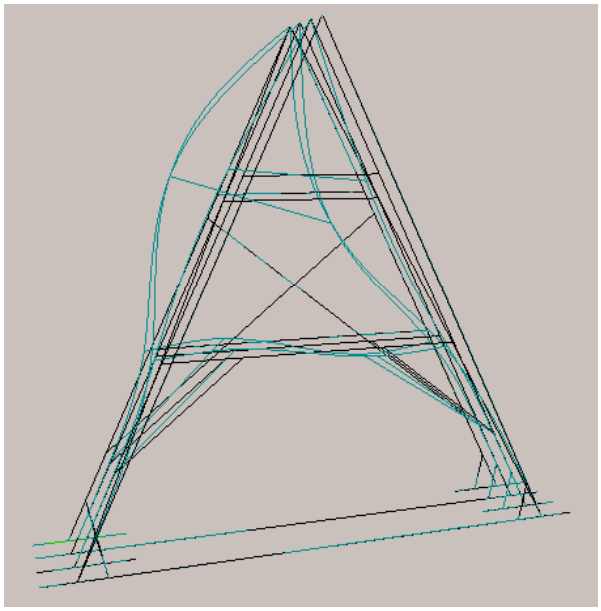

Figure 41 Shape of the structure at failure due to linear stability for load combination 1.35 DL +1.5 WL case 2, internal pressure

Examining the deflected shapes at the critical loading, the results are not as expected. The shape for 1.35 DL +1.5 WL case 2 shown in Figure 41 is unsymmetrical, despite the symmetric trusses and loadings. It would be expected that, if any, the load combinations using wind case 1 would produce this type of shape, as those loadings are unsymmetrical. The failure shapes shown in Figure 40 are logical as there are no lateral restraints on inside elements of the truss.

10.3.3 Summary of structural integrity

Table 18 Load multiplier, k, required for failure by different paths

FINE comparison		**k**
Buckling, $w < (10/9)\ w_0$ limit		1.8
Buckling, $w < (4/3)\ w_0$ limit		4.6
Limit on II order validity, $w < 1.15\ w_0$		2.3
Linear stability (most critical load combo)		13.9
Eurocode	**Limit (≤ 1)**	
Bearing	0.424	2.4
Shear	0.110	9.1
Bending and axial tension	0.290	3.4
Bending and axial comp (material failure)	0.354	2.8
Buckling	0.878	1.1
Lateral torsional buckling	0.864	1.2

The buckling limits in Table 18 are compared to the values of 4.3, 5.8, and 11.5 for limits $w < (10/9)\ w_0$, $w < 1.15\ w_0$, and $w < (4/3)\ w_0$, respectively for a standard truss. The stiffest truss had 1.93 times the loading on a standard truss, and there are differences between the standard truss and this three-dimensional model. There are missing members in three of the trusses, and the two diagonal members connecting the trusses redistribute some of the load. The two dimensional model of the standard truss does not allow for movement perpendicular to the truss, while the three-dimensional model does, and the critical load causes failure in this direction for various load combinations. Accounting for these differences, the load multipliers causing failure are acceptable.

By accounting for the stiffness in the roofing boards, loading is transferred from the trusses with lower stiffness to those with higher, and this section of the truss is found to be very safe.

10.4 End of the roof

The capacity and failure methods of the east end of the roof are examined.

Figure 42 Exernal views of the east end of St Anne's Church

On Figure 42, the roof is bowed in on the second picture. Inspection of the roofing boards at this location on the inside of the church does not reflect this situation, and there is no evidence of any bowing. The bowing likely happened during the reconstruction of the roofing.

Figure 43 Internal views of the east end of of the church

10.4.1 Analysis of FINE results: Eurocode 5 [15]

The member is modeled as a simply supported beam, and the forces are shown in the following figure.

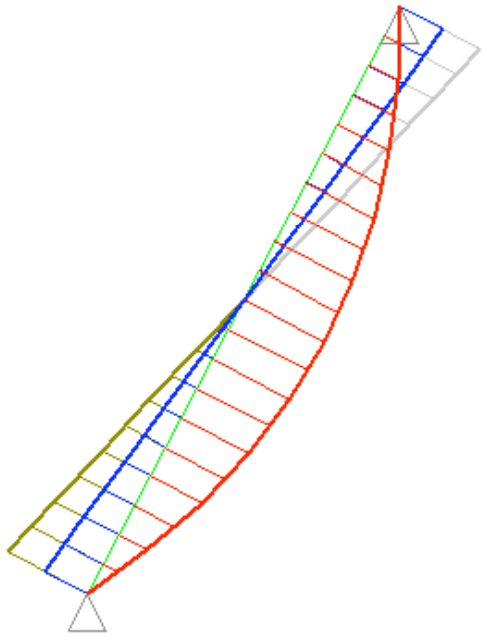

Figure 44 Bending moment (red), axial force (grey), and shear force (blue) diagrams for a member on the end of the roof

The capacity of the member under different failure paths is shown in Table 19.

Table 19 Load multiplier, k, required for failure by different paths

Eurocode	**Limit (≤ 1)**	**k**
Bearing	0.146	6.8
Shear	0.053	18.9
Bending and axial tension	0.230	4.3
Bending and axial comp (material failure)	0.922	1.1

Buckling will not occur as the roofing boards along the entire length of the member restrain it. The member acts as a composite member in combination with the roofing membrane. The area and second moment of inertia is calculated for this composite section. A rectangular section with the same cross sectional area and moment of inertia is used in the FIN 2D model.

The maximum deflection occurring under serviceability limit states is 58.2 mm, which corresponds to span / 224. This is for load case DL + LL, and an acceptable limit for this loading case is span / 240 for inelastic roof coverings. This requirement is not quite met. However, the model was conservative, as it did not account for the roof tapering, which

lowers the load on the member. As well, due to the shape of the roof, deflections will be somewhat restricted by the adjacent roof sections that are not in the same plane.

10.5 Irregularities due to damages, deteriorations, and imperfections

Irregularities were observed in a few locations on the trusses. Damage from long horn beetles was present on a few trusses, but was not very extensive, and there was no evidence of it being recent. A very small area of 4 cm by 4 cm appeared to have been attacked by a type of rot. Various models were made in FIN 2D to determine the loss of capacity resulting from these irregularities.

10.5.1 Decreased cross section due to missing material

One of the members at the base of the truss was missing material.

Figure 45 Truss member with material missing, and the location of the member on the truss

If this member were entirely lost, the truss would still be stable as this portion is statically indeterminate. The remaining cross section has dimensions 11 cm by 11cm. A FIN 2D model is created using a reduced section at this location, where the cross section is reduced for a length of 25 cm.

The FIN 2D model results are virtually identical to that of the standard truss, with the difference in reactions, displacements, and stresses not exceeding 0.35%, with the exception of this particular member. Examining this member, the axial load ranges from 1.05 kN in tension to 4.00 kN in compression. These values are between 3 and 8 % lower than those in the standard truss, and result in stresses ranging from 0.087 MPa in tension to 0.33 MPa in compression. The axial load runs through the center of the member, and the reduced cross section changes the center of area of the section, so the axial load causes biaxial bending. The increased stress ranges from 0.30 MPa in tension to 1.14 MPa in compression. There is no risk of buckling or material failure in this member. It has been found that this member has very little importance.

10.5.2 Decreased cross section due to beetle damage

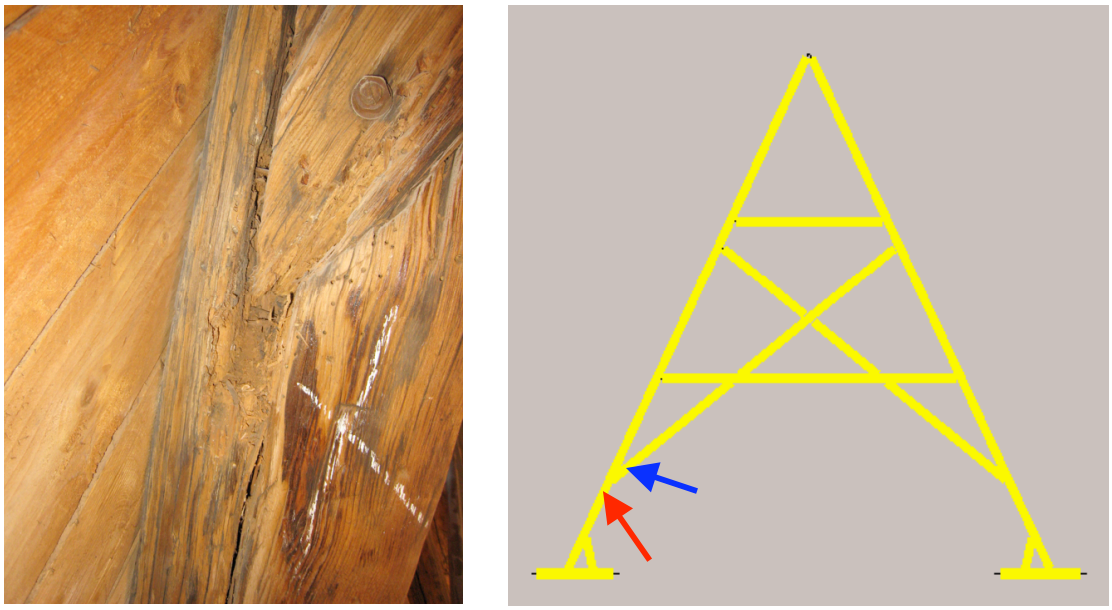

Figure 46 Truss members with significant and unsignificant damage, marked by the red and blue arrows, respectively

Long horn beetles have caused loss of material in certain locations, particularly at this joint. The deteriorated wood can easily be broken away, and has very little resistance. There is no evidence of movement around this joint.

The modulus of elasticity is assumed to be much lower for the damaged wood. Because FINE uses beam elements, it is not possible to change the modulus of elasticity across the cross section, only along the length by subdividing the beam into smaller elements. The damage extends along the member for 30 cm, but does not attack the entire cross section. Because the undamaged material is much stiffer than the damaged, it is more accurate to model a reduced cross section than a cross section with a lower modulus of elasticity. The location of the damage is indicated by red arrow in Figure 46. The end of the member marked by the blue arrow has a small damaged area, but it is past the bolt at the very tip of the member, and does not affect the structural capacity.

A FIN 2D model was created with a reduced cross section of 120 mm by 200 mm for a length of 300 mm. Similar to the previous damage model, the results do not differ from those of the standard truss model.

Examining the stresses at the location of reduced cross section, this section of the member only experiences compression. Compared to the standard truss model, the axial force is the same, but the stress is higher corresponding to the decreased cross section. A compressive stress of 1 204 kPa is present at the location of the damage, compared to 722 kPa at the same location on the undamaged truss. This accounts for the load eccentricity with respect to the center of area of the section at the damaged location. This is well below the 15 000 kPa capacity.

Buckling is not a concern for the exterior members of the truss because the stiff roofing prevents it.

10.5.3 Truss irregularity

Figure 47 Poor connection, with a large gap between the members

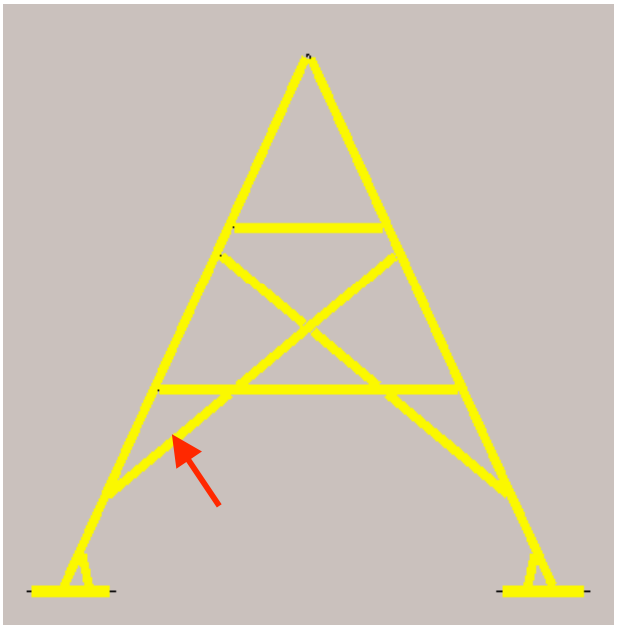

Figure 48 Location of the member on the truss

This irregularity occurs at a window, and the gap between member and wood is 1.5 cm. A bolt connects the members. The truss is modeled without this member, as considerable movement is required before the member would transfer forces.

Table 20 Load multiplier, k, required for failure by different paths compared to those for a standard truss

	Standard truss		**Missing member**	
FINE comparison		**k**		**k**
Buckling, $w < (10/9)\ w_0$ limit		4.3		4.1
Buckling, $w < (4/3)\ w_0$ limit		11.5		11.3
Limit on II order validity, $w < 1.15\ w_0$		5.8		5.6
Eurocode	**Limit (≤ 1)**		**Limit (≤ 1)**	
Bearing	0.262	3.8	0.253	4.0
Shear	0.090	11.2	0.087	11.5
Bending and axial tension	0.102	9.8	0.103	9.7
Bending and axial comp (material failure)	0.189	5.3	0.194	5.2
Buckling	0.567	1.8	0.581	1.7
Lateral torsional buckling	0.555	1.8	0.567	1.8

When compared to the standard truss, the critical values are very close. The missing member does not considerably affect the capacity. The deflected shape, shown below for loading combination 1.35 DL + 1.5 LL, is noticeably unsymmetrical due to the missing member.

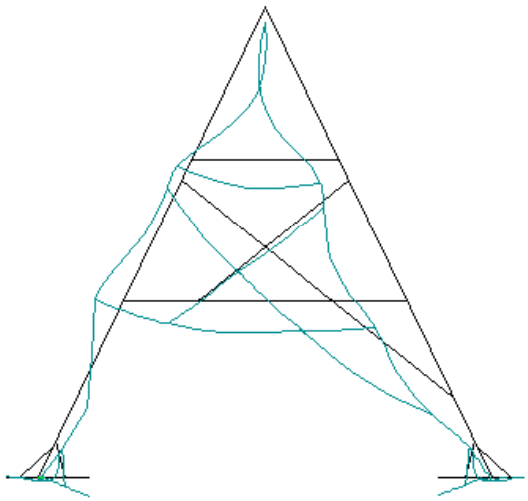

Figure 49 Deflected shape of the truss with one member removed

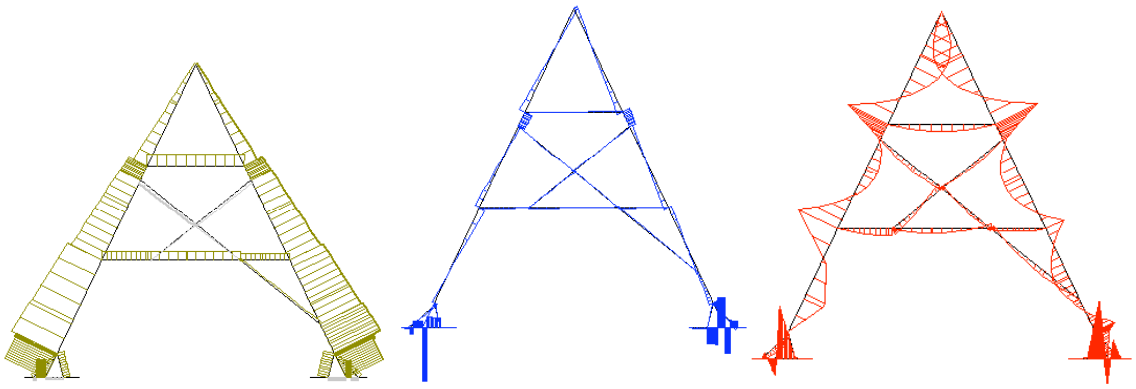

Figure 50 Axial force, shear force, and bending moment diagrams for the truss with a missing member, for load combination 1.35 DL + 1.5 LL

Despite the deflected shape being asymmetric due to the missing member, the axial force, shear force, and bending moment diagrams are not considerably affected by the missing member. Figure 50 shows these diagrams for the load combination 1.35 DL + 1.5 LL. The other loading combinations are similar in that the differences between the standard truss and the truss with the missing member are very small.

These results fit with the low forces present in this member for the standard truss.

10.5.3.1 Summary of irregularities

The irregularities modeled produced very close results to those of the standard truss. One reason is that there is a lot of reserve in the standard truss, as the capacity is four times higher than the load. One exception is the suction wind load case, which would cause the roof to blow off the building, but this is not affected by irregularities in the members.

10.6 Summary of analysis

The loading on St Anne's Church was determined using the Eurocode, with a return period of 500 years to account for the predicted life of the structure. The load of the roofing tiles was increased to 100 kg/m^2, in case ceramic tiles are used in the future. A standard truss from the structure was analyzed using FIN 2D, and the Eurocode was used to check deflections and stresses. In addition to the Eurocode, first and second order results were compared to check stability. In order to compare the methods, the load

multiplier, k, was calculated so that k multiplied by the load causes failure. The Eurocode buckling check found $k = 1.8$, and the first and second order results comparison found $k = 4.3$ for $w < (10/9)\, w_0$ limit, and $k = 11.5$ for $w < (4/3)\, w_0$ limit. These limits are derived from limits for comparing axial load to the critical buckling load used in Czech Republic and the rest of Europe. Keeping differences between first and second order analysis to $w < (10/9)\, w_0$ provided around twice that of the Eurocode under buckling, while the limit $w < (4/3)\, w_0$ provided much more allowance than the Eurocode, but is inaccurate. The limit on validity on second order analysis in the program FINE, $w < 1.15\, w_0$, resulted in a load multiplier of 5.8.

Examining failure modes other than buckling found the truss to be well within the requirements, as it can handle loads 3.8 times higher than those applied.

Some joints of the truss had two continuous members passing each other, but cut back so that they fit into each other. These joints were modeled as fixed, pinned, and spring connections, and there were negligible differences between the three cases.

Irregularities in the trusses were modeled in FINE, such as four trusses in the center with a different geometry, two members in different trusses that were damaged from beetles, and one member with a poor connection that was not taking any load. Due to the close spacing of the trusses at 0.84 m, and the stiff roof membrane of two 20 mm layers of boards, the loading redistributes if the stiffness between trusses differs. For the four trusses of different geometry, the loading was redistributed so that each truss had the same displacement at mid-span of the exterior members. The individual trusses that were damaged were modeled with the standard load, as the loss of part of the truss in these cases did not significantly affect the stiffness. In the case of an entire truss being lost, the adjacent trusses are fully capable of withstanding the extra load. The members at the end of the roof were checked according to the Eurocode, and met all requirements.

The roof structure of St Anne's is capable of withstanding the loading from the Eurocode for a 500-year return period. Significant reserve is present, in case of any future damages.

11 Conclusions

Of the structures in Prague with original Gothic roof trusses, access was possible to St Anne's Church. In examining this church, relevant documents relating to historic constructions were followed, including "Evaluation and analysis of old timber structures," [1] which uses non-destructive techniques, the Venice Charter [2], and the ICOMOS document "Principles for the preservation of historic timber structures" [3].

The entire roof structure is very stable, and capable of withstanding loading of a 500 year return period with 100 kg/m^2 tiles. Exterior members are subject to higher bending moments and axial forces than the interior members, but also have larger cross sectional dimensions. From the top to the bottom of the truss, the axial load increases and the unsupported span lengths decrease for the exterior members, making it well designed against buckling. Irregularities that are present in some trusses are missing members, beetle damage, minor rot, and reduced cross sections. The roof structure is entirely capable of withstanding the required loading despite these damages.

Employing second order analysis, comparing the results to first order, and using established limits for comparing the axial load to the critical axial load is used to check stability. Second order analysis provides an accurate representation of the structure when the second order deflections are within 15% of first order. The established limit in the Czech Republic $P < (1/4)\ P_{crit}$, and elsewhere in Europe $P < (1/10)\ P_{crit}$ are checked in FINE finite element software. The stability of the structure or portion of is examined, which is more accurate than the Eurocode equations that check each member individually. This offers a viable alternative to the Eurocode equations.

St Anne's Church meets the stability check used in Czech Republic and elsewhere in Europe, and also meets the requirements set out in the Eurocode. Table 14 is repeated below, showing the load multiplier, k, required to cause failure.

Table 14 Load multiplier, k, required for failure by different paths

FINE comparison		**k**
Stability, $P < (1/10)\ P_{crit}$ limit		4.3
Stability, $P < (1/4)\ P_{crit}$ limit		11.5
Limit on II order validity, $w < 1.15\ w_0$		5.8
Eurocode	**Limit (≤ 1)**	
Bearing	0.262	3.8
Shear	0.090	11.2
Bending and axial tension	0.102	9.8
Bending and axial comp (material failure)	0.189	5.3
Buckling	0.567	1.8
Lateral torsional buckling	0.555	1.8

It is concluded that the roof structure St Anne's Church is very safe. The stability criteria $P < (1/10)\ P_{crit}$ produced over twice the capacity when compared to the buckling check in the Eurocode. Second order analysis more accurately represents the true state of the structure and provides more allowance than the Eurocode, but is limited as it is not accurate when the deflections are more than 15% different than those from first order analysis.

St Anne's Church is in very good condition, and with proper monitoring and maintenance, will survive for many more centuries. It is recommended that a thorough inspection and mapping of deteriorations from beetles and rot be done on a regular basis. The trusses are very stable and capable of withstanding four times the current loading. If damages occur to a part of the structure, it is important to acknowledge this before any repair works are done. It is important to maintain the historic material and geometry as much as possible, and the high capacity of the trusses can mean that replacement of missing members can be avoided.

Regular maintenance and monitoring of historic constructions is important for prevention of structural failure or irreversible damage, particularly for wood constructions because they are susceptible to rot and beetle infestation. As many privately owned historic constructions might not receive the necessary attention, universities can play an important role in their conservation.

12 References

1. Ceccotti, A. (2004). Evaluation and analysis of the old timber structures. In *Proceedings of the Fourth International Seminar on Structural Analysis of Historical Constructions, 10-13 Nov. 2004, Padova, Italy, Volume 1, p. 43-50.*
2. ICOMOS, (1964). International Charter for the Conservation and Restoration of Monuments and Sites. Retrieved May 3, 2009, from The Venice Charter Web site: http://www.icomos.org/venice_charter.html
3. ICOMOS, (1999). Principles for the preservation of historic timber structures. *12th General Assembly* Mexico.
4. Map of Prague heritage reservation. Retrieved May 1, 2009, from Preservation of Monuments Web site: http://pamatky.praha-mesto.cz/38819_Map-of-Prague-heritage-reservation-gif-4-5MB
5. Dagmar and Václav Havel Foundation VIZE 97. (2005). *Prague Crossroads* [Brochure]. Prague, Czech Republic.
6. European Standard, Eurocode 1: Action on Structures, April 2002
7. Kuipers, J. 1986. Effect of Age/or Load on Timber Strength. In *Proceedings of CIB W18 meeting, Paper 19-6-1*. Florence, Italy.
8. Kuklik, Petr (2009). *Structural Timber Presentation*.
9. Holzforschung München. (2004). *Product Information: Structural Sawn Timber.*
10. Fine Ltd, (2007). Fine Civil Engineering Software. Retrieved May 16, 2009, from Fin 3D user manual Web site: http://www.fine.cz/
11. Beer, F.P., Johnston,Jr., E.R., & DeWolf, J.T. (2004). *Mechanics of Materials*. New York: McGraw-Hill.
12. Ghali, A., Neville, A.M., & Brown, T.G. (2003). *Structural analysis: a unified classical and matrix approach*. Suffolk: Spon Press.
13. Kuklik, Petr (2009). *Design of timber structures, basis of design and members*.
14. Green, D.W., Winandy, J.E., & Kretschmann, D.E. (1999). *Wood handbook: wood as an engineering material*. Madison, WI: Forests Products Laboratory.
15. European Standard, Eurocode 5: Design of timber structures, December 2003

13 Appendix A: Loading calculation for St Anne's Church

The load calculation is based on the Eurocode 1: Actions on structures [4]

13.1 Dead load (DL)

There are two layers of wood planks, each of thickness 20 mm directly on top of the trusses. The roof is covered with shingles

- The weight of the wood planks = 0.104 kN/m^2 assuming a density of 530 kg/m^3
- The weight of the shingles and roofing felt = 0.122 kN/m^2 assuming shingles weighting 225 lb/ 100ft^2 and roofing felt weighing 30 lb/ 100 ft^2

Current dead load:

- DL = 0.12 kPa

Consider heavier tiles that may be used in the future:

- 100kg/m^2 = 0.981 kPa
- Total possible dead load = 1.10 kPa

13.2 Live load (LL)

According to Eurocode EN 1991-1-1, roofs shall be categorized according to their accessibility as shown in EN 1991-1-1:2002 Table 6.9 (Table A1 below). In our case, the roof is classified as Category H, which is not accessible except for normal maintenance and repair.

Table A1: Categorization of roofs

Categories of loaded area	Specific Use
H	Roofs not accessible except for normal maintenance and repair.
I	Roofs accessible with occupancy according to categories A to D
K	Roofs accessible for special services, such as helicopter landing areas

The imposed loads for roofs of category H is listed in EN 1991-1-1:2002 Table 6.10 (not shown).

- Live loads on roof q_k = 0.4 kN/m2 or a point load of Q_k = 1 kN

13.3 Snow Load (SL)

The slope of the roof is 64.1°, which is higher than the 60° limit, so the snow would slide off the roof and the load case does not need to be considered.

Table A2: Snow load shape coefficients

Angle of pitch of roof α	$0° \le \alpha \le 30°$	$30° < \alpha < 60°$	$\alpha \ge 60°$
μ_1	0,8	0,8(60 - α)/30	0,0
μ_2	0,8 + 0,8 α/30	1,6	--

$s = \mu_i C_e C_t s_k = 0$ kPa

13.4 Wind Load (WL)

13.4.1 Basic wind velocity (v_b)

The basic wind velocity in Prague is $v_{b,0}$ = 20 m/s.

The basic wind velocity (v_b)

$v_b = C_{dir} \ C_{season} \ v_{b,0}$

C_{dir} = Directional factor = 1.0

C_{season} = Season factor = 1.0

$v_b = C_{dir} \ C_{season} \ v_{b,0}$ = 20 m/s

13.4.2 Reference height (z_e)

For a duo pitch roof, the reference height is equal to the actual height.

Reference height (z_e) = 29.61 m

13.4.3 Terrain category

In Eurocode, the terrain is categorized according to the terrain roughness. Recommended values are given in EN 1991-1-4 Table 4.1 (Table A3 below).

Table A3: Terrain categories and terrain parameters

Terrain category		z_0 m	z_{min} m
0	Sea or coastal area exposed to the open sea	0,003	1
I	Lakes or flat and horizontal area with negligible vegetation and without obstacles	0,01	1
II	Area with low vegetation such as grass and isolated obstacles (trees, buildings) with separations of at least 20 obstacle heights	0,05	2
III	Area with regular cover of vegetation or buildings or with isolated obstacles with separations of maximum 20 obstacle heights (such as villages, suburban terrain, permanent forest)	0,3	5
IV	Area in which at least 15 % of the surface is covered with buildings and their average height exceeds 15 m	1,0	10
The terrain categories are illustrated in Annex A.1.			

Buildings surround the site, so the terrain category is IV

z_0= 1.0 m

z_{min}= 10 m

13.4.4 Peak Velocity Pressure

As stated in Eurocode EN 1991-1-4, the peak velocity pressure ($q_p(z)$) depends on the exposure factor ($c_e(z)$) and the basic wind pressure (q_b).

$q_p(z) = c_e(z)\, q_b$

The exposure factor is a function of height above terrain and it is shown in EN 1991-1-4 Figure 4.2 (Figure A1 below).

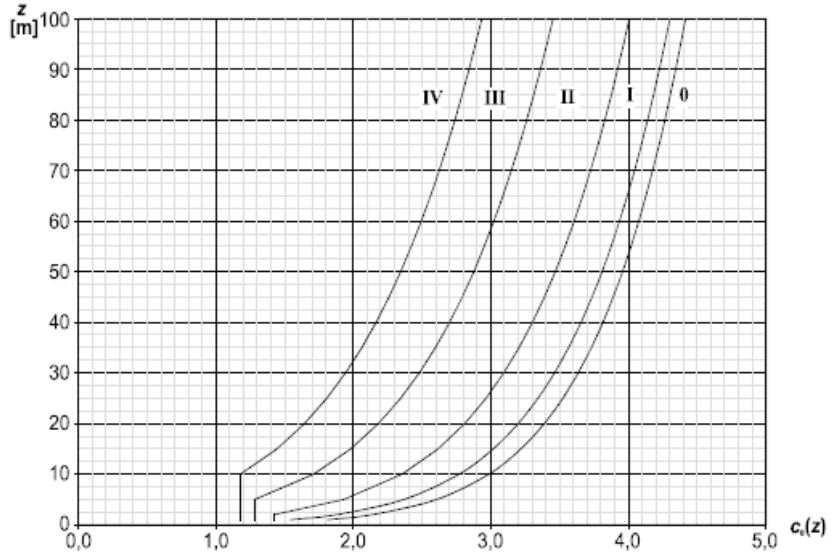

Figure A1: Illustrations of the exposure factor $c_e(z)$ for c_0 = 1.0, k = 1.0

When the height is 30 m and the site is zone IV

c_e(30 m)= 1.95

The basic wind pressure (q_b)

It was calculated as

$q_b = 0.5\ \rho\ v_b^2$

ρ = air density = 1.25kg/m^2

q_b= 250 N/m^2

The Peak Velocity Pressure

q_p(30m)= 250 N/m^2 * 1.95 = 0.488 kN/m^2

13.4.5 External pressure

The wind pressure acting on the external surface is determined as

$W_e = q_p(z_e)\ c_{pe}$

$q_p(z_e)$ = peak velocity pressure

c_{pe} = pressure coefficient for the external pressure

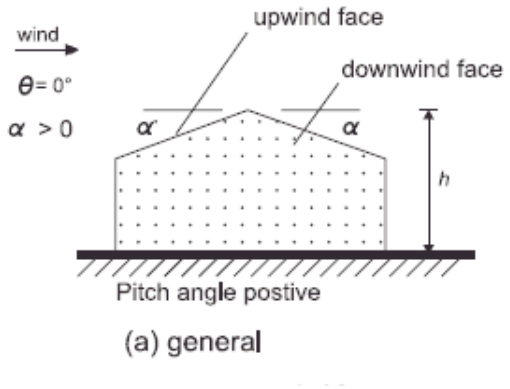

Figure A2: Wind loading on a structure

The external pressure coefficient for duo pitch roofs is determined by using Eurocode EN 1991-1-4: 2004 Table 7.4 a – b (Tables A4 and A5 below) and interpolated with reference to the pitch angle.

13.4.6 Probability of Exceedance

$$c_{prob} = \left(\frac{1 - K \cdot \ln(-\ln(1-p))}{1 - K \cdot \ln(-\ln(0{,}98))} \right)^n$$

K = is the shape parameter depending on the coefficient of variation of the extreme-value distribution (recommended 0.2)

n = the exponent (recommended 0.5)

For p = 0.002, c_{prob} = 1.122355

Multiply the basic wind pressure (q_b) by c_{prob}

It was calculated as

$q_b = 0.5\ \rho\ v_b^2$

with

ρ = air density = 1.25kg/m^2

q_b= 374 N/m^2

The Peak Velocity Pressure

$q_p(30m) = 374\ N/m^2 * 1.95 = 0.729\ kN/m^2$

Table A4: External pressure coefficients for duopitch roofs

Pitch Angle α	Zone for wind direction $\Theta = 0°$									
	F		G		H		I		J	
	$C_{pe,10}$	$C_{pe,1}$	$C_{pe,10}$	$C_{pe,1}$	$C_{pe,10}$	$C_{pe,1}$	$C_{pe,10}$	$C_{pe,1}$	$C_{pe,10}$	$C_{pe,1}$
-45°	-0,6		-0,6		-0,8		-0,7		-1,0	-1,5
-30°	-1,1	-2,0	-0,8	-1,5	-0,8		-0,6		-0,8	-1,4
-15°	-2,5	-2,8	-1,3	-2,0	-0,9	-1,2	-0,5		-0,7	-1,2
-5°	-2,3	-2,5	-1,2	-2,0	-0,8	-1,2	+0,2		+0,2	
							-0,6		-0,6	
5°	-1,7	-2,5	-1,2	-2,0	-0,6	-1,2	-0,6		+0,2	
	+0,0		+0,0		+0,0				-0,6	
15°	-0,9	-2,0	-0,8	-1,5	-0,3		-0,4		-1,0	-1,5
	+0,2		+0,2		+0,2		+0,0		+0,0	+0,0
30°	-0,5	-1,5	-0,5	-1,5	-0,2		-0,4		-0,5	
	+0,7		+0,7		+0,4		+0,0		+0,0	
45°	-0,0		-0,0		-0,0		-0,2		-0,3	
	+0,7		+0,7		+0,6		+0,0		+0,0	
60°	+0,7		+0,7		+0,7		-0,2		-0,3	
75°	+0,8		+0,8		+0,8		-0,2		-0,3	

NOTE 1 At $\Theta = 0°$ the pressure changes rapidly between positive and negative values on the windward face around a pitch angle of $\alpha = -5°$ to $+45°$, so both positive and negative values are given. For those roofs, four cases should be considered where the largest or smallest values of all areas F, G and H are combined with the largest or smallest values in areas I and J. No mixing of positive and negative values is allowed on the same face.

NOTE 2 Linear interpolation for intermediate pitch angles of the same sign may be used between values of the same sign. (Do not interpolate between $\alpha = +5°$ and $\alpha = -5°$, but use the data for flat roofs in 7.2.3). The values equal to 0,0 are given for interpolation purposes

Table A5: External pressure coefficients for duopitch roofs

Pitch angle α	Zone for wind direction $\Theta = 90°$							
	F		G		H		I	
	$C_{pe,10}$	$C_{pe,1}$	$C_{pe,10}$	$C_{pe,1}$	$C_{pe,10}$	$C_{pe,1}$	$C_{pe,10}$	$C_{pe,1}$
-45°	-1,4	-2,0	-1,2	-2,0	-1,0	-1,3	-0,9	-1,2
-30°	-1,5	-2,1	-1,2	-2,0	-1,0	-1,3	-0,9	-1,2
-15°	-1,9	-2,5	-1,2	-2,0	-0,8	-1,2	-0,8	-1,2
-5°	-1,8	-2,5	-1,2	-2,0	-0,7	-1,2	-0,6	-1,2
5°	-1,6	-2,2	-1,3	-2,0	-0,7	-1,2	-0,6	
15°	-1,3	-2,0	-1,3	-2,0	-0,6	-1,2	-0,5	
30°	-1,1	-1,5	-1,4	-2,0	-0,8	-1,2	-0,5	
45°	-1,1	-1,5	-1,4	-2,0	-0,9	-1,2	-0,5	
60°	-1,1	-1,5	-1,2	-2,0	-0,8	-1,0	-0,5	
75°	-1,1	-1,5	-1,2	-2,0	-0,8	-1,0	-0,5	

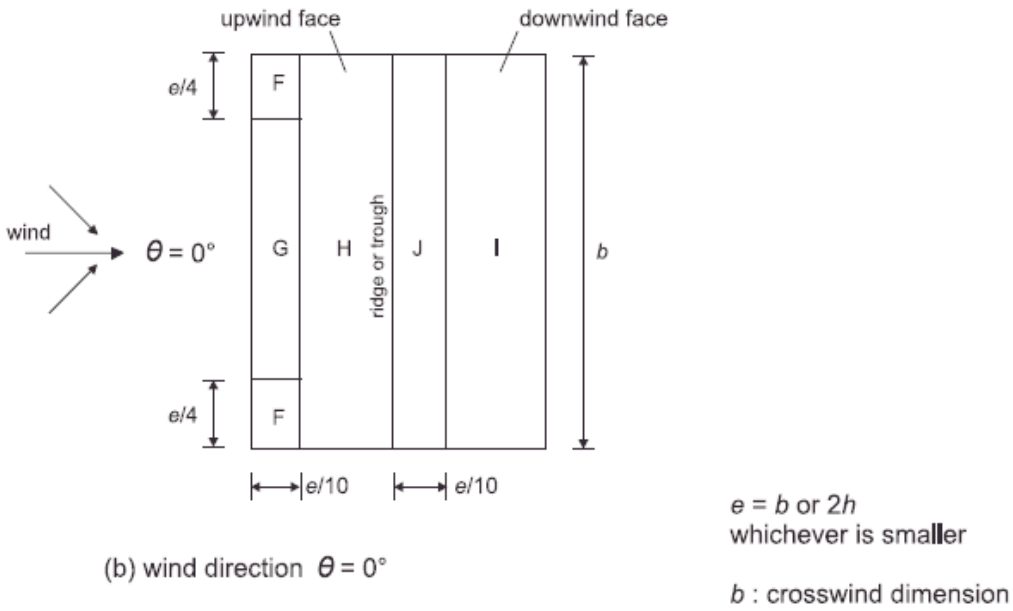

(b) wind direction $\theta = 0°$

External coefficient ($c_{pe,10}$) at wind direction θ = 0º

Zone	F	G	H	I	J
$c_{pe,10}$	0.727	0.727	0.727	-0.200	-0.300
W_e (kPa)	0.355	0.355	0.355	-0.098	-0.146

Figure A3 External coefficient ($c_{pe,10}$) at wind direction θ = 0º (Pitch angle = 64 º), e = 44m, for a 50 year return period

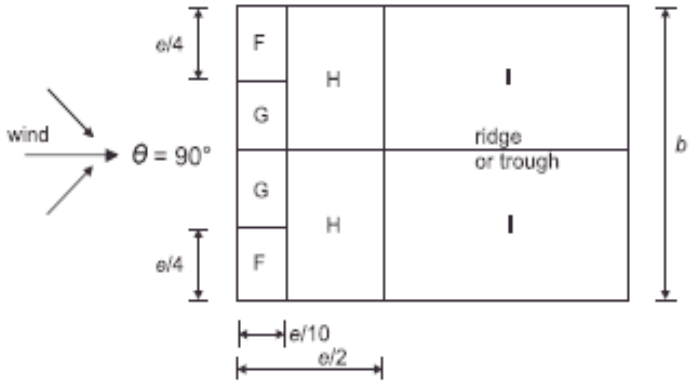

(c) wind direction $\theta = 90°$

External coefficient ($c_{pe,10}$) at wind direction θ = 90º

Zone	F	G	H	I
$c_{pe,10}$	-1.100	-1.200	-0.800	-0.500
W_e (kPa)	-0.537	-0.586	-0.390	-0.244

Figure A4 External coefficient ($c_{pe,10}$) at wind direction θ =90º (Pitch angle = 64 º), e = 12.6m, for a 50 year return period

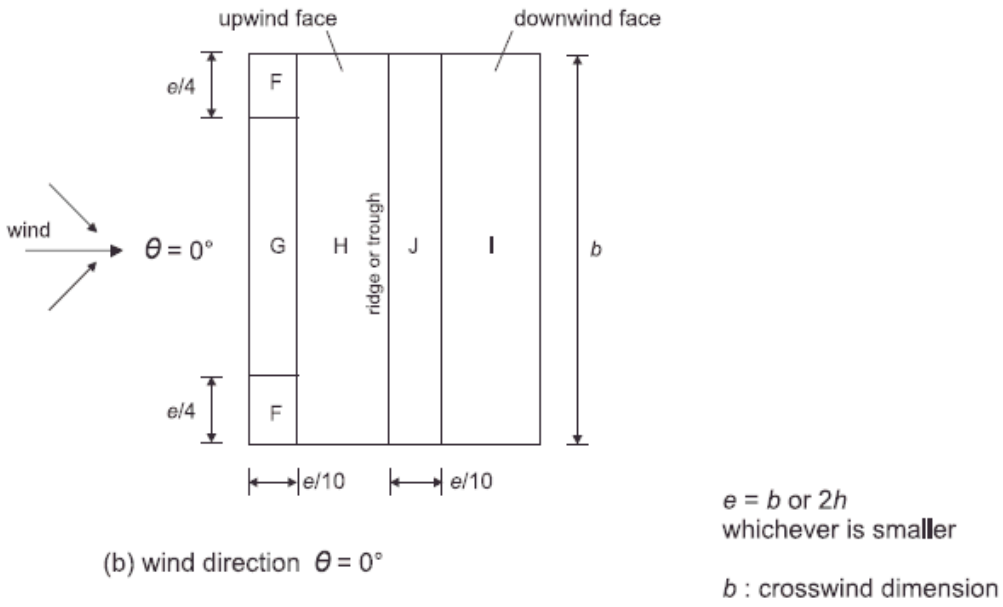

(b) wind direction $\theta = 0°$

External coefficient ($c_{pe,10}$) at wind direction θ = 0º

Zone	F	G	H	I	J
$c_{pe,10}$	0.727	0.727	0.727	-0.200	-0.300
W_e (kPa)	0.530	0.530	0.530	-0.146	-0.219

Figure A5: External coefficient ($c_{pe,10}$) at wind direction θ =0º (Pitch angle = 64 º), coefficient e = {smaller of 2h = 60, or b = 44m} = 44m, for a 500 year return period

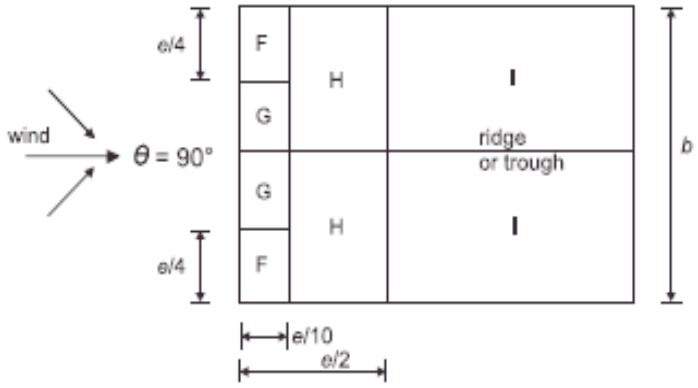

(c) wind direction $\theta = 90°$

External coefficient ($c_{pe,10}$) at wind direction θ = 90º

Zone	F	G	H	I
$c_{pe,10}$	-1.100	-1.200	-0.800	-0.500
W_e (kPa)	-0.802	-0.875	-0.583	-0.365

Figure A6: External coefficient ($c_{pe,10}$) at wind direction θ =90º (Pitch angle = 64 º), coefficient e = {smaller of 2h = 60, or b = 12.6} = 12.6 m, for a 500 year return period

13.4.7 Internal pressure coefficient

There is no dominant face to the building. The internal pressure coefficient shall be taken as 0.200 or -0.300, whatever one is critical. W_i (kPa) = -0.098 or 0.146.

14 Appendix B: Timber grading criteria, as per DIN 4074-1 [9]

Grading rule

Structural Sawn Timber

graded according to DIN 4074-1
"Strength grading of wood – Part 1: coniferous sawn timber"

Grading rule for boards and planks (*Bretter, Bohlen*), grade S7

◆ **Knots *(3 grading criteria)***

Knots with a diameter < 5 mm not taken into consideration

▸ ***Single Knot***

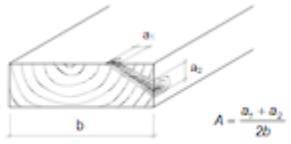

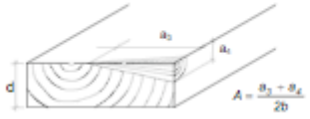

if $a_4/d \leq 1/2$, than $A = \frac{a_4}{2b}$

↳ ***Permissible limit: A ≤ 1/2***

▸ ***Sum of knots***

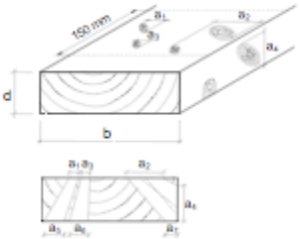

$A = \frac{a_1 + a_2 + a_3 + a_4 + a_5 + a_6 + a_7}{2b}$

↳ ***Permissible limit: A ≤ 2/3***

▸ ***Edge knot***

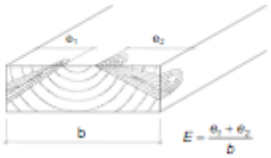

↳ ***Permissible limit: allowed***

◆ **Further characteristics**

Rate of growth:
Average ring width:

general:	≤ 6 mm
Douglas fir:	≤ 8 mm

Slope of grain: ≤ 16 %

Pith: allowed

Wane: ≤ 1/3

Warp (over 2 m length):

Bow or Spring	≤ 12 mm
Cup	≤ 1 / 20
Twist	≤ 2 mm / 25 mm width

Discolouration, Compression wood:
Up to 3/5 of cross section of surface allowed

- bluestain	allowed
- brown and white rot	not allowed

Insect attack:
Holes up to 2 mm diameter allowed

Fissures:
Lightning cracks and ring shakes not allowed

Grading rule

Structural Sawn Timber

graded according to DIN 4074-1
"Strength grading of wood – Part 1: coniferous sawn timber"

Grading rule for boards and planks (*Bretter, Bohlen*), grade S10

◆ **Knots *(3 grading criteria)***

Knots with a diameter < 5 mm not taken into consideration

▸ ***Single Knot***

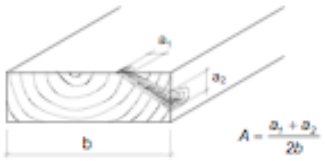

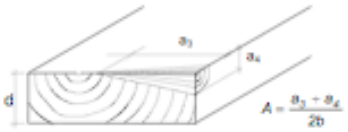

if $a_4/d \leq 1/3$, than $A = \frac{a_4}{2b}$

↳ ***Permissible limit: A ≤ 1/3***

▸ ***Sum of knots***

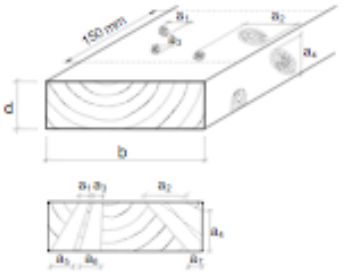

↳ ***Permissible limit: A ≤ 1/2***

▸ ***Edge knot***

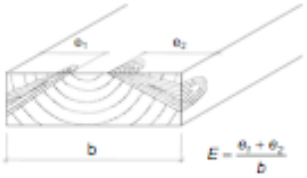

↳ ***Permissible limit: E ≤ 2/3***
(for glued laminated timber allowed)

◆ **Further characteristics**

Rate of growth:
Average ring width:

general:	≤ 6 mm
Douglas fir:	≤ 8 mm

Slope of grain: ≤ 12 %

Pith: allowed

Wane: ≤ 1/3

Warp (over 2 m length):

Bow or Spring	≤ 8 mm
Cup	≤ 1 / 30
Twist	≤ 1 mm / 25 mm width

Discolouration, Compression wood:
Up to 2/5 of cross section of surface allowed

- bluestain	allowed
- brown and white rot	not allowed

Insect attack:
Holes up to 2 mm diameter allowed

Fissures:
Lightning cracks and ring shakes not allowed

Grading rule

Structural Sawn Timber

graded according to DIN 4074-1
"Strength grading of wood – Part 1: coniferous sawn timber"

Grading rule for boards and planks (*Bretter, Bohlen*), grade S13

◆ **Knots *(3 grading criteria)***

Knots with a diameter < 5 mm not taken into consideration

▸ ***Single Knot***

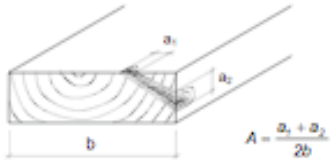

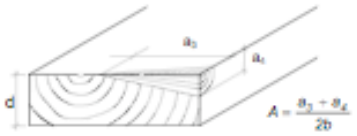

if $a_4/d \leq 1/5$, than $A = \frac{a_4}{2b}$

↳ ***Permissible limit: A ≤ 1/5***

▸ ***Sum of knots***

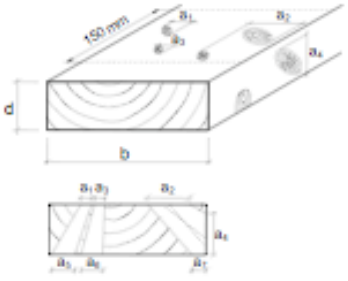

$$A = \frac{a_1 + a_2 + a_3 + a_4 + a_5 + a_6 + a_7}{2b}$$

↳ ***Permissible limit: A ≤ 1/3***

▸ ***Edge knot***

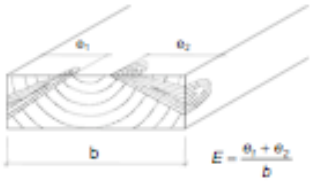

↳ ***Permissible limit: E ≤ 1/3***
(for glued laminated timber allowed)

◆ **Further characteristics**

Rate of growth:
Average ring width:

general:	≤ 4 mm
Douglas fir:	≤ 6 mm

Slope of grain: ≤ 7 %

Pith: not allowed

Wane: ≤ 1/4

Warp (over 2 m length):

Bow or Spring	≤ 8 mm
Cup	≤ 1 / 50
Twist	≤ 1 mm / 25 mm width

Discolouration, Compression wood:
Up to 1/5 of cross section of surface allowed

- bluestain	allowed
- brown and white rot	not allowed

Insect attack:
Holes up to 2 mm diameter allowed

Fissures:
Lightning cracks and ring shakes not allowed

15 Appendix C: Derivation of equations

15.1 Buckling of an ideal column [11] from page 40

Line 2 on Figure 13 is that of an ideal column using the approximate equation for curvature:

$$\frac{1}{\rho} \approx -w'' \qquad \text{[Eq. 8]}$$

$$w'' = \frac{M}{EI} = \frac{-Pw}{EI} \qquad \text{[Eq. 9]}$$

This differential equation is solved for

$$p^2 = \frac{P}{EI} \qquad w = A\sin(px) + B\cos(px)$$

Boundary conditions: When $x = 0$, $w = 0$ and $B = 0$

When $x = l$, $w = 0$ and $0 = A\ sin(pl)$

This is true when either $A = 0$ which is the case for a perfectly straight column, or it is true when $sin(pl) = 0$ since $sin(n\pi) = 0$ when 'n' is an integer

$$\sin(pl) = 0 \qquad p = \frac{n\pi}{l} \qquad p^2 = \frac{P}{EI} \qquad P = \frac{n^2 \pi^2 EI}{l^2}$$

The smallest integer is $n = 1$, providing

$$P_{cr} = \frac{\pi^2 EI}{l^2}$$

Returning to $0 = A\ sin(pl)$ the constant A is still unknown. It cannot be solved for because the equation

$$\frac{1}{\rho} \approx -w''$$

Was used instead of

$$\frac{1}{\rho} = -\frac{w''}{\left(1 + w'^2\right)^{3/2}}$$

Therefore, the deflection at failure is unknown.

When $P < P_{cr}$ the equation $sin(pl) = 0$ cannot be satisfied, and therefore, the column is straight.

15.2 Buckling of a column with an initial deformation [10] from page 41

As no column is perfect in terms of geometry or material, a column (Line 1 on Figure 13) is examined with an initial deformation given as

$$w_0(x) = e_0 \sin\left(\frac{\pi x}{l}\right) \qquad \text{[Eq. 11]}$$

Modifying equation 9 to account for the initial deflection given by equation 11:

$$(w(x) - w_0(x))'' = \frac{-Pw(x)}{EI} \qquad \text{[Eq. 12]}$$

Previously

$$w(x) = A \sin\left(\frac{\pi x}{l}\right) \qquad w''(x) = -A\left(\frac{\pi^2}{l^2}\right) \sin\left(\frac{\pi x}{l}\right)$$

And with

$$w_0(x) = e_0 \sin\left(\frac{\pi x}{l}\right) \qquad w'' + p^2 w = w_0''$$

$$-A\left(\frac{\pi^2}{l^2}\right) \sin\left(\frac{\pi x}{l}\right) + p^2 A \sin\left(\frac{\pi x}{l}\right) = -e_0\left(\frac{\pi^2}{l^2}\right) \sin\left(\frac{\pi x}{l}\right)$$

Solve for

$$A = \frac{e_0}{1 - \frac{p^2 l^2}{\pi^2}}$$

And with

$$p^2 = \frac{P}{EI} \qquad P_{cr} = \frac{\pi^2 EI}{l^2} \qquad A = \frac{e_0}{1 - \frac{P}{P_{cr}}}$$

And

$$w = \left[\frac{e_0}{1 - \frac{P}{P_{cr}}}\right] \sin\left(\frac{\pi x}{l}\right) \qquad w = \frac{w_0}{1 - \frac{P}{P_{cr}}}$$

15.3 Eurocode buckling equations [15] from page 67

The following formulas use the stresses from first order analysis.

$$\frac{\sigma_{c,0,d}}{k_{c,y} f_{c,0,d}} + \frac{\sigma_{m,y,d}}{f_{m,y,d}} + k_m \frac{\sigma_{m,z,d}}{f_{m,z,d}} \le 1$$

$$\frac{\sigma_{c,0,d}}{k_{c,z} f_{c,0,d}} + k_m \frac{\sigma_{m,y,d}}{f_{m,y,d}} + \frac{\sigma_{m,z,d}}{f_{m,z,d}} \le 1 \qquad \text{[Eq. 38]}$$

This criteria is met as $0.243 \le 1$.

The factors $k_{c,y}$ and $k_{c,z}$ consider buckling of the member.

$$k_{c,y} = \frac{1}{k_y + \sqrt{k_y^2 - \lambda_{rel,y}^2}}$$

$$k_{c,z} = \frac{1}{k_z + \sqrt{k_z^2 - \lambda_{rel,z}^2}}$$

$$k_y = 0.5\left(1 + \beta_c\left(\lambda_{rel,y} - 0.3\right) + \lambda_{rel,y}^2\right)$$

$$k_z = 0.5\left(1 + \beta_c\left(\lambda_{rel,z} - 0.3\right) + \lambda_{rel,z}^2\right)$$

$$\lambda_{rel,y} = \frac{\lambda_y}{\pi}\sqrt{\frac{f_{c,0,k}}{E_{0.05}}}$$

$$\lambda_{rel,z} = \frac{\lambda_z}{\pi}\sqrt{\frac{f_{c,0,k}}{E_{0.05}}}$$